UNIVERSIDADE FEDERAL DE SÃO CARLOS
CENTRO DE CIÊNCIAS EXATAS E DE TECNOLOGIA
DEPARTAMENTO DE QUÍMICA
PROGRAMA DE PÓS-GRADUAÇÃO EM QUÍMICA

LAYERED DOUBLE HYDROXIDE AS MATRICES FOR PHOSPHATE INTERACTION: PHYSICO-CHEMICAL ASSESSMENT AND APPLICATIONS

Marcela Piassi Bernardo*

Thesis presented as part of the requirements to obtain the title of DOCTOR IN SCIENCES, concentration area: CHEMISTRY.

Advisor: Dr. Caue Ribeiro de Oliveira
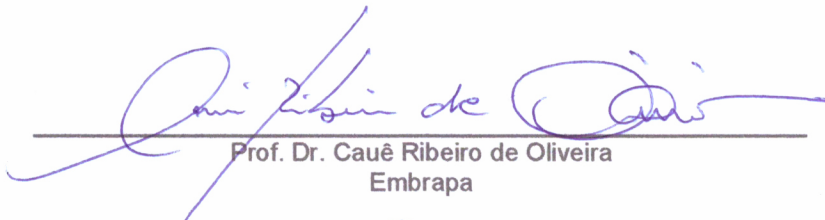
*scholarship: Capes

São Carlos - SP
2018

Folha de Aprovação

Assinaturas dos membros da comissão examinadora que avaliou e aprovou a Defesa de Tese de Doutorado da candidata Marcela Piassi Bernardo, realizada em 27/02/2018:

Prof. Dr. Cauê Ribeiro de Oliveira
Embrapa

Prof. Dr. Francys Kley Vieira Moreira
UFSCar

Profa. Dra. Elaine Cristina Paris
Embrapa

Profa. Dra. Ângela Albuquerque Teixeira Neto
CNPEM

Profa. Dra. Sandra Helena Pulcinelli
UNESP

"Que a gente não desista porque ninguém acredita"

Machado de Assis

Dedico este trabalho a todos que estiveram comigo durante esta jornada

Agradecimentos

Ao Dr. Caue Ribeiro pela orientação e paciência durante o desenvolvimento do trabalho.

Ao Prof. Dr. Francys Moreira pela inestimável cooperação neste trabalho, pela amizade e pelos bons conselhos.

A Embrapa Instrumentação pela excelente infraestrutura sem a qual este trabalho não poderia ter sido realizado. Agradeço ao pessoal, Adriana, Silviane, Viviane, Joana, Paulinho, Matteo, Alice por todo apoio, trabalho, paciência e companheirismo.

Ao Programa de Pós-Graduação em Química da Universidade Federal de São Carlos (PPGQ-UFSCar), pela oportunidade que me foi dada de realizar o doutorado. Agradeço a CAPES pela bolsa de doutorado e a todas instituições de fomento que financiaram esta pesquisa.

Aos meus amigos, João Otávio e Camila que muitas vezes me deram forças para continuar em frente. Agradeço as nossas infinitas conversas, as nossas risadas e nosso apoio!

Ao Flávio que está comigo nessa jornada desde termodinâmica, meu muito obrigada, por toda a ajuda nesse período. Agradeço também pela sua amizade.

Agradeço aos companheiros de Embrapa: ao Fábio por sempre me socorrer nas horas de aperto; ao Gelton por toda a paciência, cooperação e amizade; Kele, Jéssica, Fernando, Gelson, Paulo, Ricardo, Gabi pelas boas conversas e auxílios.

Ao meu namorado, Osmando, pelo apoio, carinho e incentivo, que já existiam mesmo antes de namorarmos.

Agradeço a minha mãe, Eliana, por ter me dado todo o suporte para chegar até aqui, por ter acreditado em mim e me incentivado.

Ao meu irmão Vitor, por sempre estar presente; ao meu pai, Reinaldo, que mesmo de longe sempre me incentivou. A toda a minha família que sempre acreditou de mim.

A todos que direta ou indiretamente contribuíram para a realização deste trabalho.

Table List

Figure List

Resumo

HIDRÓXIDOS DUPLOS LAMELARES COMO MATRIZES PARA INTERAÇÃO COM FÓSFORO: AVALIAÇÃO FÍSICO-QUÍMICA E APLICAÇÕES. O fósforo é um elemento essencial para todos os seres vivos e imprescindível para diversas atividades econômicas, especialmente para a agricultura. O desenvolvimento de sistemas de liberação controlada de fosfato é uma importante e necessária alternativa para que o fosfato seja entregue aos meios necessários evitando perdas econômicas e ambientais. Os hidróxidos duplos lamelares (HDL) por suas singulares características são excelentes materiais para serem explorados como matrizes para a interação com o fosfato. No entanto, não há consenso na literatura sobre como os fatores estruturais podem favorecer ou prejudicar o processo de interação do ânion com HDL. Dessa forma, nesta tese, foi investigado o papel que o cátion metálico (M^{2+}) da estrutura do HDL possui na capacidade de adsorção e dessorção e na estabilidade da estrutura quando em contato com fosfato. Hidrotalcita, o tipo mais comum de HDL, foi inicialmente estudada pois sua composição ($M^{2+}= Mg^{2+}$), tem menor raio iônico e a estrutura mais aberta. Observou-se que em baixas e intermediárias concentrações de fosfato a estrutura de [Mg-Al]-HDL é preservada, com intercalação do ânion. Já em concentrações mais elevadas, a estrutura do [Mg-Al]-HDL é substituída por novos precipitados formados por magnésio e fósforo. A partir desses resultados avaliou-se a interação do fosfato com HDL de estrutura intermediária, em relação ao tamanho do raio iônico de M^{2+}, agora formado por Zn^{2+}. A formação de novas fases aconteceu em concentrações menores que aquelas observadas para Mg^{2+}, e a concentração adsorvida por esses materiais também foi menor. No entanto, esses materiais foram apropriados para a liberação de fosfato quando incorporados em resinas odontológicas, podendo contribuir para a remineralizarão e manutenção do esmalte dentário. Neste caso também foram investigadas as propriedades de reforço deste HDL na matriz polimérica odontológica. Por fim, a interação do fosfato com a estrutura mais fechada de HDL, formada por Ca^{2+} foi estudada. De forma similar ao [Zn-Al]-HDL, novas fases foram formadas em concentrações intermediárias de fosfato. Porém, devido as suas características, esses materiais foram utilizados como fonte de fosfato às bactérias nitrificantes, extremamente importantes ao cultivo de leguminosas. [Ca-Al-PO_4]-HDL foi capaz de estimular o crescimento destas bactérias. Já havia sido constatada a capacidade de liberação de fosfato de [Mg-Al-PO_4]-HDL em água, assim, esse material também foi utilizado para a liberação de fosfato em um sistema dinâmico, como fertilizante para culturas de trigo. Em curto período de tempo [Mg-Al]-HDL foi capaz de fornecer a mesma nutrição de fosfato que as outras fontes estudadas com a vantagem de aumentar o pH do solo, prevenindo a imobilização do fosfato. Além disso, análises do solo após o cultivo revelaram que o solo cultivado com [Mg-Al-PO_4]-HDL possui maior quantidade de fosfato, cerca de 1,5 vezes maior que das outras fontes estudadas. Isso pode implicar na redução de aplicação de fosfato em cultivos posteriores.

Palavras-Chave: Liberação controlada. Fertilizante. Eutrofização. Reforço polimérico. *Bradyrhizobium*. Adsorção.

Abstract

LAYERED DOUBLE HYDROXIDE AS MATRICES FOR PHOSPHATE INTERACTION: PHYSICO-CHEMICAL ASSESSMENT AND APPLICATIONS: Phosphorus is an essential element for all living organisms and is indispensable for diverse economical activities, specially agriculture. The development of control release systems is an important and necessary alternative to correct delivery of phosphorus to the necessary mediums, avoiding economic and environmental losses. Layered Double Hydroxides (LDH) due to the singular characteristics are excellent materials to be explored as matrices for phosphate interaction. However, there is no consensus in literature about the structural factors which may favor or harm the interaction process between LDH and the anion. This thesis, was investigated the role of the metallic cation (M^{2+}) of LDH structure has on adsorption and desorption process and on stability of the structure when in contact with phosphate. Hydrotalcite, the most common LDH, was first studied due to the M^{2+} composition ($M^{2+}=Mg$), which has the short ionic radius and then the structure slightly open. It was notice that in low and intermediate phosphate concentrations the [Mg-Al]-LDH structure is well preserved, with anion intercalation, while at elevated concentrations, the [Mg-Al]-LDH structure is replaced by new precipitates formed by magnesium and phosphorus. From these results, were evaluated the interaction of LDH with Zn^{2+} in the structure (intermediate ionic radius). The formation of new phases happens in minor concentrations than that observed for Mg^{2+} and fewer amount of phosphate was adsorbed. However, these materials were appropriated for phosphate release when incorporated in dental resins, and may contribute to remineralization and maintenance of dental enamel. Besides, the reinforcement properties of this LDH on dental polymeric matrix were evaluated. Lastly, the interaction of phosphate with a more closed structure of LDH, formed by Ca^{2+} was studied. Similarly to [Zn-Al]-LDH, new phases were formed at intermediated phosphate concentrations. Due to [Ca-Al]-LDH characteristics, these materials were used as phosphate source for nitrifying bacteria, extremely important for legume cultivation. [Ca-Al-PO$_4$]-LDH was able to increase the bacterial growth. About [Mg-Al-PO$_4$]-LDH, the capacity of phosphate release from its structure had already been verified in aqueous medium, therefore this material was used to phosphate release in a dynamic system, as fertilizer for wheat crops. [Mg-Al-PO$_4$]-LDH was able to provide the phosphate nutrition than the other sources investigated, in a shorter time, with the advantage of increasing the soil pH, preventing the soil immobilization of phosphate. Soil analysis, after the cultivation, revealed that [Mg-Al-PO$_4$]-LDH has potential to provide phosphate in longer times, around 1.5 fold longer than commercial fertilizers.

Keywords: Controled release. Fertilizer. Eutrophication. Polymeric reinforcement. *Bradyrhizobium.* Adsorption.

Summary

1 - Introduction

1.1   - Background

According to ONU the world population in 2050 may achieve 9.2 billion of people. With this remarkable population growth, the search for a highly productive agriculture is urgent. The increase of agricultural production is directly linked to the use of fertilizers, agrochemicals and climatic factors. New fertilizer technologies are an important tool to avoid deforestation of new areas for food production.[1-4] However, Brazil is not self-sufficient for fertilizers production: approximately 90% of potassium (K), 70% of nitrogen (N) and 50% of phosphorus used for fertilizing of Brazilian lands are imported.[5,6] Among the three primary macronutrients (nitrogen, phosphorus and potassium), the phosphorus is the less required (in mass) by plants. However, this is the nutrient used in Brazil that limits crop production. Besides the direct importance that phosphorus has to agriculture, it is an essential element for all living organisms, once it is a cellular and energetic molecular constituent.[7] The adequate phosphorus supply allows the growth and normal function of cells. Considering other applications, phosphorus supply is essential for bones and teeth being one of the main responsible elements to guarantee the quality of tooth enamel and consequently oral health, in general.[8]

However, these activities and other economic sectors, generate effluents with high phosphorus content, which may achieve water bodies and cause eutrophication and consequently biodiversity lost.[9] The control or slow release of P is ideal to avoid waste of phosphorus, economical losses and environment damage. Layered double hydroxides are an important class of ceramic materials, whose properties go in favor of the objective of controlling the applied amount of this element.

1.2   - Layered Double Hydroxides

Layered Double Hydroxides (LDH) were discovered in the mid-19th century, in 1842 in Sweden. Briefly, the LDH structure is based on brucite ($Mg(OH_2)$) layer structure, where part of the divalent cations is isomorphically replaced by trivalent cations, originating in the layer a positive charge excess which is counter-balanced by intercalation of anions (and water) between the layers.[10,11] Each positive layer is formed by octahedral units containing metal cations in the center and hydroxyl anions groups positioned at their vertices. These octahedral units share the edges, forming planar layers, which positive charges are neutralized by the presence of anions between the layers (FIGURE 1.1).[12]
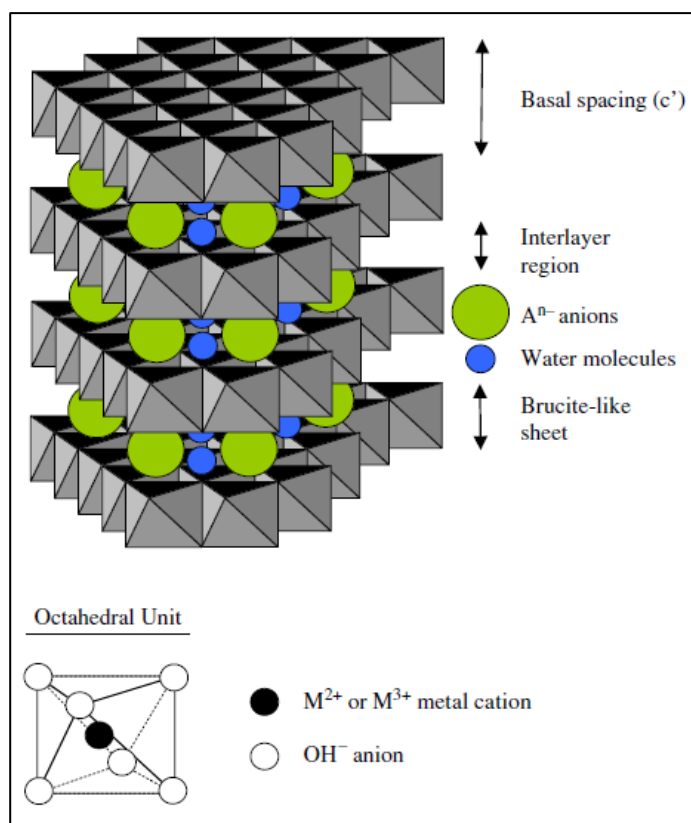
FIGURE 1.1- Schematic representation of the LDH structure (Available at Goh and co-authors (2008)[13]).

LDH have the general formula $M^{2+}_{1-x}M_x^{3+}(OH)_2]^{x+} (A^{n-})_{x/n} \cdot yH_2O$, where M^{2+} are bivalent cations, such as Ni^{2+}, Co^{2+}, Cu^{2+}, Zn^{2+} and Ca^{2+}, and M^{3+} are trivalent cations, such as Al^{3+}, Cr^{3+}, Fe^{3+}, Ga^{3+}. A^{n-} is a charge-balancing anion, and x is the molar ratio ($M^{3+}/(M^{3+}+M^{2+})$) ranging from 0.1 to 0.5 (TABLE 1.1). This versatility concerning the LDH structure allows the synthesis of different LDH with particular characteristics and applications on different fields.[14]

TABLE 1.1 - Possible combinations of metallic cations M^{2+} and M^{3+} at LDH (Adapted from Crepaldi and co-authors (1997)[15]).

Divalent cation	Trivalent cation														
	Al	Fe	Cr	Co	Mn	Ni	Sc	Ga	Ti[1]	La	V	Sb	Y	In	Zr[1]
Mg	o	o	o	o	o		o	o		o	o	o	o	o	o
Ni	o	o	o	o	o	o		o		o					
Zn	o	o	o					o							
Cu	o		o												
Co	o	o	o	o					o	o					
Mn	o		o		o			o							
Fe	o	o													
Ca	o														
Li[2]	o														
Cd	o														

(1) Tetravalent (2) Monovalent

The "bottom-up" LDH synthesis is a traditional aqueous coprecipitations process.[16] There are three main methods of precipitation used: (i) titration with NaOH and/or $NaHCO_3$ (sequential precipitation, or increasing pH method); (ii) constant pH at low supersaturation: The pH is controlled by the slow addition in a single container of two diluted streams: the first stream contains the M^{2+} and the M^{3+} ions, and the second one the base (KOH, NaOH, $NaHCO_3$); (iii) constant pH at high supersaturation; the solutions containing the M^{2+} and M^{3+} are added very quickly to the one containing $NaHCO_3$ or NaOH.[17,18]

LDH layers can be stacked in two symmetries, rhombohedric or hexagonal unit cells. Most of the synthetic LDH display rhombohedric unit cell; only LDH with M^{2+}/M^{3+} ratio equals to 1 exhibit orthorhombic unit cell.[14] Powder X-ray diffraction (PXRD) is an extremely important tool for the study of LDH structure. Information about crystalline structure, lattice parameters, crystal morphology and crystallite size may be obtained from this technique, where a single PXRD diagram is enough for a precise determination of the lattice parameters of these compounds.[19] For example, the lattice parameter c corresponds to three times the spacing between two consecutive layers (FIGURE 1.1). It can be calculated from XRD diagrams for rhombohedric unit cell, specifically from the position of the first peak: $c = 3d(003)$, or averaging the positions of the three harmonics, $c = d(003) + 2d(006) + 3d(009)$ (FIGURE 1.2). It is noteworthy that the peak (009) is sometimes overlapped with those from other non-basal planes, which are usually broad because of disorder of the anions and the water molecules in the interlayer space. The first peak of the doublet is originated from diffraction by planes (110) and its value corresponds to one half of lattice parameter a, i.e., $a = 2d(110)$.[19] The parameter a is very sensitive to the nature of the layer cations (ionic radius), while c strongly depends on the nature and orientation of the interlayer anion. For instance, c increases linearly with the number of carbon atoms in the organic anion, and for the halogens.[17]
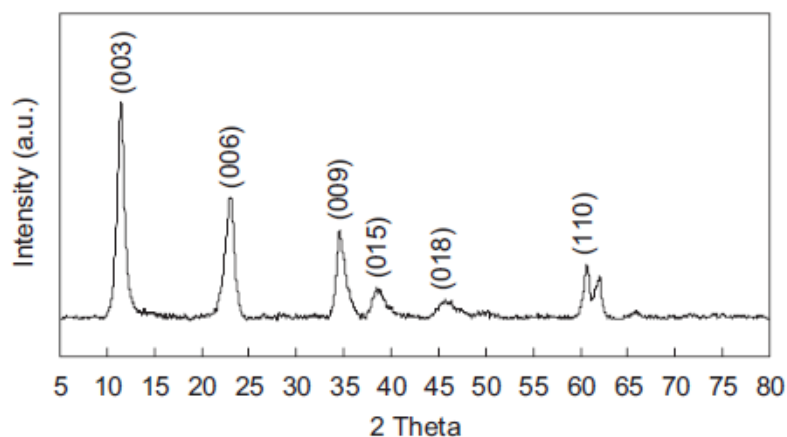
FIGURE 1.2- Typical XRD pattern of LDH with rhombohedric unit cell (Available at Goh and co-authors (2008)[13]).

The gallery size of LDH is estimated by subtracting the thickness of the brucite-like layers from the basal spacing determined by X-ray diffraction (XRD), in the case of layers formed by Mg^{2+} and Al^{3+} the thickness is assumed to be 0.48 nm, in other words, the basal distance is calculated as 0.48 + interlayer spacing, where the interlayer spacing includes the van der Waals radius of appropriate external atoms of the anion. The interlayer space of LDH is occupied by the counter-balance anions and water molecules, which interacts with the hydroxyl layer groups, anions and water molecules through a complex network of hydrogen bonding but due to the substantially disorder of the interlayers, the hydrogens bonds are in continuous ressonance, and consequently, the precise nature of interactions at the interlayer space is extremely complex.[11,20] Electrostatic effects are also involved between the bonding of octahedral layers and the interlayer content. Every interlayer anion has to satisfy the excess positive charges on both sides of the octahedral layers, which are electrically balanced by two neighboring interlayers.[21]

LDH have an interesting structural property called "memory effect". In this case, the calcination performed at proper temperature breakdown partially the hydroxyls from layer and convert interlayer anion into volatile, forming a double oxide. After calcination, if the double oxide get in contact with water or a solution of anion of interest, the original layered structure of LDH is regenerated with new intercalated anion. In general, during regeneration process, pH is raised, so it must be corrected to avoid hydroxyl from occupying the interlayer space.[22-24] Besides that important characteristic, LDH has the property of anion exchange. When in a medium, surrounding by anion which LDH has great

affinity (multivalent anions>OH⁻>F⁻>Cl⁻>Br⁻>NO₃⁻>I⁻), LDH are able to exchange the previous interlayer anion by that present at external medium (FIGURE 1.3).[25]
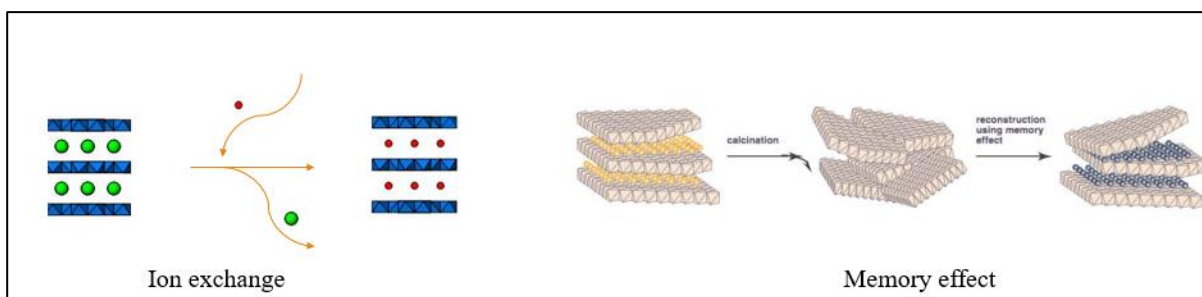
FIGURE 1.3- Representation of LDH properties: ion exchange and memory effect (Adapted from Sipiczki, 2013 [26]).

1.3 - Applications of LDH

Synthetic LDH containing exchangeable anions are less known and diffuse in nature than cationic clays, therefore the applications of these materials are less explored. However, these materials are almost the unique materials able to host molecules at anionic form. Due to the great versatility in the chemical composition of LDH, these materials have many and different potential applications. Besides that, other properties are essential for some applications, such as the high basicity of mixed oxides formed after thermal decomposition; the so-called "memory effect"; and the anion exchange capacity (AEC), usually larger for LDH than for cationic clays. [17,24]

1.3.1 - Catalysis

LDH are relatively easy to synthesize, thus they are inexpensive, versatile and potential recyclable source of a variety of catalyst supports, catalyst precursors or actual catalysts. LDH have an important role as catalysts in natural gas conversion and environmental catalysis.[27] Also, they have been explored as support for different catalysts, including enzymes.[28-30] The potential role of LDH for important organic reactions has been explored: Corma and co-authors (1992)[31] studied catalyst for the synthesis of chalcones of pharmaceutical interest through the Claisen-Schmidt condensation between benzaldehyde and acetophenone. They found that a Mg/Al (3:1) mixed oxide with water content of 35 wt.% was the optimized solid- base catalyst, and could be used in the synthesis of several chalcones with anti-inflammatory, antineoplasic, and diuretic activities.

1.3.2 - Ion exchange and adsorption

Other important field for application of LDH is the removal of negatively charged species which may be considered as contaminant depending on the environment and

concentration. The removal may happen by two main mechanisms: surface adsorption and interlayer anion-exchange.[32] The remarkable uptake levels of anionic species can be associated with their large surface area and high anion-exchange capacities (AEC) and flexible interlayer space, which is accessible to polar molecular species as well as anions, and can accommodate very diverse materials such as contaminants from soils, sediments and water.[33] Another interesting mechanism for anions removal is the elegant "memory effect". Over the thermal treatment, organic contaminants, CO_2 and water are eliminated, thus negative species could be removed or adsorbed by LDH, including inorganic anions and organic species.[34]

1.3.3   - Pharmaceutics

LDH also have gained importance in the pharmaceutics field. LDH is not only used as antacid and antipepsin agents[35] but also as important delivery matrices of strategic drugs. The great biocompatibility, the variable chemical composition, the ability to intercalate anionic drugs, and LDH alkaline character are desirable characteristics for delivery of drugs to different parts of the human body. Sun and co-authors (2017)[36] used LDH as drug delivery system for sustained release of brimonidine, for treatment of several glaucoma. LDH was effectively in delivery the drug which relief of intraocular pressure. Liang and co-authors (2014)[37] have shown great potential of LDH in bioimaging, targeted drug delivery and cancer therapies. In similar way, O'Hare's group has intercalated a series of different pharmaceutic active compounds, including ibuprofen, naproxen and 4-biphenylacetic acid. The results showed that the intercalation of pharmaceutically active compounds that form stable anions is a feasible approach for the storage and subsequent controlled release of bioactive agents.[38,39]

The application of LDH in biochemistry is attracting attention. Vitamins,[40] macromolecules (DNA, ATP and nucleosides) were intercalated in LDH and were protected from degradation and were delivered to specific targets.[41] In this way, LDH can act as a new type of inorganic carrier that is completely different from existing non-viral vectors in terms of chemical bonding and structure. [27]

1.3.4   - Photochemistry

The importance and application of LDH can be expanded to photochemistry, where LDH can provide a novel environment for photochemical reactions of guest molecules.[42] Zhu and co-authors (2017),[43] developed a novel and efficient photocatalyst composed of Zn/Ti-LDH and C60 molecules. The experiments have shown higher photocatalytic activity for this nanocomposite. Usually used in the textile industry, the

organic dyes are highly toxic major waste products causing severe harmful environmental pollution. Several studies have shown that LDH as active photo-catalysts, with good results about the degradation of these pollutants.[44,45]

1.3.5 - Eletrochemistry

Inorganic materials such as zeolites, clays or microporous solids are attractive to be used as modified electrodes since they have much better stability, tolerance to high temperatures and oxidizing conditions, and chemical inertness. Luo and co-authors (2017)[46] performed electrochemical measurements $NiCo_2S_4$/Ni–Co LDH nanocomposites by cyclic voltammetry and galvanostatic charge–discharge techniques. This electrode achieved a capacity of 1765 F g^{-1} at 1 A g^{-1} and a capacity of 940 F g^{-1} at 10 A g^{-1}. Layered nickel hydroxide can be used as an electrode for alkaline secondary cells.[27] For example, Chen and co-authors (1998)[47] reported the electrochemical performance [Ni-Al]-LDH with appropriate additives in Ni-metal hydride batteries. They found that the addition of Mg^{2+} increases the unit cell parameters and the charge and discharge potentials, and decreases the electrochemical polarization.

1.3.6 - Additives in functional polymer materials

LDH has been used with polymers to improve some properties from polymers, for example, mechanical resistance, flame retardance, thermal stability, among others. Liu and co-authors (2008)[48], considerable increased the thermal stability of poly(vinyl chloride)- PVC by the use of exfoliated LDH and the authors noticed that thermal stability time increased with LDH content. Similar results were obtained by Manzi-Nshuti and co-authors (2009), who used [Zn-Al]-LDH as modifier of polyethylene (PE).[49] Also, the ability of nanocomposite (polymer + LDH) incorporate molecules was evaluated. The nanocomposite was able to incorporate more diclofenac than control material.[50]

1.3.7 - Agriculture

Agroproducts, such as fertilizers, pesticides, herbicides are frequently applied at higher doses than needed to crop growth. Regarding the use of fertilizers – especially of N and P – the amounts used of this agricultural inputs are increasing due to the constant need for high agricultural production. However, the real efficiency of fertilizers are low due to fixation in the soil (in the case of P) or volatilization (in case of N) of the required elements.[51] Therefore, LDH have been applied as inorganic matrix to provide this nutrients in an efficient and sustainable way.

LDH with nitrate are simply prepared as synthesis intermediated. Berber and co-authors (2014)[52] synthesized and characterized a $MgAl$-NO_3-LDH. This material was

used as source of sustainable-release of NO_3^- to soil. Nitrate release was monitored at different media with solutions that simulate soil composition, one simulating an acid soil solution and other a basic one. The results for the different pH and temperature conditions encourage the use of these materials as sources for slow release of NO_3^- in soil. In a similar way, LDH are able to intercalate and release phosphate, but this subjected has not been deep explored so far. Despite the great knowledge about LDH structure, the interactions that LDH isostructures – that formed by M^{2+} with different ionic radius- has with phosphorus anion has not been completely described and understood. There is lack in the knowledge related to physico-chemical understanding of this interaction and the consequences to release process of this anion to dynamic systems.

2 - Goals and Overview

The main goal of this thesis was to explore LDH, formed by cations with different ionic radius, as inorganic matrixes for phosphate adsorption, with the main purpose of obtaining materials for a multifunctional phosphate release and understand the mechanisms involved in both process.

Specific goals:

- To understand the physico-chemical interactions between LDH and PO_4^{3-} ions;
- To identify and understand the formation of other phases from LDH-phosphate contact interaction;
- To evaluate the LDH capacity for phosphate exchange and the influence of the ionic radius of M^{2+} on the desorption process;
- To evaluate the phosphate release from LDH in dynamic systems.

Summary of each chapter

The main idea of this thesis was to investigate the role played by that the cation (M^{2+}) on the sorption capacity and stability of LDH when contacting phosphate ions considering the different ionic radius of M^{2+} on LDH structure.

Initially we synthetized the most common LDH, the hydrotalcite-like ([Mg-Al]-LDH). The hydrotalcite-like has open structure due to the ionic radius of Mg^{2+} (1.73Å). We aimed to understand if there is phosphate interaction and if so, how it occurs in physico-chemical terms. Therefore, a study of adsorption process of high concentrations of phosphate, by the reconstruction method (or memory effect) was performance and the main results of this part are present in Chapter I.

After that, we proposed to study the phosphate interaction with LDH when the M^{2+} has larger ionic radius, thus a LDH with closer structure. We compared the phosphate adsorption by ion exchange of [Zn-Al]-LDH and [Mg-Al]-LDH. The main results of this part are presented in Chapter II.

With the same purpose of Chapter II, the Chapter III describes the phosphate adsorption by [Zn-Al]-LDH, with Zn^{2+} ionic radius of 2.01 Å, through the structural reconstruction method. These materials were investigated as phosphate release sources and mechanical reinforcement for dental resins.

The Chapter IV was guided by the following question: "the release tendency is confirmed with increase on ionic radius of M^{2+} ?" To answer this question, LDH composed of [Ca-Al]-LDH (Ca^{2+} radius: 2.31 Å) was synthetized and exposed to phosphate

by the two main routes, the ion exchange and structural reconstruction. To evaluate the release tendency, these materials were applied in a dynamic system, as phosphate source for important nitrifying bacteria.

Finally, we exposed the hydrotalcite-like with high phosphate content (obtained by reconstruction method) to dynamic system as phosphate source. The material was used as phosphate nanofertilizer for wheat crops. The main results are exposed at Chapter V.

Chapter VI presents the main conclusions of this work.

3 - Chapter I: Do LDH with open structure interact with phosphate? How does it occur?

The content of this chapter is an adaptation of the article entitled **"Physico-chemical assessment of [Mg-Al-PO$_4$]-LDHs obtained by structural reconstruction in high concentration of phosphate"** by Marcela P. Bernardo, Francys K.V. Moreira, Luiz A. Colnago and Caue Ribeiro published for Colloids and Surfaces A: physicochemical and engineering aspects..

Contents lists available at ScienceDirect

Colloids and Surfaces A: Physicochemical and Engineering Aspects

journal homepage: www.elsevier.com/locate/colsurfa

Physico-chemical assessment of [Mg-Al-PO$_4$]-LDHs obtained by structural reconstruction in high concentration of phosphate

CrossMark

Marcela P. Bernardo [a,b,*], Francys K.V. Moreira [b], Luiz A. Colnago [b], Caue Ribeiro [a,b]

3.1   - Introduction

Phosphorus (P) is a vital element for all living organisms, in which it makes up DNA, RNA, phospholipids, and many other biomolecules involved in metabolic reactions, and storage and transport of energy. Phosphorus is also a crucial element in agriculture since phosphate (PO_4^{3-}), its naturally occurring form, is one of the three main nutrients of fertilizers. With growing world population and consequent need to increase food production, the natural reserves of phosphate are deteriorating progressively, and the cost of these mineral will be rising in the future which indubitably could provoke a strong impact on agriculture.[53,54] Developing technologies to optimize the use of phosphate in plantations has been considered to be urgent. In this context, controlled-release fertilizers have emerged as powerful tools to improve management of nutrients in agriculture, thereby reducing environmental threats while maintaining high crop yields.[55]

Layered double hydroxides (LDH) have gained considerable importance in agriculture and environmental science due to their large anionic exchange capacity and affinity to phosphate and other multivalent anions.[56] LDH are also known as anionic clays and have the general formula $[M^{2+}_{1-x}M^{3+}_x(OH)_2]^{x+}[A^{n-}]_{x/n}\cdot yH_2O$, where M^{2+} and M^{3+} are di- and trivalent metallic cations, respectively, A^{n-} is a charge-balancing anion, and x is the molar ratio $M^{3+}/(M^{3+} + M^{2+})$ ranging from 0.1 to 0.5.[57] The LDH crystalline structure consists of positively charged brucite ($Mg(OH)_2$)-like lamellas in which trivalent cations replace isomorphically divalent cations at the octahedral sites.[18] The net positive charge on the LDH lamellas is then counter-balanced by A^{n-} species in the interlamellar domains.[58]

Thermal treatment provides important physicochemical properties to LDH[59]: (i) a "memory effect" of the hydroxide lattice, which allows different anionic species to be incorporated into the LDH interlamellar space (ii) a larger surface area, which increases adsorption of anions and (iii) elimination of the interlayer carbonate (CO_3^{2-}), which strongly hinders anion exchange processes in LDH.[57,60]

Currently, the increasing interest on LDH arise mainly from their versatile intrinsic properties in terms of chemical composition both of layer and interlayer domains, their high and tunable charge density, and anion exchange capacity.[61] Several reports have shown the potential of LDH for anion exchange technologies, including for example, fluoride,[62] selenite,[63] arsenate[64] and perchlorate.[65] Studies on adsorption of dilute concentrations of phosphate in LDH have also been reported in literature,[32,66,67] however the physico-chemical changes in LDH when they are exposed to high concentrations of phosphate have not been investigated yet.

In the present study, we demonstrate the potential of hydrotalcite-like LDH as inorganic host matrixes for phosphate aiming at slow release fertilizer applications. We have explored the so-called "memory effect" (or reconstruction method) to incorporate high loadings of phosphate into the 2D LDH architecture. The influence of the phosphate concentration and the Mg^{2+}/Al^{3+} ratio on the phosphate uptake process was examined. The reconstructed [Mg-Al-PO$_4$] LDH were characterized by adsorption experiments, XRD, NMR, and other techniques. The phosphate release from the LDH was also investigated.

3.2 - Experimental

3.2.1 - Materials

Magnesium chloride hexahydrate, aluminum chloride hexahydrate, sodium hydroxide and monobasic potassium phosphate were purchased from Synth, Brazil. Commercial hydrotalcite ([Mg-Al]c), $CH_{16}Al_2Mg_6O_{19}.4H_2O$, was purchased from Sigma Aldrich. All reagents were used as received. Decarbonated MiliQ H_2O (ρ = 18.2 MΩ cm) obtained by a Milli-Q system (Barnstead Nanopure Diamond, Thermo Fisher Scientific Inc., Dubuque, IA, USA) was used exclusively in all experimental procedures.

3.2.2 - Synthesis of [Mg-Al$_x$-Cl] LDH

The hydrotalcite-like [Mg-Al$_x$-Cl] LDH with Al^{3+} molar fractions (x) of 0.25 ([Mg-Al$_{0.25}$-Cl] LDH), 0.3 ([Mg-Al$_{0.3}$-Cl] LDH) and 0.4 ([Mg-Al$_{0.4}$-Cl] LDH) were synthesized by the co-precipitation at high supersaturation method.[14] The syntheses were carried out in an all-glass reactor (capacity of 300 mL) which was attached to a water circulating system in order to control accurately the temperature at 75 ºC ($\pm$0.5). In a typical reaction, a mixed salt chloride solution (0.5 mol L^{-1}) containing Mg^{2+} and Al^{3+} cations was gradually injected at the rate of 0.5 mL min^{-1} into the reactor containing a vigorously agitated NaOH solution (1.0 mol L^{-1}). Once completed the injection, the stirring was prolonged for 1 hour to age the precipitate in the mother liquid. Subsequently, the mixture was centrifuged at 11.200 g for 10 min to remove the excess NaCl. The precipitate was then purified by three washing-centrifugation cycles using 1:1 water-ethanol solution, and finally resuspended in water for storage in a freezer and lyophilized under a vacuum of 1.33×10^{-4} bar (Supermodulyo Freeze Dryer, Thermo Fisher Scientific Inc., Kansas City, MO, USA) to yield white powders.

3.2.3 - Structural reconstruction of [Mg-Al$_x$]-LDH in high concentrations of PO$_4{}^{3-}$

LDH samples were loaded with PO$_4{}^{3-}$ anions by using the so-called reconstruction method.[68] The experimental conditions required to form crystalline LDH products were previously set by testing the structural reconstruction of calcined LDH

samples in pure water at temperatures of 25 °C and 75 °C, and mixing times of 4 h and 24 h (Appendix A- FIGURE A1). Samples were designated according with the step of the reconstruction method, that is: calcined (C), and reconstructed (R), and no designation corresponded to the untreated sample ([Mg-Al]c, C-[Mg-Al]c, and R-[Mg-Al]c correspond to the original, calcinated, and reconstructed [Mg-Al]c, respectively, as an example).

First, LDH samples ([Mg-Al]c or [Mg-Al $_x$-Cl]-LDH) were thermally treated at 550 ºC for 2 h in a muffle using a programmed heating rate of 30 °C min^{-1}. Next, 500 mg of the calcined product was added to 250 mL of KH_2PO_4 solution previously equilibrated at 75 °C and pH adjusted to 7 using 0.1 M NaOH. The mixture was continuously agitated for 24 h and then centrifuged at 11.200g for 10 min. The supernatant was used to quantify the concentration of PO_4^{3-} at equilibrium (C_e), whereas the pellet was lyophilized for solid-state characterizations. The incorporation of PO_4^{3-} anions was studied under conditions of molar saturation by varying the PO_4^{3-} concentration from 6.6 mM (1:1 Al^{3+}:PO_4^{3-} molar ratio) to 99.3 mM (1:15 Al^{3+}:PO_4^{3-} molar ratio). For all conditions, the final pH of the suspension was found to be approximately 12. Considering the pKa^{III} of the phosphoric acid (pKa^{III} = 12.67) the predominant anion in suspension is PO_4^{3-}, but it may also be possible that other dissociated forms of phosphoric acid ($H_2PO_4^-$ and HPO_4^{2-}) occurred in the medium at some extent.

The kinetics of PO_4^{3-} desorption was studied at 35 °C using two NaOH solutions with concentrations of 0.01 M (pH 12) and 0.005 M (pH 7.5) as releasing mediums. The experiments were conducted on LDH samples treated with 16.6 mM KH_2PO_4 solution. Briefly, 50 mg of the PO_4^{3-}-loaded LDH were immersed into 150 mL of releasing medium and continuously stirred for 60 h. Aliquot parts were taken at different intervals of time and centrifuged at 11.200g for 10 min to determine the concentration of phosphorus in the supernatant. The precipitate was also characterized.

The concentration of phosphorus was determined according to a procedure reported elsewhere:[69,70] 5 mL of supernatant was mixed with 2 mL of ascorbic acid solution (0.4 M), 0.2 mL of citric acid solution (0.03 M), and 2 mL of a reactant consisting of sulfuric acid solution (4.7 M), 5.5 mL ammonium molybdate (0.08 M), and 0.6 mL of antimony and potassium tartrate (0.05 M). This mixture was then allowed to react for 15 minutes in a water bath at 50 °C to form a phosphoantimonylmolybdenum blue complex, which had its concentration determined by UV-Vis spectrophotometry on a Lambda 25 UV-Vis spectrophotometer (Perkin Elmer) operating at selected wavelength of 880 nm. All quantifications were performed in duplicate.

3.2.4   - Characterizations

Powder X-ray diffraction (PXRD) measurements were conducted on a Shimadzu XRD 6000 diffractometer using Ni-filtered Cu K_α radiation (λ = 1.5405 Å). PXRD patterns were taken over the 2θ range of 5° – 70° with a scan speed of 2° min^{-1}. Interlamellar spaces were calculated using the Brag's law. Fourier Transform Infrared (FT-IR) analyses were performed on a Bucker spectrometer using spectral resolution of 2 cm^{-1}. Specific surface area measurements were done by isothermal nitrogen adsorption through the BET (Brunauer–Emmett–Teller) method on ASAP 2020 equipment (Micrometrics). Scanning electron microscopy (SEM) was conducted on a JEOL microscope running at 15 kV. ^{27}Al and ^{31}P MAS NMR experiments were carried out on 9.4 T Avance III HD spectrometer (Bruker) operating at a frequency of 104.215 MHz for ^{27}Al and 161.904 MHz for ^{31}P, respectively. The ^{31}P spectra were acquired using a 90° pulse (2.5 μs), proton decoupled, 25 ms of acquisition time, 10 s of recycle delay and 1000 scans. The ^{27}Al spectra were acquired using a 30° pulse (1.5 μs), without proton decoupling, 16 ms of acquisition time, 1s of recycle delay and 500 scans. The samples for ^{31}P and ^{27}Al analyses were packed in a 5 mm cylindrical zirconium rotor and were spun at the magic angle sample spinning (10 kHz).

3.3. -Results and discussion

3.3.1   - Reconstruction of $_x$[Mg-Al] LDH

The occurrence of the so-called "memory effect" in the [Mg-Al$_x$]-LDH was examined by a series of PXRD and FTIR measurements. The overall trend is illustrated by the PXRD patterns of the [Mg-Al]c and [Mg-Al$_{0.25}$-Cl]-LDH samples as given in FIGURE 3.1 (PXRD patterns of [Mg-Al$_{0.3}$-Cl]-LDH and [Mg-Al$_{0.4}$-Cl]-LDH are in Appendix A-FIGURE A2.) The set of diffraction peaks exhibited by untreated [Mg-Al]c corresponded to the rhombohedral crystalline symmetry (Rl3m, JCPDS 54-1030) as expected (FIGURE 3.1A). In addition, the basal spacing of the (003) reflection was calculated to be 0.76 nm, which is in accordance with values typically reported for hydrotalcite.[14,17] Untreated [Mg-Al$_{0.25}$-Cl]-LDH had also a rhombohedral LDH symmetry, and no other phases were observed in its PXRD pattern (FIGURE 3.1D). After calcination at 550 °C, both samples (C-[Mg-Al]c and C- [Mg-Al$_{0.25}$-Cl]-LDH) only exhibited reflections indexed to the cubic periclase phase of MgO (Fm-3m, JCPDS 45-0946) and AlO (JCPDS 75-0278), meaning that the LDH structure was efficiently collapsed by thermal dehydration. However, it is observed that further immersing into water at 75 °C led to reappearance of the LDH reflections in the PXRD patterns of R-[Mg-Al]c and R- [Mg-Al$_{0.25}$-Cl]-LDH. This confirmed that the as-

synthetized [Mg-Al$_x$]-LDH could regenerate their layered stacking by hydration at low temperature.

The structural reconstruction of the [Mg-Al]-LDH was also supported by FTIR spectroscopy, FIGURES 3.1G-I. It is observed the presence of O-H stretching vibration bands (3600 – 3100 cm^{-1}) of hydroxyl groups in the brucite-like layer for all R-[Mg-Al$_x$]-LDH samples after hydration in opposition to the FTIR spectra with no active bands of the oxide-rich C-[Mg-Al$_{0.25}$]-LDH, C-[Mg-Al$_{0.3}$]-LDH, and C-[Mg-Al$_{0.4}$]-LDH samples. The shoulder at approximately 3000 cm^{-1} ascribed to hydrogen bonding between H$_2$O and interlayer anion further confirmed the reconstruction of the [Mg-Al$_x$] LDH.[17] Additional chemical information was provided by the vibration band at 1360 cm^{-1} assigned to CO$_3^{2-}$ in a D3h planar symmetric environment, thus suggesting that [Mg-Al$_x$]-LDH samples incorporated CO$_3^{2-}$ anions through the reconstruction process. The XRD data and surface area of the [Mg-Al]-LDH have been summarized in TABLE 3.1.
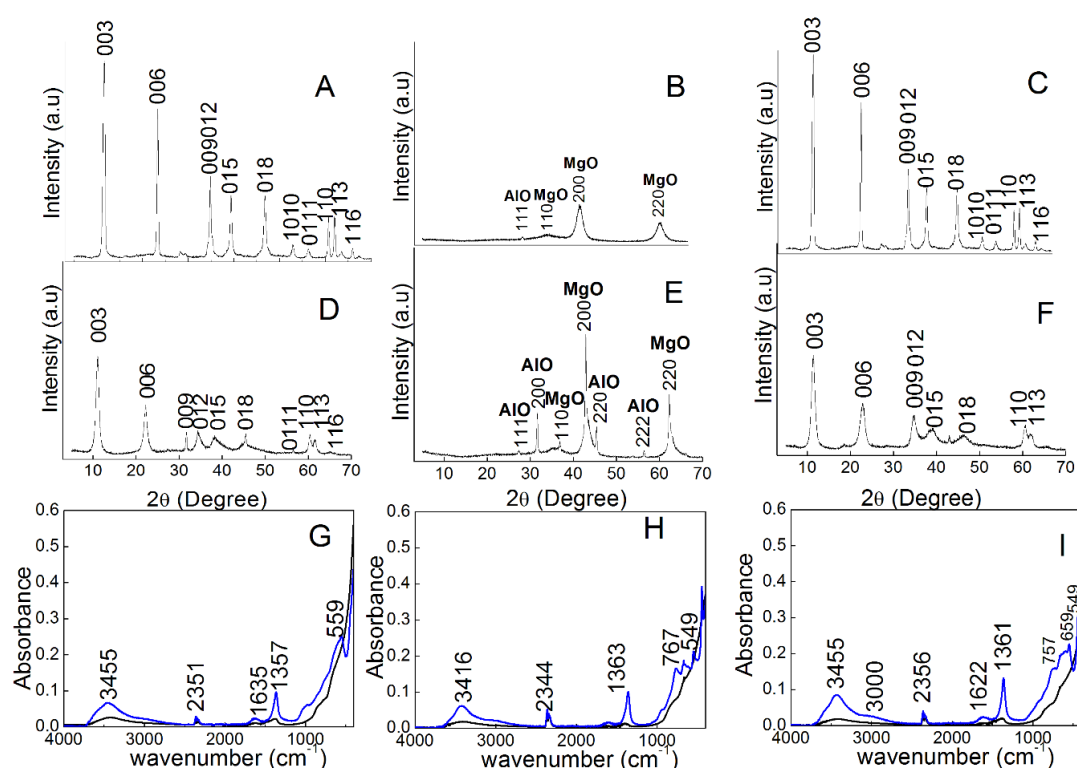
FIGURE 3.1 - PXRD and FTIR measurements denoting the memory effect of LDH. PXRD patterns of (A) [Mg-Al]c; (B) C-[Mg-Al]c; (C) R-[Mg-Al]c; (D) [Mg-Al$_{0.25}$-Cl]; (E) C-[Mg-Al$_{0.25}$-Cl]; (F) R-[Mg-Al$_{0.25}$-Cl]. FTIR spectra of (G) [Mg-Al$_{0.25}$-Cl]; (H) [Mg-Al$_{0.30}$-Cl]; (I) [Mg-Al$_{0.40}$-Cl].

TABLE 3.1 - Structural and textural data of commercial and co-precipitated [Mg-Al]-LDH.

LDH sample	I_{003}/I_{110}	d_{003} (nm)*	d_{006} (nm)*	S_{BET} (m^2 g)
[Mg-Al]c	4.4	0.763	0.381	2.9
[Mg-Al$_{0.25}$]	4.0	0.801	0.400	44.6
[Mg-Al$_{0.30}$]	3.5	0.795	0.397	51.9
[Mg-Al$_{0.40}$]	2.3	0.776	0.392	69.4
C-[Mg-Al]c	-	-	-	11.9
C- [Mg-Al$_{0.25}$]	-	-	-	123.3
C- [Mg-Al$_{0.30}$]	-	-	-	84.6
C- [Mg-Al$_{0.40}$]	-	-	-	110.0
R-[Mg-Al]c	3.8	0.767	0.382	2.6
R-MgAl0-25	3.3	0.777	0.390	48.8
R-MgAl0-30	5.2	0.772	0.385	45.3
R-MgAl0-40	3.9	0.760	0.381	55.2

*Calculated by Bragg's equation. [Mg-Al]c – commercial hydrotalcite; [Mg-Al$_x$] – synthesized LDH with varying molar coefficient (*x*); C – calcined sample; R – reconstructed sample.

3.3.2 - Adsorption of PO$_4^{3-}$ in [Mg-Al]-LDH by structural reconstruction

The commercial [Mg-Al]c sample was used to understand the uptake behavior of PO$_4^{3-}$ anions by LDH through the structural reconstruction route (FIGURE 3.2A and 3.2B). Initially, the PO$_4^{3-}$ concentration was fixed at 6.6 mM (1:1 Al^{3+}:PO$_4^{3-}$ molar ratio), at which the adsorption was expected to occur mainly through a charge counterbalancing mechanism involving the cationic sites of the [Mg-Al]c lattice, and further increased up to 99.3 mM (1:15 Al^{3+}:PO$_4^{3-}$ molar ratio) in order to test the adsorption of high loadings of PO$_4^{3-}$ by reconstructed LDH. FIGURE 3.2A shows that the quantity of PO$_4^{3-}$ anions adsorbed on C-[Mg-Al]c increased as its initial concentration was increased. Additionally, the curve displayed in FIGURE 3.2B can be classified as an *S*-type isotherm, which suggests a "co-operative adsorption" of PO$_4^{3-}$ anions.[71] This is most likely to happen due to a first electrostatic anchoring of the anions on the positively charged sites (Al^{3+} centers) of the LDH lamellas until a monolayer is formed with resulting adsorption of more PO$_4^{3-}$ anions as upper adsorbate layers.

The co-precipitated [Mg-Al $_x$]-LDH were used to examine the influence of the Al^{3+} molar content (stoichiometric coefficient, *x*) on the PO$_4^{3-}$ adsorption process. The adsorption isotherms were collected in the PO$_4^{3-}$ concentration range of 6.6 – 33.1 mM as shown in Figure 3.2C. The isotherms suggest that the adsorption process follows the charge distribution (CD) model at concentrations up to 16.6 mM.[74] This indicates that the positive charges (Al^{3+} sites) of the LDH lamellas are counter-balanced by the PO$_4^{3-}$ anions, thus the

layered stacking is regenerated and the PO_4^{3-} anions are trapped in between the hydroxide lamellas.[75]   Various studies on adsorption of PO_4^{3-} in LDH by ion exchange routes and involving dilute PO_4^{3-} solutions have been extensively reported in literature, and the PO_4^{3-} adsorption capacities were compared with the data found in the present work. For instance, adsorption capacities of 47.3 mg P/g LDH, 38 mg PO_4^{3-}g LDH, and 54 % have been reported for [Mg-Al]-LDH exhibiting a Mg^{2+}/Al^{3+} ratio of 2-4, respectively.[67,76,77] In contrast, the adsorption capacities found in this work, considering analogous LDH compositions and initial PO_4^{3-} concentrations, were found to be 310 mg P/g LDH, 182 mg PO_4^{3-}/g LDH, and 61 %, respectively. These comparisons undoubtedly indicate that the memory effect plays a significant role in extending the adsorption capacity of [Mg-Al]-LDH. This can be explained by the increase of surface area as a consequence of the unstacking of the LDH lamellas (TABLE 3.1). This possibly resulted in the exposure of a large number of positively charged Al^{3+} sites to interact with PO_4^{3-} anions.

The adsorption of PO_4^{3-} anions in [Mg-Al]-LDH through structural reconstruction was examined using the Langmuir and Freundlich models, which have been extensively used to describe the adsorption process of anionic species.[71] The linear forms of the (1) Langmuir and (2) Freundlich equations are given as follows:

$$C_e/q_e = C_e/b + 1/(K_L b) \tag{1}$$

$$\log q_e = \log K_F + (1/n) \log C_e \tag{2}$$

Where C_e is the ion concentration (mmol L^{-1}) at equilibrium, q_e denotes the ion adsorbed per unit mass of sorbent (mmol g^{-1}), K_F and K_L are constants related to the adsorption capacity, n is the experimental constant related to the adsorption intensity, and b is the maximum adsorption capacity for a monolayer coverage. The parameters concerning the adsorption of PO_4^{3-} anions by the reconstructed [Mg-Al]-LDH are reported in Table 3.2.

It is observed that both models did not fit the adsorption data correctly for [Mg-Al]c-, [Mg-Al$_{0.25}$]-, and [Mg-Al$_{0.30}$]-LDH, with $R^2 < 0.9$. However, the Freundlich model fit well the adsorption data of the [Mg-Al$_{0.40}$]-LDH sample ($R^2 = 0.93$). One possible explanation for this bad fitting is that the PO_4^{3-} adsorption in reconstructed LDH is ruled by more than one rate-determining step when it involves high concentrations of PO_4^{3-}. This is supported by previous reports in which the Langmuir and Freundlich models described very well the uptake of low concentrations of PO_4^{3-} by hydrotalcite-like LDH.[67] The results

presented here indicate that the PO_4^{3-} adsorption is not limited to happen at the external surface of LDH particles, as expected for the memory effect mechanism.
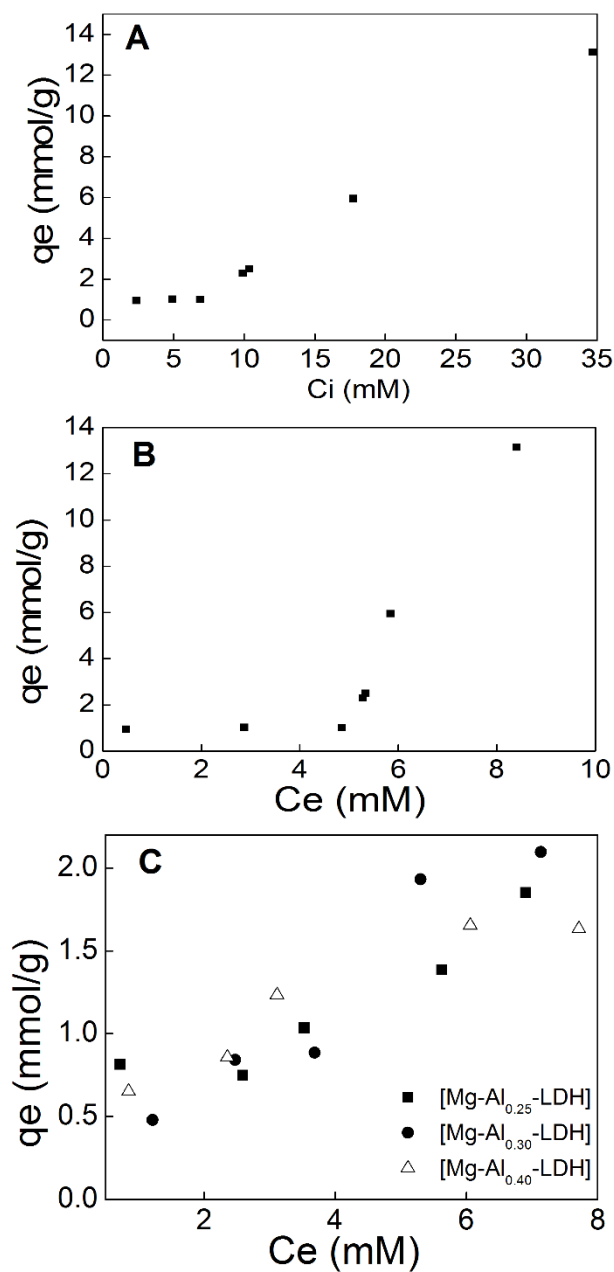
FIGURE 3.2 - (A) Representation of adsorption curve in commercial hydrotalcite ([Mg-Al]c) reconstructed in PO_4^{3-} solution (6.6 mM to 99.3 mM, pH = 7) in fuction of the initial concentration and (B) in function of equilibrium concentration (C) Full adsorption isotherm (75ºC) of PO_4^{3-} anions in 0.25[Mg-Al], 0.30[Mg-Al], 0.40[Mg-Al] reconstructed in PO_4^{3-} solution (6.6 mM to 33.1 mM, pH=7).

TABLE 3.2 - Parameters for PO_4^{3-} adsorption in reconstructed [Mg-Al]-LDH.

Sample	Langmuir			Freundlich		
	R^2	K_l	b	R^2	N	K_f
[Mg-Al]c	0.33	0.18	7.44	0.49	2.72	1.47
[Mg-Al$_{0.25}$]	0.46	0.08	7.74	0.42	3.08	1.25
[Mg-Al$_{0.30}$]	0.31	0.004	7.29	0.86	1.14	0.95
[Mg-Al$_{0.40}$]	0.85	0.076	9.14	0.93	1.99	1.16

*Units: K_l, L mmol^{-1}; b, mmol g^{-1}; K_f, mmol$^{(1 - 1/n)}$ g^{-1} L$^{1/n}$.

Observations by scanning electron microscopy (SEM) further indicated the presence of PO_4^{3-} in the LDH. FIGURE 3.3A revealed a plate-like morphology of the [Mg-Al]c particles, which is consistent with the crystalline LDH structure.[58] Individual [Mg-Al]c plates had irregular edges and diameters of approximately 1 μm. From the SEM micrograph of R-[Mg-Al]c reconstructed in presence of phosphate shown in FIGURE 3.3B, it is possible to observe a resembling hollow architecture of [Mg-Al]c particle agglomerates which appeared smoothly impregned by another phase, thus suggesting that a large amount of PO_4^{3-} anions was incorporated in [Mg-Al]c. The incorporation of other anions, such as PO_4^{3-} and F$^-$, in reconstructed [Mg-Al-CO$_3$]-LDH has also been reported.[72] The morphological changes suggested by FIGURE 3.3B may be attibuted to the growth of PO_4^{3-} rich phases on the R-[Mg-Al]c surface.[73]

PXRD was used to assess the crystalline structure of the [Mg-Al]-LDH reconstructed in presence of PO_4^{3-}. FIGURE 3.4 summarizes the PXRD patterns of R-[Mg-Al]c and R-[Mg-Al$_x$]-LDH samples as a function of the PO_4^{3-} concentration. For 1:1 Al^{3+}:PO_4^{3-} molar ratio, the typical reflections of LDH can be seen in the patterns of all samples, indicating an effective structural reconstruction in presence of PO_4^{3-} anions. Furthermore, the PXRD pattern of R-[Mg-Al]c (FIGURE 3.4 A-1) displayed a broadening and slight displacement of basal reflections ‹003› and ‹006› to lower 2θ values and the appearance of a new peaks at 8.4° and 16.6° of 2θ. These features may be ascribed to multiple states of adsorption of the PO_4^{3-} anions onto the R-[Mg-Al]c structure. The new peak at 8.4° may also indicate an unfolding of the series ‹003› due to intercalation of PO_4^{3-}. The corresponding *d*-value of this new peak was 1.05 nm and a comparison with the original d_{003}-value (TABLE 3.1) shows that the basal spacing of R-[Mg-Al]c increased to 0.57 nm in presence of PO_4^{3-}. This was in good agreement with the size of the anion (0.476 nm),[13] strongly indicating that PO_4^{3-} anions were intercalated into R-[Mg-Al]c.
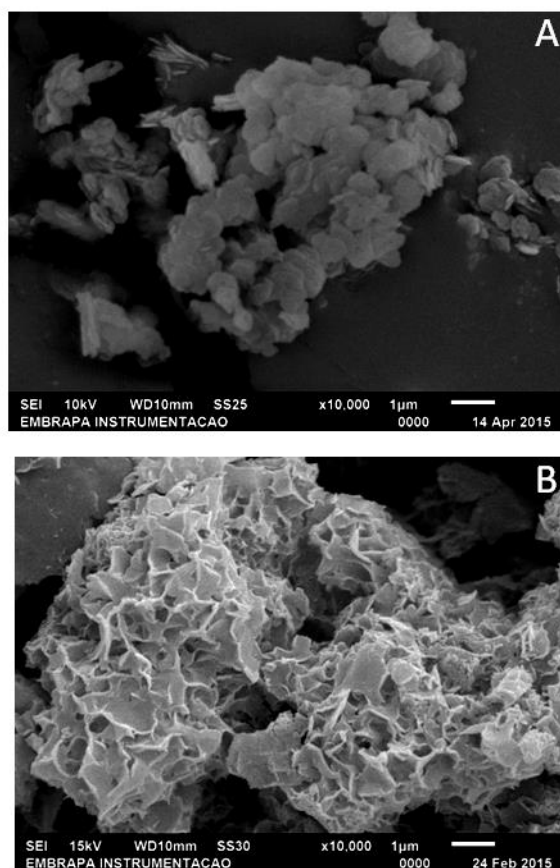
FIGURE 3.3 - Representative scanning electron microscopy (SEM) micrographs of R-[Mg-Al]c (A) reconstructed in pure water and (B) reconstructed in 16.6 mM PO_4^{3-} solution. The scale bar is 1 µm.

The PXRD pattern of R-[Mg-Al]c in FIGURE 3.4A-1 further exhibited peaks belonging to the MgO phase, thus indicating that the presence PO_4^{3-} anions also interfered on the reconstruction of R-[Mg-Al]c at some extent.

In the case of higher $Al^{3+}:PO_4^{3-}$ molar ratios, the PXRD patterns showed reflections of crystalline phases different from hydrotalcite and periclase. For PO_4^{3-} concentrations between 11.6 mM (1:1.75 $Al^{3+}:PO_4^{3-}$ ratio, FIGURE 3.4A-2) and 33.1 mM (1:5 $Al^{3+}:PO_4^{3-}$ ratio, FIGURE 3.4A-3) the new peaks in the PXRD patterns could be indexed to the monoclinic bobierrite phase of $Mg_3(PO_4)_2 \cdot 8H_2O$ (C2/c, JCPDS 33-0877). This suggests that the intercalation of PO_4^{3-} and the precipitation of bobierrite on [Mg-Al]-LDH occurred in parallel at moderately high PO_4^{3-} concentrations. Precipitation of metal phosphates has been generally assumed to be the main adsorption mechanism at high concentrations of PO_4^{3-}.[78] In the present case, the precipitation of magnesium phosphate was found to happen preferentially during reconstruction of [Mg-Al]-LDH at a PO_4^{3-}

concentration of 33.1 mM, as suggested by the more intense reflections of bobierrite in the PXRD pattern of FIGURE 3.4A-3.

FIGURE 3.4A-5 displays the crystalline phases grown on R-[Mg-Al]c from the highest concentration of PO_4^{3-} (99.3 mM, 1:15 Al^{3+}:PO_4^{3-}). Interestingly, the reflections belonging to hydrotalcite and bobierrite vanished and new peaks indexed to the orthorhombic newberyite phase of $MgHPO_4.3H_2O$ (Pbca, JCPDS 97-001-5330) are noticed in the PXRD pattern. The precipitation of magnesium phosphate is therefore able to occur through distinct mechanisms depending on the extent of PO_4^{3-} anions available to react with the calcinated [Mg-Al]-LDH. Overall, newberyite is suggested to be a predominant phase at high concentrations of both Mg^{2+} and PO_4^{3-}.[79] Similar compositional trends were found to occur in the $[Mg-Al_x-PO_4]$-LDH with varying Mg^{2+}/Al^{3+} ratio (FIGURES 3.4 B-D).
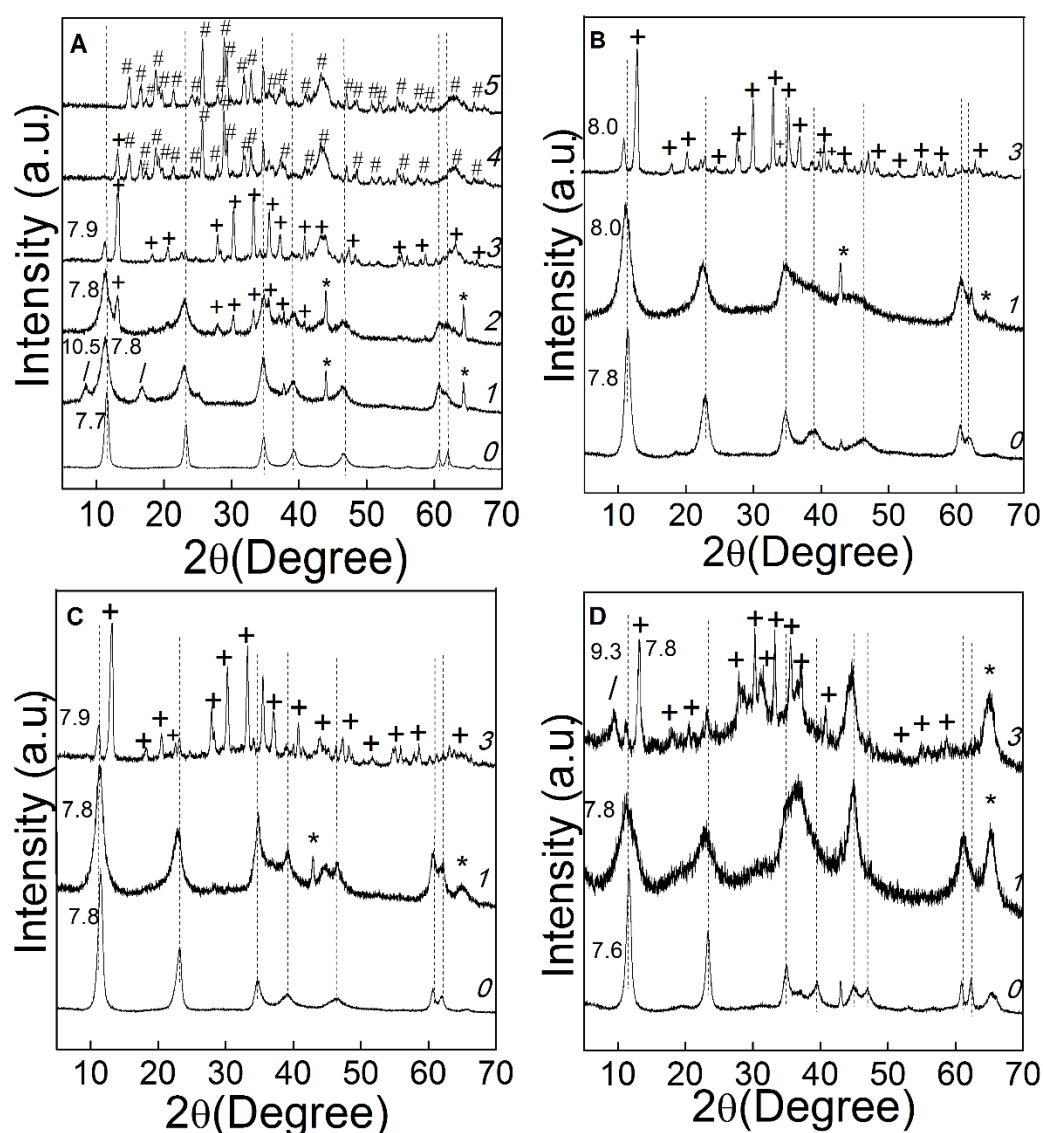
FIGURE 3.4 - Powder X-ray diffraction (PXRD) patterns (A) R-[Mg-Al]c, (B) R[Mg-Al_{0.25}], (C) R[Mg-Al_{0.30}], and (D) R-[Mg-Al_{0.40}] reconstructed in presence of PO_4^{3-} anions. Al^{3+}:PO_4^{3-} molar ratios (PO_4^{3-} concentration): 0 = pure water; 1 = 1:1 (6.6 mM), 2 = 1:1.75

(11.6 mM); 3 = 1:5 (33.1 mM); 4 = 1:10 (66.2mM); 5 = 1:15 (99.3mM). /: multiple states of adsorption of the PO_4^{3-}anions; * :spinel phase, +: bobierrite phase, #: newberyite phase. The d-spacing values are in angstroms.

The chemical environment of the ^{27}Al and ^{31}P atoms in the PO_4^{3-} loaded LDH was assessed by NMR (FIGURE 3.5 and Appendix A-FIGURE A3). All chemical shifts detected in the ^{31}P NMR and ^{27}Al NMR spectra have been summarized in TABLE 3.3. For comparison purposes, the ^{31}P NMR spectrum of pure KH_2PO_4 was also recorded (FIGURE 3.5A-1), which exhibited a single resonance at 4.0 ppm assigned to ^{31}P atoms in a tetrahedral molecular geometry.[80] The ^{31}P NMR spectrum of R-[Mg-Al]c reconstructed in 6.6 mM PO_4^{3-} (1:1 Al^{3+}:PO_4^{3-}) (FIGURE 3.5A-3) displayed an broadened resonance signal as a result of multiple chemical environments of the PO_4^{3-} anions adsorbed on the [Mg-Al]c lamellas, as previously indicated by PXRD. By increasing PO_4^{3-} concentration up to 33.1 mM, this broadened resonance signal disappeared and a new peak at 4.72 ppm assigned to tetrahedral coordination of P atoms in the bobierrite lattice was observed (FIGURE 3.5A-6). [78] Further increase on the PO_4^{3-} concentration led to the presence of a new resonance at -7.59 ppm corresponding to octahedral coordination of P atoms in the newberyite lattice.[81] Accordingly, only this resonance signal was detected in the ^{31}P NMR spectrum of R-[Mg-Al]c obtained in 99.3 mM PO_4^{3-} (FIGURE 3.5A-8). From these results it is confirmed that the PO_4^{3-} concentration is a key parameter governing the uptake of PO_4^{3-} during structural reconstruction of LDH, in particular changing the state of intercalation into a mixture of solid phases having different extents of bobierrite and newberrite precipitates.

FIGURE 3.5B presents a series of ^{27}Al NMR spectra for [Mg-Al]c reconstructed in different PO_4^{3-} solutions to typify the chemical environments of Al atoms in [Mg-Al] LDH undergoing reconstruction with high loadings of PO_4^{3-}. FIGURE 3.5B-2 displays a single resonance at 9.5 ppm for R-[Mg-Al]c reconstructed in pure water, which is assigned to octahedral coordinated Al atoms of [Mg-Al]c lattice, as previously documented.[82] Only for a PO_4^{3-} concentration equal or larger than 26.5 mM, a further broad and weak resonance signal at 66 ppm was observed, which is most likely related to tetrahedral coordinated Al atoms in aluminum oxide phase.[83]

The chemical shift measured by NMR shows excellent agreement with the PXRD characterizations, except for the fact that the NMR technique confirms the presence of hydrotalcite phase in all [Mg-Al-PO4]-LDH. It can be suggested from this result that the magnesium phosphate phases grew onto the LDH lamellas according to a "down-top" mechanism rather than being formed through reaction with MgO.

On the other hand, the NMR results confirms that very high PO_4^{3-} concentration hinder Al^{3+} cations to be incorporated into the LDH lattice during the structural reconstruction process.
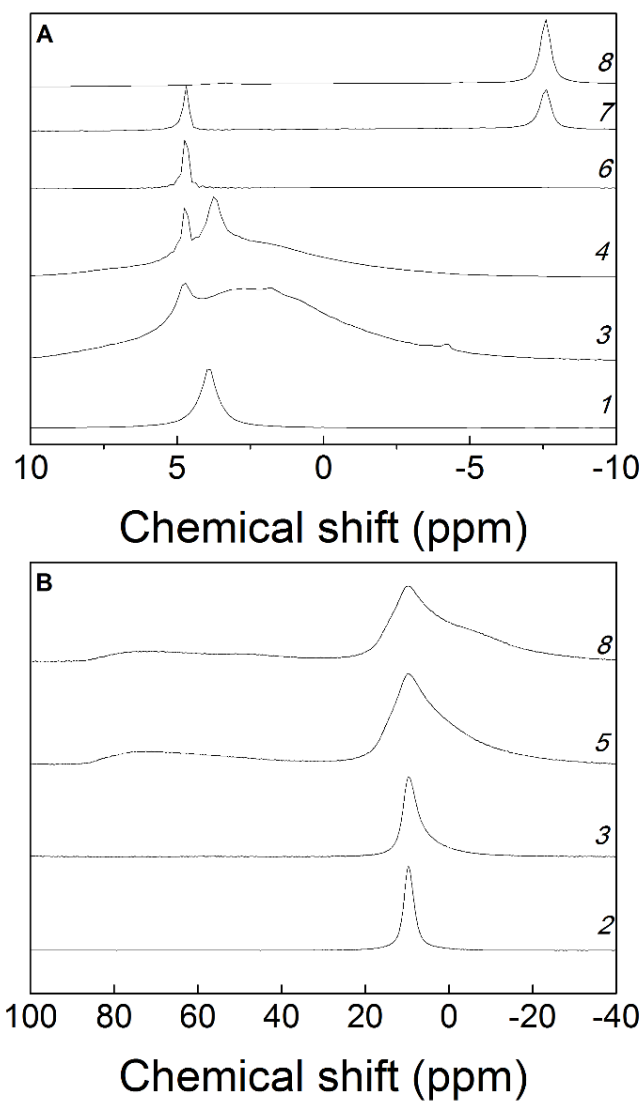
FIGURE 3.5 - (A) ^{31}P NMR spectra for [Mg-Al]c (B) ^{27}Al NMR spectra for [Mg-Al]c. 1 = KH_2PO_4; 2 = [Mg-Al]c; 3 = 1:1 (6.6 mM); 4 = 1:2,5 (16.6 mM); 5 = 1:4 (26.5 mM); 6 = 1:5 (33.1 mM); 7 = 1:7,5 (49.7mM); 8 = 1:15 (99.3 mM).

TABLE 3.3 - Chemical shifts of ^{31}P NMR and ^{27}Al NMR resonances for [Mg-Al]c and [Mg-Al $_x$]-LDH reconstructed in different PO_4^{3-} solutions.

PO_4^{3-} (mM)	R-[Mg-Al]c		R- [Mg-Al$_{0.25}$]		R- [Mg-Al$_{0.3}$]		R- [Mg-Al$_{0.4}$]	
	^{31}P	^{27}Al	^{31}P	^{27}Al	^{31}P	^{27}Al	^{31}P	^{27}Al
0		8.39		9.83		9.79		9.83
6.6	4.72 1.78 -4.13	9.64	3.07	9.27	2.93	9.40	4.66 2.33	9.40 66.60
11.6	4.63 3.91	9.64	4.98 3.09	9.78	4.87 2.93	9.53	4.76	9.48 66.46
16.6	4.72 3.74	9.49	4.78 2.75	9.23	4.87 2.75	9.07	4.75	9.61 66.13
26.5	4.72	9.69 65.75	4.65 2.19	9.32	4.65	9.40 65.03	4.73	10 66.13
33.1	4.72	9.64 65.14	4.65	9.39	4.65	9.07 65.80	4.75 1.33 -0.03 -1.89 -2.17	9.61 66.59
49.7	4.68 7.6	9.76 66.07						
66.2	4.71 -7.55	9.61 65.14						
99.3	-7.59	9.69 66.72						

3.3.3 - Kinetics of PO_4^{3-} desorption

The typical characteristic of tropical soils is the high acidity and consequently low fertility.[84,85] The liming process has been employed to correct the pH of these soils, turning them into alkaline soils, and thus improving fertility and agricultural yields.[86] Developing a system able to release phosphorus species in a slow manner was the main goal of this work. Earlier studies have already shown that PO_4^{3-} desorption is ideally achieved in high-pH mediums.[25,34,76,87] FIGURE 3.6 displays the percentage of PO_4^{3-} anions released into alkaline medium (pH 12) and neutral medium (pH 7.5) from R-[Mg-Al]c and R-[Mg-Al$_x$]-LDH formerly reconstructed in 16.6 mM PO_4^{3-} solution. It can be seen that at pH 12, R-[Mg-Al]c released 93.3 % of its PO_4^{3-} loading over 60 h, whereas the R-[Mg-Al$_{0.30}$]- and R-[Mg-Al$_{0.40}$]-LDH released 90.4 % and 98.2 % of PO_4^{3-} loading, respectively, over 60 h. Conversely, a PO_4^{3-} release percentage of 69 % was found for the [Mg-Al$_{0.25}$]-LDH sample. At pH = 7.5, the release of PO_4^{3-} was slightly reduced over time (R-[Mg-Al]c = 56.5%; [Mg-Al$_{0.25}$] $_=$ 49.3%; [Mg-Al$_{0.30}$] = 57.2% and [Mg-Al$_{0.40}$] = 76.4%). This was possibly due to the

negligible concentration of exchangeable anions in the medium at pH 7.5, confirming that the phosphate release is dependent of the pH. Similar trends have been previously reported, for example, a moderately fast desorption of PO_4^{3-} (63 % in 4 h) for a [Mg-Al]-LDH in 0.1 N NaOH. [34] and a PO_4^{3-} release of 80 % for [Mg-Al]-LDH treated with 20 w/v% NaOH solution.[76]

The results suggest that hydroxyl (OH^-) ions interacted with the LDH surface at high pH, thereby replacing the PO_4^{3-} ions.[93] Thus, the PO_4^{3-} release process into an alkaline environment is predominantly a surface ion-exchange reaction.[94] Overall the successful release of PO_4^{3-} from reconstructed [Mg-Al]-LDH demonstrates a promising potential of [Mg-Al]-LDH as recyclable carriers for slow release of phosphorus.
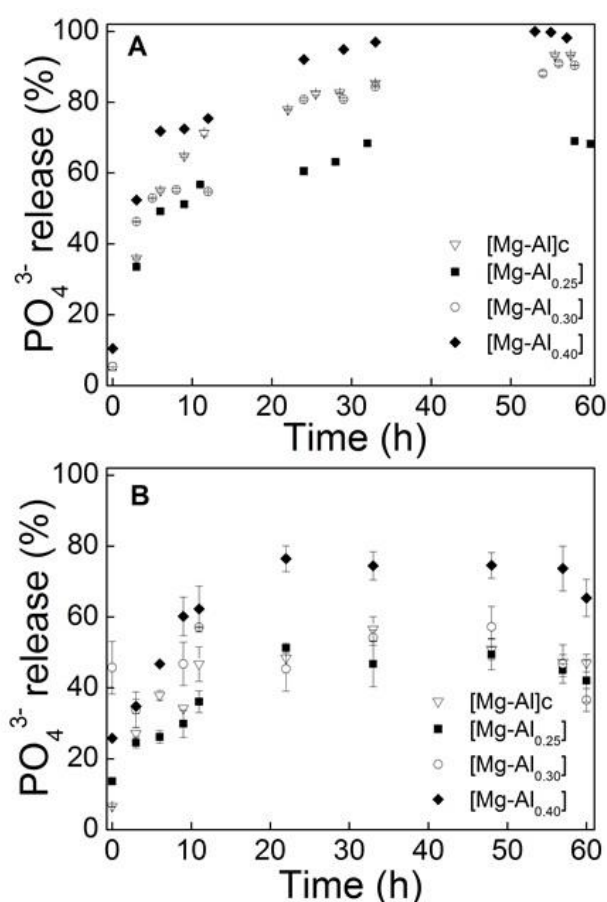
FIGURE 3.6 - (A) Phosphate release profile in 0.01 M NaOH solution (pH = 12) for [Mg-Al]c and [Mg-Al $_x$]-LDH reconstructed in 16.6 mM PO_4^{3-} solution. (B) Phosphate release profile in 0.005 M NaOH solution (pH = 7.5) for [Mg-Al]c and [Mg-Al $_x$]-LDH reconstructed in 16.6 mM PO_4^{3-} solution

In order to gain a better understanding of the PO_4^{3-} release process, kinetics calculations were performed using the (3) zero-order kinetics, (4) first-order kinetics, (5) Higuchi, and (6) Hixson–Crowell classical models, whose mathematical forms are:

$$Q_t - Q_0 = K_0 t \tag{3}$$

$$\ln(M_t)/M_\infty = K t \tag{4}$$

$$R_t = K_H t^{1/2} \tag{5}$$

$$W_0^{1/3} - W_t^{1/3} = K_S t \tag{6}$$

Where Q_0, M_∞, and W_0 are the initial amount (concentration) of PO_4^{3-} in [Mg-Al]c; Q_t, M_t, W_t is the amount (concentration) of PO_4^{3-} remaining in [Mg-Al]c at a time t; K_0 is the constant of proportionality; K is the first order rate constant; R_t is the amount of PO_4^{3-} released at a time t; K_H is the Higuchi dissolution constant; K_S is the constant incorporating the surface-volume relation.[88-92]

The zero order kinetics model is based on the slow release of the substance from a substrate that remains intact. The first-order kinetic model shows that the adsorbate release is proportional to the amount of adsorbate in the matrix. The Higuchi model describes the adsorbate release velocity from the matrix system. The model of Hixson-Crowell recognizes that the particles' regular area is proportional to the cube root of its volume, thereby describing the adsorbate release from systems in which there is a change of surface area and diameter of particles.[91]

The kinetics parameters obtained from the models are summarized in TABLE 3.4. The PO_4^{3-} release data were best fitted with the Higuchi model which describes that (i) initial PO_4^{3-} concentration in [Mg-Al]-LDH is much larger than phosphate solubility; (ii) PO_4^{3-} diffusion takes place only in one dimension (edge effect must be negligible); (iii) PO_4^{3-} ions are much smaller than matrix thickness; (iv) PO_4^{3-} diffusivity is constant; and (v) perfect sink conditions are always attained in the releasing medium.[91] According to the results presented in FIGURE 3.6, the [Mg-Al]c and [Mg-Al$_x$]-LDH exhibited a potential to be used as host matrixes for slow release of phosphate, once more than 90 % of the adsorbed PO_4^{3-} content were found to be released over a period of time of 60 h.

The [Mg-Al]-LDH submitted to the release experiments were scrutinized by PXRD in order to assess their recycling potential. Their PXRD patterns were confronted with those of the analogous samples before and after reconstruction in 16.6 mM PO_4^{3-} solution (FIGURE 3.7). It is clearly observed that after PO_4^{3-} release, the reflections of bobierrite precipitate disappeared, remaining only the characteristic reflections of the LDH phase. This suggests that bobierrite is involved in the PO_4^{3-} release process in highly loaded

[Mg-Al-PO$_4$]-LDH. Accordingly, it is possible to observe peaks of bobierrite in the PXRD pattern of [Mg-Al$_{0.25}$]-LDH because the PO$_4^{3-}$ release percentage for this sample was of only 69 %.

TABLE 3.4 -Kinetics parameters for PO$_4^{3-}$ release at pH 12 and pH 7.5 from reconstructed [Mg-Al] LDH.

Sample	Zero order		First order		Higuchi model		Hixson–Crowell	
	K_0	R^2	K	R^2	K_H	R^2	K_S	R^2
pH 12								
[Mg-Al]c	0.27	0.5799	0.04	0.9258	8.53	0.9218	0.02	0.8277
[Mg-Al$_{0.25}$]	0.13	0.4762	0.01	0.6300	6.64	0.8709	0.01	0.5801
[Mg-Al$_{0.30}$]	0.17	0.6818	0.03	0.9156	5.90	0.9415	0.02	0.8554
[Mg-Al$_{0.40}$]	0.25	0.5612	0.10	0.9831	12.18	0.9275	0.04	0.9086
pH 7.5								
[Mg-Al]c	0.01	0.35	0.01	0.22	1.09	0.62	0.00	0.27
[Mg-Al$_{0.25}$]	0.07	0.50	0.01	0.46	0.80	0.72	0.00	0.48
[Mg-Al$_{0.30}$]	0.03	0.33	0.00	0.34	0.26	0.45	0.00	0.34
[Mg-Al$_{0.40}$]	0.13	0.44	0.11	0.40	0.68	0.68	0.00	0.42
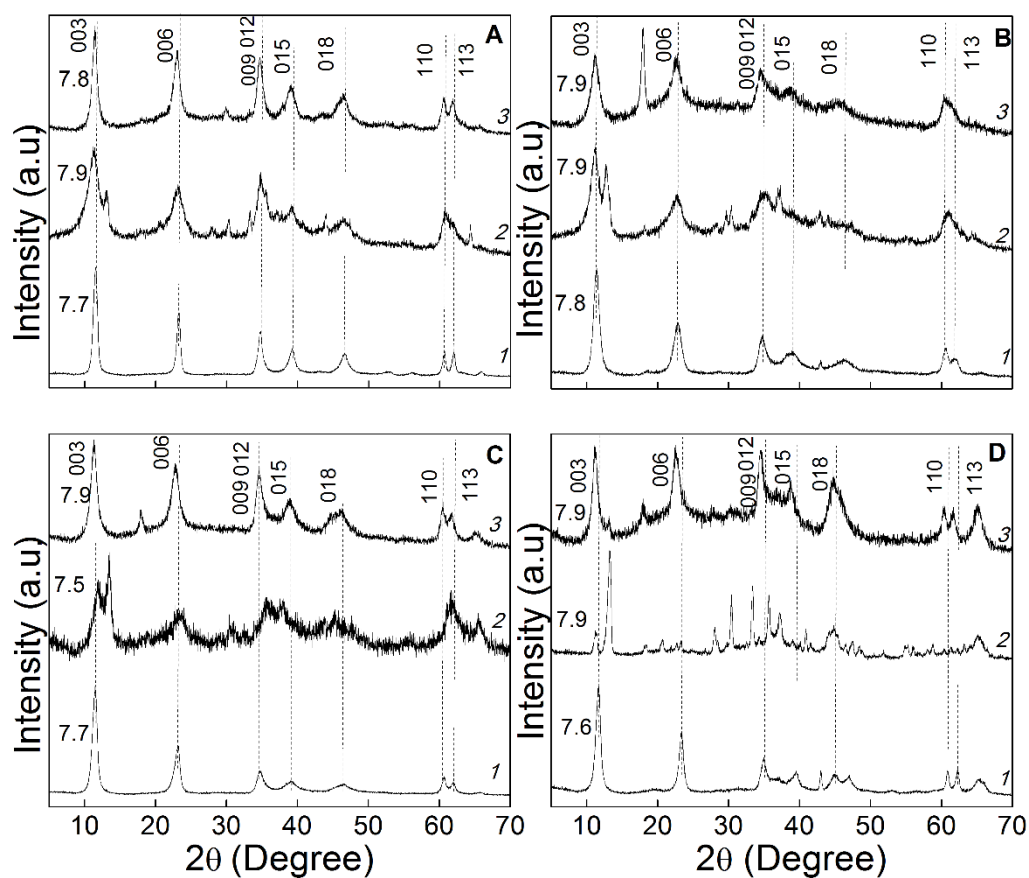
FIGURE 3.7 - PXRD patterns for phosphate release for (A) [Mg-Al]c (B) [Mg-Al$_{0.25}$] (C) [Mg-Al$_{0.30}$] (D) [Mg-Al$_{0.40}$]. 1: reconstructed sample; 2: sample loaded with 16.6 mM; and 3: sample after phosphate desorption. The d-spacing values are in angstroms.

In conclusion, we have investigated the "memory effect" of LDH to create slow release fertilizers highly incorporated with PO_4^{3-} anions. Our results confirmed a significant concentration dependence of PO_4^{3-} adsorption process in reconstructed LDH in which intercalation and precipitation occurs as concurrent steps at variable extents. At high PO_4^{3-} concentrations, Mg- and PO_4^{3-} rich phases (bobierrite and newberyte-like compounds) are precipitated at expense of LDH regeneration. Regardless of the adsorption mechanism, more than 90 % of the PO_4^{3-} amount incorporated into the LDH can be released to alkaline medium. Our results suggest that PO_4^{3-} desorption process is essentially an ion-exchange reaction that occurs at both interlamellar domains and outer surface of LDH structure. The PO_4^{3-}-loaded LDH are found to exhibit recycling properties, indicating the possibility of using these PO_4^{3-} slow release systems in many adsorption-desorption cycles. Ultimately, this research provides a new path to design new slow release fertilizers of strategic nutrients employing LDH as host matrices.

4 - Chapter II: Changing the cation, is there phosphate interaction?

The content of this chapter is an adaptation of the article entitled **"[Mg-Al]-LDH and [Zn-Al]-LDH as Matrices for Removal of High Loadings of Phosphate"** by Marcela Piassi Bernardo and Caue Ribeiro, published for Materials Research.

[Mg-Al]-LDH and [Zn-Al]-LDH as Matrices for Removal of High Loadings of Phosphate

Marcela Piassi Bernardo[a,b] , Caue Ribeiro[a,b]*

[a]Departamento de Química, Universidade Federal de São Carlos, Rodovia Washington Luís, 13565-905, São Carlos, SP, Brasil
[b]Laboratório Nacional de Nanotecnologia Aplicada ao Agronegócio (LNNA), Embrapa Instrumentação, Rua XV de Novembro, 1452, 13560-970, São Carlos, SP, Brasil

4.1   - Introduction

Wastewaters from different economic sectors and from human activities are concerns due to the high phosphate content of these effluents. Swine wastes can achieve phosphate concentrations around 1000 mg.L^{-1},[95] while the wastewater produced by the cochineal extract process to obtain the carminic acid colouring pigment (carmin red E120) has high concentrations of phosphates, about 3500 mg.L^{-1}.[96] In a similar way, other activities generate wastewater with high phosphate concentration, like agriculture, animal breeding and domestic activities.[97-100]

In most of the cases, the effluents are not treated and are simply thrown into rivers where they contribute to eutrophication, which occurs when the concentrations of nutrients in water bodies increase, resulting in intense reproduction of autotrophic organisms, especially algae and cyanobacteria. The increased respiration of autotrophs then leads to environments that are hypoxic or anoxic, threatening the aerobic fauna and flora.[101,102] Thus, the treatment of the wastewaters prior the discharge is of crucial importance.

It is extremely important the development of technologies capable of removing phosphate from effluents with medium to high phosphate concentration content. Biological methods of recovery have been employed since the 1950s, although such techniques typically remove only 10-30% of the phosphate present. Another effective and economic technological option for phosphate removal is the use of adsorbents.[103]

Layered double hydroxides (LDH) are excellent materials for removal of phosphate from contaminated area due to their unique structure, high specific surface area, and low synthesis costs.[104] LDH are a class of two-dimensional nanostructured anionic clays whose crystalline structure can be described as positive layers of brucite ($Mg(OH)_2$), in which trivalent cations replace isomorphically divalent cations at the octahedral sites. The net positive charge of the LDH lamellae is then counterbalanced by A^{n-} species in the interlamellar domains. Water molecules can also occupy the free space in the interlamellar region. [13,14,17,27]

LDH can be represented by the following general formula: $[M^{2+}_{1-x}M^{3+}_{x}(OH)_2]^{x+}.(A^{n-})_{x/n}.mH_2O$, where M^{2+} and M^{3+} are divalent and trivalent cations, respectively; the value of x is equal to the molar ratio $M^{3+}/(M^{2+}+M^{3+})$; A is the interlamellar anion with valence of n^{-}. Variation of M^{2+}, M^{3+}, x, and A^{n-} enables the formation of a broad class of isostructural materials with different physical-chemical properties.[13,14] LDH have

high ion exchange capacity, since the interlamellar regions are flexible in terms of the content of anionic species. This important characteristic provides LDH with excellent potential for use in the removal of contaminants by ion exchange processes.[13]

The adsorption at LDH can occur in, at least, two ways involving superficial adsorption or ion exchange in the interlamellar space. Superficial adsorption involves the adhesion of ionic compounds on the LDH surface, with the formation of molecular or atomic films. The ion exchange process is mainly influenced by the anionic charge balance in the interlamellar space and the charge density of the lamellae.[13] It has been observed that divalent anions (A^{2-}) of LDH can be easily replaced by monovalent anions. [105]

LDH have been employed for the removal of a variety of anions including fluorite,[62] selenium, [63] arsenate, [106] perchlorate, [65] chromium, [107] and phosphate.[66,69] However, the mechanisms of adsorption of phosphate by LDH have received little attention and remain poorly understood. [32] The aim of this work was to compare the effects of magnesium and zinc on LDH adsorption properties of high phosphate concentrations, since both have the same valence but very different ionic sizes. The [Mg-Al]-LDH is the best known and explored type of layered double hydroxide and it was used as reference to phosphate adsorption comparison. On the other hand, [Zn-Al]-LDH has been extensively used, as selenium and fluoride adsorbent.[62,63] These materials may have different adsorption properties, due to the intrinsically associated differences in the structure, since different ionic radius will influence on the size of each adsorption site. In this sense, the [Mg-Al]-LDH and [Zn-Al]-LDH were chosen as inorganic matrices for phosphate adsorption study.

4.2   - Materials and Methods

4.2.1   - Materials

Zinc chloride ($ZnCl_2$), aluminum chloride hexahydrate ($AlCl_3 . 6H_2O$), sodium hydroxide (NaOH), sodium carbonate (Na_2CO_3), and potassium phosphate monobasic (KH_2PO_4) were purchased from Synth (Brazil). Commercial [Mg-Al]-LDH hydrotalcite (Pural) was purchased from Sasol (Germany). All reagents were used as received. Decarbonated deionized water (ρ = 18.2 MΩ cm) obtained from a Milli-Q system (Barnstead Nanopure Diamond, Thermo Fisher Scientific Inc., Dubuque, IA, USA) was used in all the experimental procedures.

4.2.2   - Synthesis of [Zn-Al]-LDH

[Zn-Al]-LDH with $M^{3+}/(M^{2+}+M^{3+})$ molar ratio (*x*) of 0.25 was synthesized by the co-precipitation method, with pH control.[14] The synthesis was carried out in an all-glass reactor (capacity of 300 mL) attached to a water circulating system to accurately

control the temperature at 25.0 ℃ (±0.5 ℃). In a typical reaction, a mixed chloride solution (0.5 mol L^{-1}) containing Zn^{2+} and Al^{3+} cations was gradually injected at a rate of 0.5 mL min^{-1} into the reactor containing sodium hydroxide solution (1.0 mol L^{-1}), under vigorous stirring. At the same time, a solution of Na_2CO_3 (2 mmol L^{-1}) was injected at a rate of 0.025 mL min^{-1} for pH control. Once injection of the solutions was completed, agitation was continued for a 1 hour, to age the precipitate. Subsequently, the mixture was centrifuged at 11,200 g for 10 min to remove the excess NaCl. The precipitate was then purified using three washing-centrifugation cycles with 1:1 water-ethanol solution, and was resuspended in water for storage in a freezer. Finally, the material was lyophilized under a vacuum of 1.33×10^{-4} bar (Supermodulyo Freeze Dryer, Thermo Fisher Scientific Inc., Kansas City, MO, USA), yielding a white powder.

4.2.3   - Phosphate adsorption by ion exchange

The phosphate adsorption capacities of the isomorphic structured LDH ([Mg-Al]-LDH and [Zn-Al]-LDH) were evaluated by ion exchange process using different potassium phosphate solutions. 500 mg of the LDH were added to 250 mL of KH_2PO_4 solution (concentration range from 112.64 mg L^{-1} to 4505.60 mg L^{-1} - this range of values includes the phosphate concentrations found at effluents from different human activities) that had been previously equilibrated at 75 °C, with adjustment of pH to 7.0 using 0.1 M NaOH, to guarantee the well preservation of LDH structure. The mixture was continuously agitated for 24 h and was then centrifuged at 11,200 g for 10 min. After the adsorption process, the LDH was lyophilized prior to solid-state characterizations analyses.

The concentration of phosphorus was determined according to the molybdate blue procedure: 5 mL of supernatant was mixed with 2 mL of ascorbic acid solution (0.4 M), 0.2 mL of citric acid solution (0.03 M), 2 mL of sulfuric acid solution (4.7 M), 5.5 mL of ammonium molybdate (0.08 M), and 0.6 mL of antimony and potassium tartrate (0.05 M). This mixture was then allowed to react for 15 min in a water bath at 50 ℃, forming a phosphoantimonylmolybdenum blue complex. The concentration of the product was determined using a Lambda 25 UV–Vis spectrophotometer (Perkin Elmer) operated at a wavelength of 880 nm.

4.2.4   - Characterizations

X-ray powder diffraction measurements were performed with a Shimadzu XRD 6000 diffractometer, using Ni-filtered CuK$_α$ radiation (λ = 1.5405 Å). The diffractograms were acquired at 2θ of 3-80º, with a scan speed of 2º min^{-1}. The FTIR analyses were performed using a Bruker spectrometer with spectral resolution of 2 cm^{-1}. The

specific surface area measurements were performed by applying the BET (Brunauer-Emmett-Teller) method to nitrogen adsorption isotherm data acquired with an ASAP 2020 instrument (Micrometrics). Scanning electron microscopy (SEM) images were obtained with a JEOL JSM-6701F microscope operated at 15 kV. The thermal properties of the LDH materials were evaluated using a TGA Q500 thermogravimetric analyzer (TA Instruments, New Castle, DE) operated under the following conditions: atmosphere of nitrogen at a flow rate of 60 mL/min; heating rate of 10 °C/min; and temperature range of 25-800 °C.

4.3   - Results and Discussion

4.3.1   - [Mg-Al]-LDH and [Zn-Al]-LDH materials

The X-ray diffractograms of the as-synthesized [Zn-Al]-LDH showed sharp and intense peaks at low values of 2θ, together with clear (110) reflections at higher values of 2θ that were typical of materials such as LDH and could be indexed by JCPDS card 48-1023. This result confirm that the synthesis method proposed was efficient to obtain crystalline [Zn-Al]-LDH material. The commercial [Mg-Al]-LDH sample also displayed the characteristic peaks of hydrotalcite and could be indexed by JCPDS card 14-0191 (FIGURE 4.1). For both materials, the indexed diffractions corresponded to a hexagonal lattice with rhombohedral 3R symmetry.[17,104]
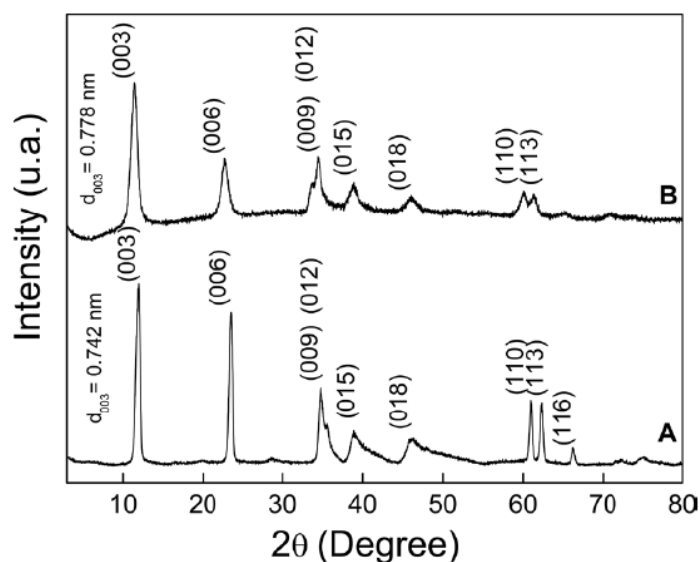
FIGURE 4.1 - XRD diffractograms for (A) commercial [Mg-Al]-LDH and (B) the synthesized [Zn-Al]-LDH.

4.3.2   - Phosphate adsorption by [Mg-Al]-LDH and [Zn-Al]-LDH

The anion exchange capacity properties of [Mg-Al]-LDH and [Zn-Al]-LDH were evaluated by placing the materials in contact with different phosphate concentrations, under vigorous stirring. The X-ray diffractograms of the LDH materials after phosphate

adsorption are shown in FIGURE 4.2. The corresponding amounts of adsorbed phosphate are provided in TABLE 4.1. Also, the adsorption isotherms are represented in Appendix B (FIGURE B1).

TABLE 4.1 - Amounts of phosphate adsorbed by the [Mg-Al]-LDH and [Zn-Al]-LDH.

Initial PO_4^{3-} concentration (mg L^{-1})	[Mg-Al]-LDH (mg $PO_4^{3-}.g^{-1}$ LDH)	[Zn-Al]-LDH (mg $PO_4^{3-}.g^{-1}$ LDH)
112.64	0.47	14.36
225.26	1.39	24.45
450.56	1.38	39.14
901.12	3.91	43.76
1576.96	12.21	54.26
2252.80	17.93	72.69
3604.48	32.62	73.87
4505.60	33.18	116.07

The crystalline structure of [Mg-Al]-LDH was well preserved, even when the material was exposed to higher phosphate concentrations. On (003) diffraction plane no displacements were observed. The highest concentration of adsorbed phosphate was 0.90% (32.62 mg $PO_4^{3-}.g^{-1}$ LDH) when the initial phosphate concentration was 3604.48 mg L^{-1}. Therefore, the adsorbed phosphate probably interacted with hydrotalcite at the external surface. A mechanism of interaction at the external surface involves electrostatic attraction between the negatively charged phosphate species and the surface, which is positively charged due to the presence of protonated hydroxyl groups ($-OH_2^+$). [32]

The crystalline structure of [Zn-Al]-LDH, was clearly modified as the amount of adsorbed phosphate increased. The typical crystalline structure of the material was well maintained up to the phosphate concentration of 1576.96 mg L^{-1}. While for 2252.80 mg L^{-1} PO_4^{3-} and higher concentrations the formation of zinc hydroxide ($Zn(OH)_2$) (JCPDS: 36-1451) was observed, in addition to the typical crystalline structure of [Zn-Al]-LDH. The formation of new phases during phosphate adsorption could be explained by the processes of dissolution and reprecipitation of [Zn-Al]-LDH, with the ion exchange process occurring in two steps, involving LDH dissolution followed by reprecipitation of the new phase.[108] The formation of new phases during the adsorption of phosphate on LDH has also been described in previous studies. [109,110]
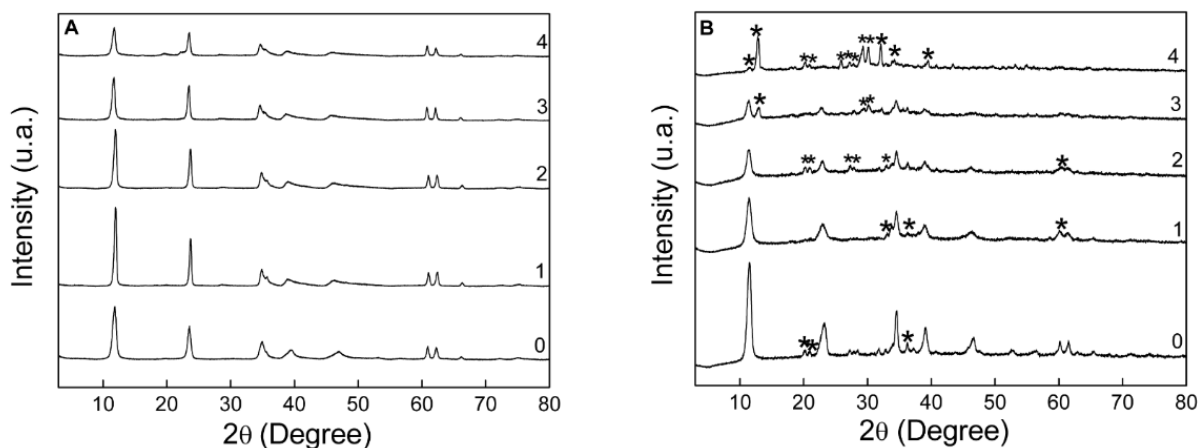
FIGURE 4.2 - X-ray diffractograms of (A) [Mg-Al]-LDH and (B) [Zn-Al]-LDH. (0) Pure water; (1) 112.64 mg L^{-1} PO$_4^{3-}$; (2) 901.12 mg L^{-1} PO$_4^{3-}$; (3) 2252.80 mg L^{-1} PO$_4^{3-}$; (4) 4505.60 mg L^{-1} PO$_4^{3-}$. *: Zinc hydroxide (Zn(OH$_2$)).

Although crystalline phosphate phases were not observed, there was interaction between the phosphate ions at [Zn-Al]-LDH, as revealed by the adsorption of 54.26 mg PO$_4^{3-}$.g^{-1} [Zn-Al]-LDH (TABLE 4.1, FIGURE 4.3B). [111] As in the case of the commercial hydrotalcite, phosphate could interact with [Zn-Al]-LDH on the external surface, but [Zn-Al]-LDH showed greater efficiency in the adsorption of phosphate by ion exchange in the interlamellar space.
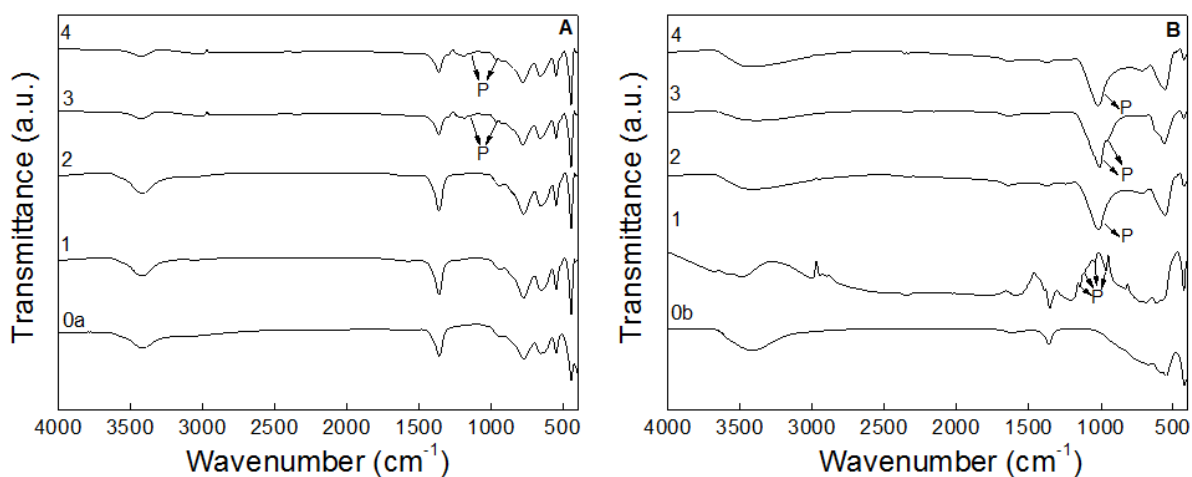
FIGURE 4.3 - FTIR spectra for (A) [Mg-Al]-LDH and (B) [Zn-Al]-LDH. (0a) Commercial [Mg-Al]-LDH; (0b) pristine [Zn-Al]-LDH; (1) 112.64 mg L^{-1} PO$_4^{3-}$; (2) 901.12 mg L^{-1} PO$_4^{3-}$; (3) 2252.80 mg L^{-1} PO$_4^{3-}$; (4) 4505.60 mg L^{-1} PO$_4^{3-}$.

Other materials, with low costs production, have been investigate for phosphorus removal from water. The steel slag is an industrial waste derived from a steel factory, however the maximum phosphate adsorption capacity of this material was

5.3 mg P/g.[112] Mesoporous silica materials has the maximum adsorption capacity around 0.40 mmol/g.[113] These results demonstrated the high potential of LDH materials as inorganic matrices for removal of phosphate by adsorption. [69]

FTIR (FIGURE 4.3) was used to identify the interaction of phosphate with [Mg-Al]-LDH and [Zn-Al]-LDH. An intense band at approximately 3450 cm^{-1} could be attributed to the vibration of water molecules present in the interlayer space, [114] while bands above 1350 cm^{-1} were indicative of the presence of CO_3^{2-}.[115] Vibrations corresponding to metal-oxygen bonds were observed at around 650, 550, and 450 cm^{-1}. [116] A successful phosphate interaction was verified by the presence of new bands at 1145 and 960 cm^{-1}, related to PO_4^{3-} stretching, confirming the interaction of phosphate with the hydrotalcite layers. Similarly, [Zn-Al]-LDH presented new bands at around 1135 and 960 cm^{-1}, suggesting strong interaction of this anion with the [Zn-Al]-LDH matrix, in accordance with the phosphate adsorption capacity of [Zn-Al]-LDH as seen at TABLE 4.1. [117,118]

FIGURE 4.4 shows SEM images of [Mg-Al]-LDH and [Zn-Al]-LDH, before and after the phosphate adsorption process. The [Mg-Al]-LDH material exhibited the typical hydrotalcite structure, composed of quasi-hexagonal layers (FIGURE 4.4A). The typical hexagonal structure was maintained even after the phosphate adsorption (FIGURES 4.4B and 4.4C) in agreement with the XRD results. In contrast, substantial modifications of the [Zn-Al]-LDH structure were observed after phosphate adsorption. FIGURE 4.4D shows the pristine [Zn-Al]-LDH, with an irregular nanostructure and layers without the presence of hexagonal structures. The XRD data (FIGURE 4.2B) showed that when intermediate phosphate concentrations were adsorbed by [Zn-Al]-LDH, two different crystalline phases were produced, one related to [Zn-Al]-LDH and the other to zinc hydroxide. The corresponding SEM image (FIGURE 4.4E) also revealed the presence of these two phases, with predominance of irregular plaques, together with evidence of the deposition of a secondary phase, which was probably zinc hydroxide. When [Zn-Al]-LDH was exposed to a high phosphate concentration (FIGURE 4.4F), the irregular plaques were replaced by elongated rods, with deposition of a secondary phase that was small and highly agglomerated, consistent with zinc hydroxide.[119]
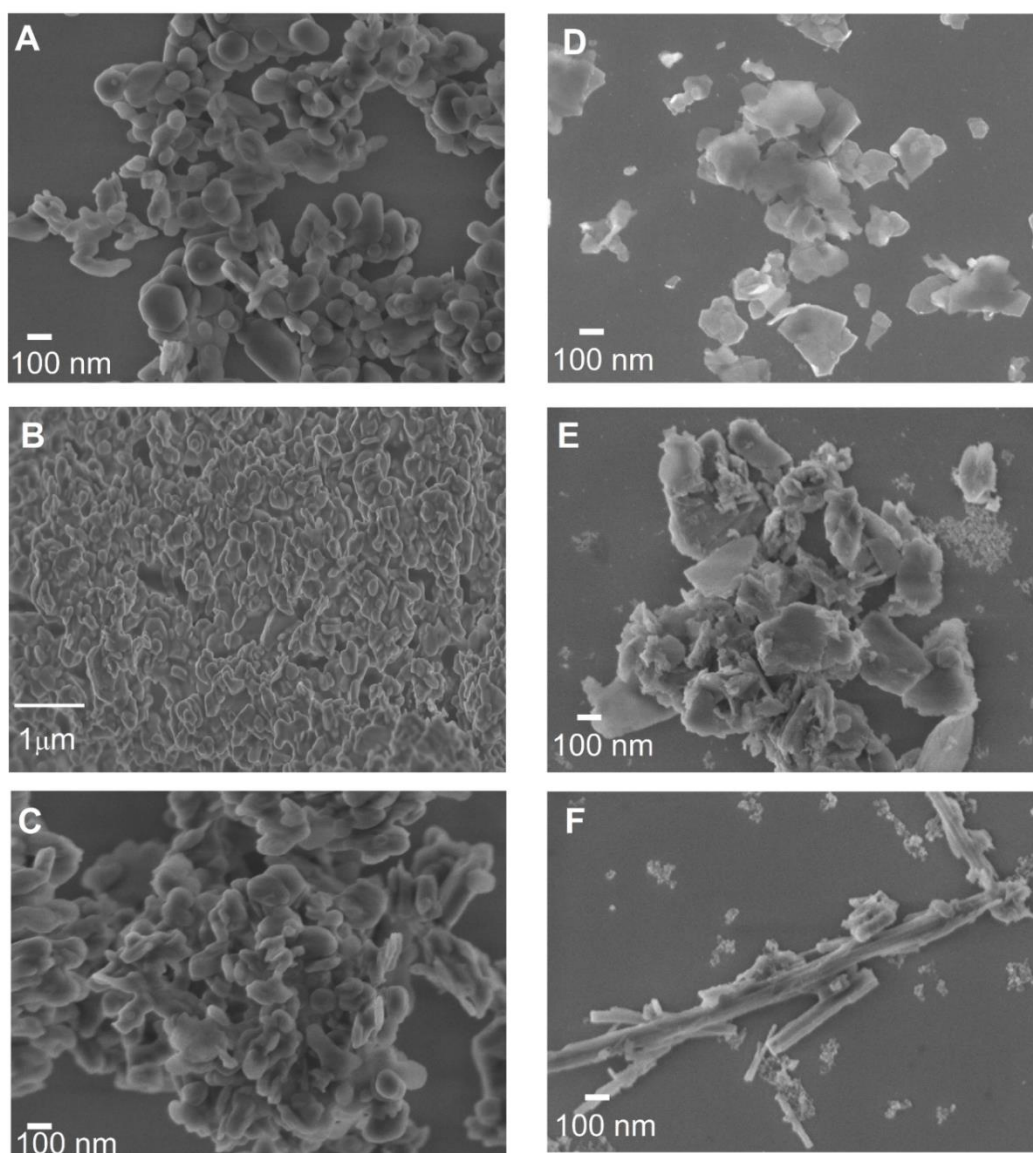
FIGURE 4.4 - SEM micrographs: (A) Commercial [Mg-Al]-LDH; [Mg-Al]-LDH after adsorption of 2252.80 mg L-1 PO43- (B) and 4505.60 mg L-1 (C); as-synthesized [Zn-Al]-LDH (D); [Zn-Al]-LDH after adsorption of 2252.80 mg L-1 PO43- (E) and 4505.60 mg L-1 (F).

The thermogravimetric and differential thermogravimetric analysis of [Mg-Al]-LDH and [Zn-Al]-LDH loaded with phosphate are shown in FIGURE 4.5 and provide further information concerning the compositions of the materials.

The TG/DTG curve for [Mg-Al]-LDH exhibited the same profiles, with sharp peaks regardless of the phosphate concentration (FIGURES 4.5A-4.5C). A small mass loss at around 39 °C could be attributed to desorption of water from the surface. [36] A mass loss of 12% above 200 °C was related to the removal of water adsorbed in the hydrotalcite layers, while a mass loss of 5% at 278 °C was associated with the dihydroxylation of [Mg-Al]-LDH. Finally, a 7% mass loss at 405 °C was due to the loss of CO_3^{2-} as CO_2. [37] The

dihydroxylation temperature for hydrotalcite is generally observed at around 300°C and indicates the thermal stability of the structure, because once dihydroxylation and the loss of the interlayer anion occurs the hydrotalcite structure collapse which leads to the formation of the metal oxide and spinel formation. There were no significant differences in the TGA profiles for the [Mg-Al]-LDH samples with different amounts of adsorbed phosphate. As the presence of phosphate on [Mg-Al]-LDH did not interfered on the thermal degradation profile, the TG/DTG technique corroborates the poor interaction of [Mg-Al]-LDH with phosphate.

However, in the case of [Zn-Al]-LDH, significant differences were observed between the thermogravimetric profiles obtained with increasing phosphate concentration (Figures 4.5 D, 4.5 E and 4.5 F). With the increase of phosphate concentration adsorbed, the temperature of loss related to surface water desorption reduces- from around 140°C to 120°C- as well as the mass loss. When 14.36 mg.L^{-1} of phosphate was adsorbed at [Zn-Al]-LDH the mass loss related to desorption of the surface water was around 9%, while the adsorption of 72.69 and 116.07 mg.L^{-1} of phosphate leads to mass loss of surface water of 5% and 6%, respectively.

This event may be related to the phosphate interaction with the surface of LDH, where phosphate may be interacting with the surface of LDH and competing with water molecules for the bond sites. Therefore, the amount of water interacting with the surface of [Zn-Al]-LDH is reduced. In addition, the bond strength between water and [Zn-Al]-LDH surface is weakened, requiring less energy to be lost, as observed by reduction of the temperature of desorption of surface water. Considering the mass loss due to the loss of structural water, only the sample with 72.69 mg.L^{-1} of phosphate adsorbed had the peak displaced to higher temperatures, therefore this phenomenon may not be related to the phosphate adsorption by [Zn-Al]-LDH.

Regardless the amount of phosphate adsorbed on [Zn-Al]-LDH, all the samples loss the phosphate around 498°C with mass loss around 4%. That means that the same fraction of phosphate is weakly interacting with [Zn-Al]-LDH, but considering the samples with higher phosphate concentration adsorbed (Figures 4.5 E and 4.5 F), a major fraction of the phosphate is forming thermostable phosphate phase.
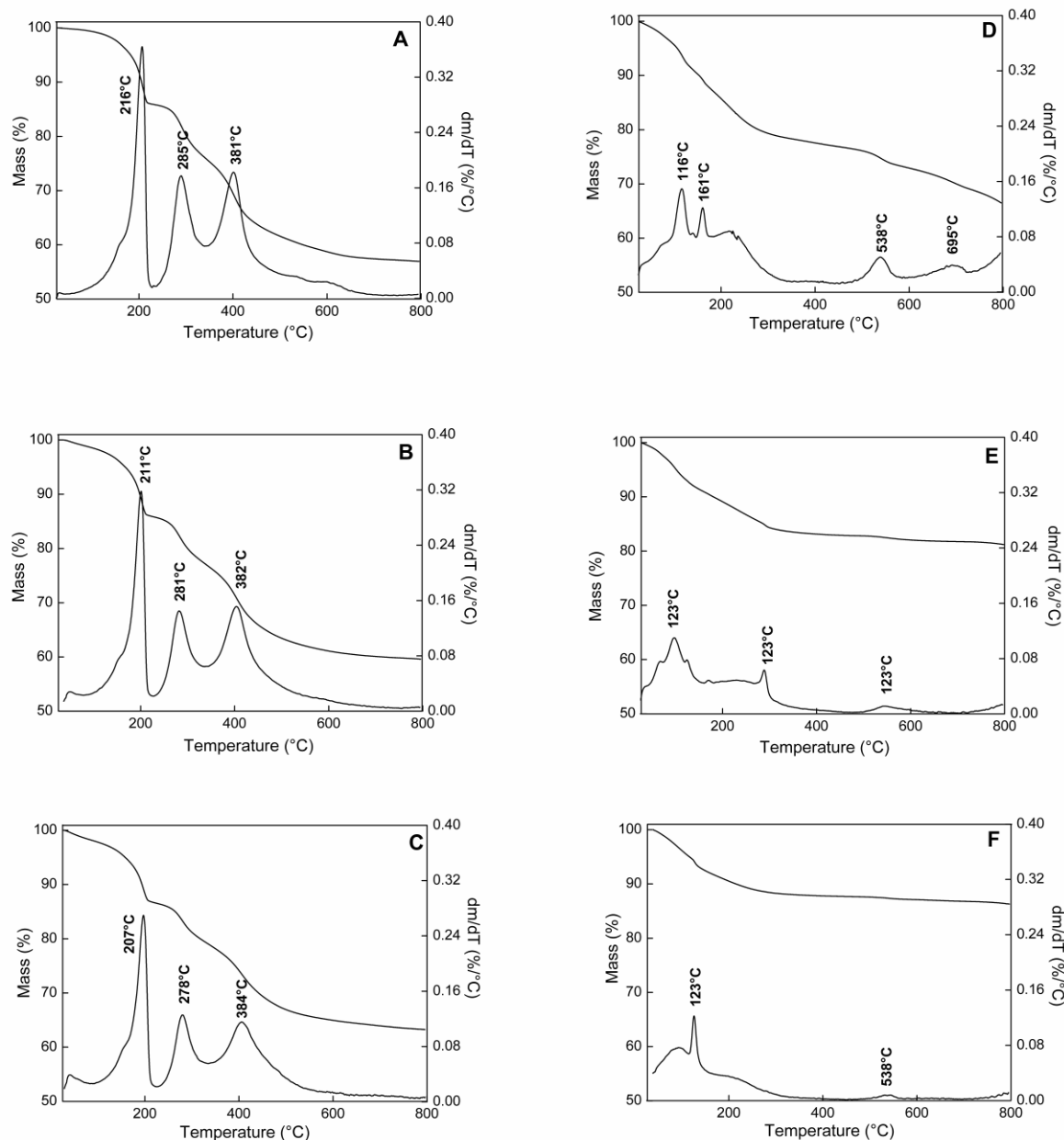
FIGURE 4.5 - Thermogravimetric (TG) and differential thermogravimetric (DTG) curves of samples loaded with PO_4^{3-} by ion exchange using different initial PO_4^{3-} concentrations: (A) [Mg-Al]-LDH (112.64 mg L^{-1} PO_4^{3-}); (B) [Mg-Al]-LDH (2252.80 mg L^{-1} PO_4^{3-}); (C) [Mg-Al]-LDH (4505.60 mg L^{-1} PO_4^{3-}); (D) [Zn-Al]-LDH (112.64 mg L^{-1} PO_4^{3-}); (E) [Zn-Al]-LDH (2252.80 mg L^{-1} PO_4^{3-}); (F) [Zn-Al]-LDH (4505.60 mg L^{-1} PO_4^{3-}).

Once the wastewater effluent is confined, the obtained phosphate loaded-LDH could be recovered by traditional techniques (flocculation and/or decantation) and be applied as phosphate fertilizer with controlled or slow release avoiding future widespread contamination by better fertilizer management over time. [111,124,125]

4.4   - *Conclusions*

This work proposes the use of layered double hydroxides (LDH) as adsorbent matrices for the removal of phosphate from effluents with high phosphate content. The [Zn-Al]-LDH adsorbent provided efficient removal of phosphate from aqueous solution by means of ion exchange processes. No alteration of the crystalline structure was observed for [Mg-Al]-LDH exposed to different phosphate concentrations. On the other hand, [Zn-Al]-LDH exhibited changes in the crystalline structure following phosphate adsorption, reflecting higher adsorption capacity. At low and intermediate concentrations of PO_4^{3-}, the crystalline structure of [Zn-Al]-LDH was well preserved, demonstrating that the ionic interaction mainly occurred on the external surface of the material. At high phosphate concentrations, there was formation of crystalline zinc hydroxide and non-crystalline zinc phosphate. The [Zn-Al]-LDH material exhibited high potential for use in phosphate removal from effluent with high phosphate concentration. In order to the effluent reach discharging standards, combination of great methods of phosphate removal could be practiced. The phosphate load-LDH recovered from the confined effluent treatments could be applied as phosphate fertilizer, avoiding future contamination by the better fertilizer management.

5 - Chapter III: Does the phosphate release occur with other phases formation?

The content of this chapter is an adaptation of the manuscript entitled **"Zn-Al-based layered double hydroxides (LDH) active structures for restorative dental materials"** by Marcela P. Bernardo and Caue Ribeiro that is under preparation.

5.1   *- Introduction*

Resin composites are important materials developed in modern biomaterials research and can replicate biological tissues in terms of both appearance and function.[126] These composites are used for a variety of applications in dentistry, including (but not limited to) restorative materials, cavity liners, and provisional restorations.[127] They are composed of three distinct phases: (i) the resin, composed of polymerizable monomers that convert from a liquid to a highly cross-linked polymer upon exposure to visible light; (ii) a filler that has several roles, including enhancement of modulus, radiopacity, alteration of thermal expansion behavior, and reduction of polymerization shrinkage by reducing the resin fraction; and (iii) the filler-resin interface, which acts as a bridge by coupling polymerizable moieties to the particle surface.[128] Exposure to various environments results in alteration of the properties of resin composites due to degradation and aging. These changes are caused by: (a) chemical breakdown by hydrolysis; (b) chemical breakdown by stress-induced effects associated with swelling and applied stress; (c) modification of chemical composition by leaching; (d) precipitation and swelling phenomena that produce voids and cracks, with leaching of the interface; and (e) loss of strength due to corrosion.[129-131]

Within each type of composite, the materials are further distinguished by the characteristics of the reinforcing fillers, especially particle size. Conventional dental composites have average particle sizes much larger than 1 μm. These "macrofill" materials are very strong, but are difficult to polish and are unable to retain surface smoothness.[127]

Efforts to identify novel options for reinforcing fillers have generally focused on nanosized materials and hybrid organic-inorganic fillers. Efforts to modify fillers have aimed at improving the properties of composites by the addition of polymer nanofibers, glass fibers, and titania nanoparticles.[132,133] Lamellar fillers, such as clays and related materials, can be good choices for improvement of polishing and unidirectional mechanical properties, due to their high aspect ratios.

Layered double hydroxides (LDH) belong to a class of anionic clays with the general formula $[M^{2+}_{1-x}M^{3+}_{x}(OH)_2]^{x+}[A^{n-}]_{x/n} \cdot yH_2O$, where M^{2+} is a divalent cation such as Mg^{2+}, Ni^{2+}, Zn^{2+}, Cu^{2+}, or Co^{2+}; M^{3+} is a trivalent metallic cation such as Al^{3+}, Cr^{3+}, Fe^{3+}, or Ga^{3+}; A^{n-} is a charge-balancing anion; and x is the molar ratio $M^{3+}/(M^{3+}+ M^{2+})$, ranging from 0.1 to 0.5.[134] LDH exhibit high anionic exchange capacity, with affinity for phosphate and other multivalent anions.[56] Thermal treatment confers important physicochemical properties to LDH[59] : (a) a "memory effect" of the hydroxide lattice, which allows different

anionic species to be incorporated into the LDH interlamellar spaces; and (b) a greater surface area, which increases adsorption of anions.[60,134] LDH have been used for the reinforcement of polymers in order to improve the mechanical properties or thermal stability,[135-137] reduction of corrosion in steel materials,[136] and reinforcement and protection against corrosion of concrete.[137] However, the effects of LDH as fillers in resin composites have received little attention.[138]

The importance of phosphate in the process of tissue mineralization is well known. Therefore, the incorporation of a phosphate releasing material as a component of dental resin is an important technique that can be used to avoid dental health problems such as caries.[139] Considering that zinc may act as a regulator of the mineralization process,[140] and given the potential of LDH as a nanofiller, here we demonstrate the potential of LDH, where M^{2+} is zinc ([Zn-Al]-LDH), for loading with high amounts of phosphate anions by means of the memory effect. Evaluation was made of the mechanical properties of dental polymeric resins containing the LDH materials as fillers, as well as the profiles of phosphate release from the reinforced dental resins in an artificial saliva medium.

5.2   - *Materials and Methods*

5.2.1   - *Materials*

Zinc chloride ($ZnCl_2$), aluminum chloride hexahydrate ($AlCl_3.6H_2O$), sodium hydroxide (NaOH), sodium carbonate (Na_2CO_3), and potassium phosphate monobasic (KH_2PO_4) were purchased from Synth (Brazil). All reagents were used as received. Decarbonated deionized water (ρ = 18.2 MΩ cm) obtained from a Milli-Q system (Barnstead Nanopure Diamond, Thermo Fisher Scientific Inc., Dubuque, IA, USA) was used in all the experimental procedures.

5.2.2   - *Synthesis of [Zn-Al]-LDH*

[Zn-Al]-LDH with $M^{3+}/(M^{2+}+M^{3+})$ molar ratio (x) of 0.25 was synthesized by the co-precipitation method, with pH control. The synthesis was carried out in an all-glass reactor (capacity of 300 mL) attached to a water circulating system in order to accurately control the temperature at 25.0 ºC (±0.5 ºC). In a typical reaction, a mixed chloride solution (0.5 mol L^{-1}) containing Zn^{2+} and Al^{3+} cations was gradually injected at a rate of 0.5 mL min^{-1} into the reactor containing sodium hydroxide solution (1.0 mol L^{-1}), under vigorous stirring. At the same time, a solution of Na_2CO_3 (2 mmol L^{-1}) was injected at a rate of 0.025 mL min^{-1} for pH control. Once injection of the solutions was complete, agitation was continued for a further hour, in order to age the precipitate. Subsequently, the mixture was centrifuged at 11,200 *g* for 10 min to remove the excess NaCl. The precipitate was then

purified using three washing-centrifugation cycles with 1:1 water-ethanol solution, and was resuspended in water for storage in a freezer. Finally, the material was lyophilized under a vacuum of 1.33×10^{-4} bar (Supermodulyo Freeze Dryer, Thermo Fisher Scientific Inc., Kansas City, MO, USA), yielding a white powder.

5.2.3   - Phosphate adsorption by structural reconstruction

Phosphate was loaded into the as-synthesized [Zn-Al]-LDH by means of structural reconstruction. The synthesis product was calcined for 4 h at two different temperatures: 300 °C ([Zn-Al]-LDH$_{c300}$) and 600 °C ([Zn-Al]-LDH$_{c600}$). Portions of 500 mg of the calcined samples were added to 250 mL of KH_2PO_4 solution, previously equilibrated at 75 °C and adjusted to pH 7.0 using 0.1 NaOH. The mixture was kept under vigorous agitation for 24 h, followed by centrifugation at 11,200 g for 10 min. The supernatant was used for quantification of the concentration of PO_4^{3-} at equilibrium, and the pellet was lyophilized prior to solid-state characterizations. Different molar ratios of PO_4^{3-} were studied by varying the PO_4^{3-} concentration from 0.83 mM (1:0.125 Al^{3+}/PO_4^{3-} molar ratio) to 33.10 mM (1:5 Al^{3+}/PO_4^{3-} molar ratio).

The concentration of phosphorus was determined according to a procedure reported elsewhere [141]: 5 mL of supernatant was mixed with 2 mL of ascorbic acid solution (0.4 M), 0.2 mL of citric acid solution (0.03 M), and 2 mL of a reactant consisting of sulfuric acid solution (4.7 M), 5.5 mL ammonium molybdate (0.08 M), and 0.6 mL of antimony and potassium tartrate (0.05 M). This mixture was then allowed to react for 15 min in a water bath at 50 °C, forming a phosphoantimonylmolybdenum blue complex. The concentration of the product was determined by UV-Vis spectrophotometry, using a PerkinElmer Lambda 25 spectrophotometer operated at a wavelength of 880 nm. All the quantifications were performed in duplicate.

5.2.4   - Characterizations

Powder X-ray diffraction (PXRD) measurements were performed using a Shimadzu XRD 6000 diffractometer, with Ni-filtered Cu K$_\alpha$ radiation (λ = 1.5405 Å). The diffractograms were acquired in the 2θ range 3-80°, at a scan speed of 2° min^{-1}. Fourier transform infrared (FTIR) analyses were performed using a Bruker spectrometer, with spectral resolution of 2 cm^{-1}. Scanning electron microscopy (SEM) analyses employed a JEOL microscope operated at 15 kV. Thermal degradation studies were performed using a TGA Q500 thermogravimetric analyzer (TA Instruments, New Castle, DE), under a flow of nitrogen at 60 mL min^{-1}, with heating at 10 °C min^{-1} from 25 to 800 °C.

5.2.5 - Incorporation of the LDH materials in dental resin and evaluation of mechanical properties

The reconstructed materials ([Zn-Al]-LDH$_{c300}$ and [Zn-Al]-LDH$_{c600}$) loaded with 33.1 mM PO$_4^{3-}$ were incorporated in commercial dental resin (Fill Magic, Coltene) at ratios of 2.5 and 4% (m/m), relative to the mass of resin. After complete and homogeneous incorporation of the samples, the composites were molded into specimens that were submitted to UV radiation (40.3 W m^{-2}) for 10 min for photo-curing. A three-point flexural test with a span of 4 cm was used to fracture the specimens, using a computer-controlled universal mechanical testing machine (Instron Corp., Canton, MA) fitted with a 50 kgf load cell and operated at a crosshead speed of 0.5 mm min^{-1}. The parameters flexural strength and elastic modulus were determined. Semi-quantitative atomic composition analysis and elemental mapping of Zn and P atoms were performed by energy-dispersive X-ray spectroscopy (EDX), using a Thermo Noran system coupled to a scanning electron microscope (JEM 2010, JEOL).

5.2.6 - Phosphate release from the reinforced dental resin

Artificial saliva with composition adapted from Appel and Reus,[142] containing KHCO$_3$ (15.01 g L^{-1}), NaCl (5.85 g L^{-1}), MgCl$_2$ (0.14 g L^{-1}), citric acid (0.002 g L^{-1}), CaCl$_2$ (0.16 g L^{-1}), and sodium carboxymethylcellulose (5 g L^{-1}) was used as the release medium for the dental resin. Resin specimens (2.8 x 1.5 x 0.225 cm) were placed in contact with 50 mL of artificial saliva under constant stirring (150 rpm) at 28 °C. The concentration of phosphate was performed using the same method described above after incubation for 0, 6, 14, 20, 27, 34, 41 and 58 days.

5.3 - Results and Discussion

5.3.1 - Synthesis of [Zn-Al]-LDH

[Zn-Al]-LDH was synthesized by the co-precipitation method with pH control. FIGURE 5.1 shows a scanning electron micrograph of the pristine LDH. The as-synthesized material presented an irregular nanostructure and layers without the presence of hexagonal structures, as well as some stacked nanoparticle flakes.[143] The PXRD patterns of the as-synthesized [Zn-Al]-LDH presented sharp and intense peak lines, with rhombohedral 3R symmetry, as expected for LDH material (JCPDS: 48-1023).[32] The d-spacing calculated using Bragg's law was 0.78 nm, in agreement with the presence of chloride ions in the interlayer space (FIGURE 5.2). The pristine [Zn-Al]-LDH was calcined at 300 °C (FIGURE 5.2-A1) and 600 °C (FIGURE. 5.2-B3). At 300 °C, the typical LDH structure was replaced by the metal oxide phase corresponding to ZnO (JCPDS: 36-1451). When the sample was

exposed to pure water, the original LDH structure was restored, confirming the "memory effect", despite some residual ZnO phase. On the other hand, calcination at 600 °C resulted in formation of not only the ZnO phase, but also a spinel phase ($ZnAl_2O_4$) (JCPDS: 05-0669), and when placed in contact with water, the sample was not reconstructed. In other words, the calcination temperature was so high that layers of LDH could not be restored. According to Cavani et al.[17] structural reconstruction is possible when the heating does not cause modification of the crystal morphology or exfoliation of the layered structure. The lamellar microstructure was retained after thermal decomposition of LDH, for 300 °C. However, the calcination at 600 °C caused microstructural changes that removed the memory effect.
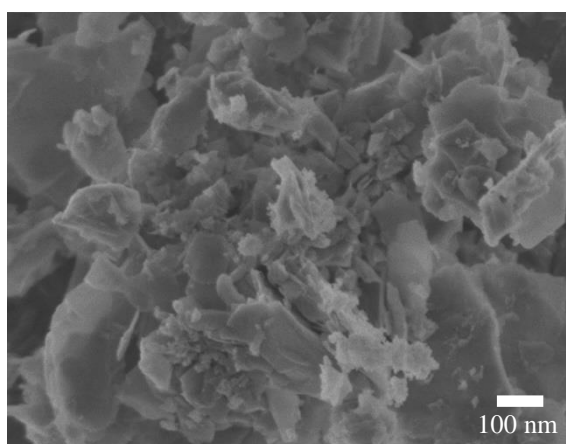
FIGURE 5.1 - Representative scanning electron micrograph of pristine [Zn-Al]-LDH.
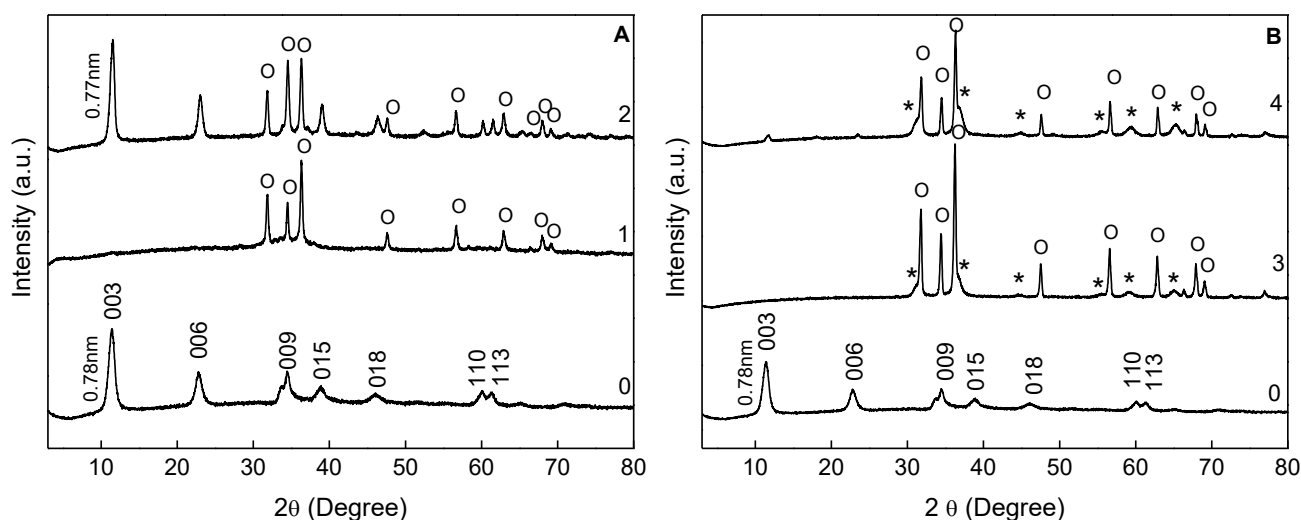
FIGURE 5.2 - PXRD patterns of pristine [Zn-Al]-LDH (A-0 and B-0); the material calcined at 300 °C ([Zn-Al]-LDH$_{c300}$) (A-1); the material calcined at 600 °C ([Zn-Al]-LDH$_{c600}$) (B-3); [Zn-Al]-LDH$_{c300}$ reconstructed in water (A-2); and [Zn-Al]-LDH$_{c600}$ reconstructed in water (B-4). *: $ZnAl_2O_4$; O: ZnO.

5.3.2   - Phosphate interaction with [Zn-Al]-LDH

Although the memory effect was not observed for [Zn-Al]-LDH$_{c600}$, the interactions with phosphate were investigated for [Zn-Al]-LDH calcined at both temperatures. The crystalline structures of the samples were assessed by PXRD (FIGURE 5.3). At lower phosphate concentrations, [Zn-Al]-LDH$_{c300}$ maintained the basic LDH crystalline structure and a ZnO phase after the thermal treatment. In this case, the interaction of phosphate with [Zn-Al]-LDH was probably due to electrostatic attraction between the external layers of the LDH and the negative PO_4^{3-} ions.[32] When the PO_4^{3-} concentration was increased, the LDH phase disappeared and was replaced by ZnO and $Zn(OH)_2$ (JCPDS: 74-0094) phases. At 33.10 mM, crystalline zinc-phosphate phases were identified. In this case, ZnO was the precursor material for phosphate interaction and the presence of OH^- groups was identified (FIGURE 5.4-A4). The PO_4^{3-} ions could exchange with OH^- groups and complex with Zn^{2+} on the surface by outer-sphere complexation or electrostatic attraction, allowing the formation of zinc-phosphate compounds.[144]

In a similar way, when [Zn-Al]-LDH calcined at 600 °C was exposed to solutions containing different concentrations of phosphate, the predominant crystalline phases were the spinel component ($ZnAl_2O_4$) and ZnO. At a phosphate concentration of 33.10 mM, the $Zn_3(PO_4)_2$ phase (JCPDS: 29-1390) was dominant. However, even at lower initial PO_4^{3-} concentrations, the interaction of phosphate with the materials was evidenced by the FTIR (FIGURE 5.4-B) and phosphate quantification analyses (TABLE 5.1). According to Lv et al.[145] phosphate causes dissolution of ZnO particles. Since ZnO was present with phosphate, a mixture of amorphous and crystalline phases of ZnO and zinc phosphate was obtained. Phosphate can react by adsorption and precipitation on solid phase surfaces, leading to a complex mixture of components and structural transformation of ZnO to zinc phosphate. In addition, the formation of amorphous zinc phosphate phases can occur due to complexation between dissolved PO_4^{3-} and Zn^{2+}.

These results can be compared to our previous findings for other LDH structures, where it was shown that at higher PO_4^{3-} concentrations, Ca-Al-based LDH converted into hydroxyapatite, and Mg-Al-based LDH converted to bobierrite.[109,110]
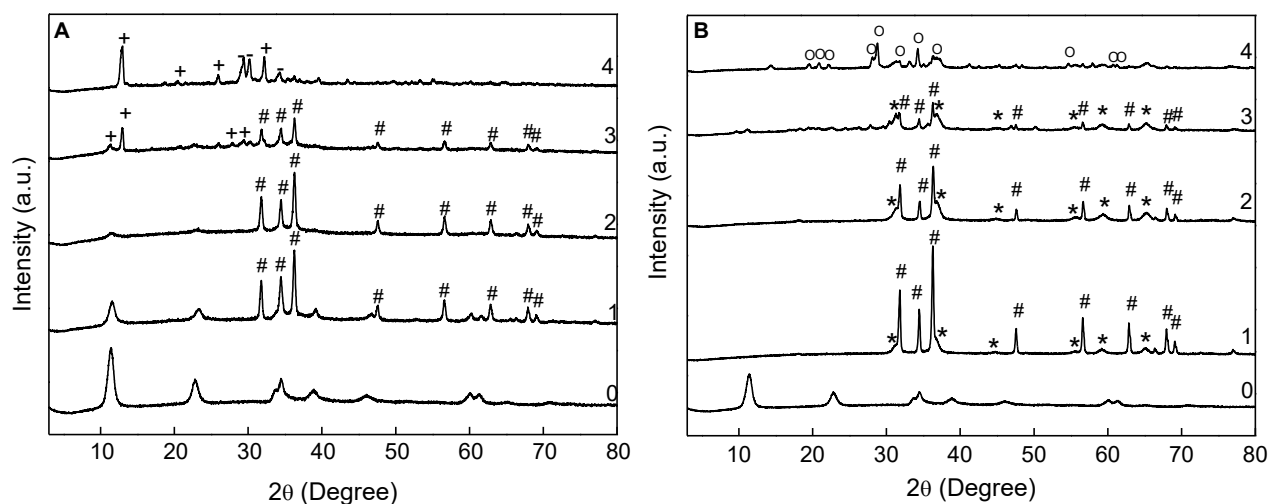
FIGURE 5.3 - Powder X-ray diffraction (PXRD) patterns for phosphate adsorption by structural reconstruction on (A) [Zn-Al]-LDH$_{c300}$ and (B) [Zn-Al]-LDH$_{c600}$. (0): pristine [Zn-Al]-LDH; (1): 0.83 mM PO$_4^{3-}$; (2): 3.31 mM PO$_4^{3-}$; (3): 16.55 mM PO$_4^{3-}$; (4): 33.10 mM PO$_4^{3-}$. (#): ZnO; (-): Zn$_2$P$_2$O$_7$; (*): ZnAl$_2$O$_4$; (+): ZnH$_2$P$_2$O$_7$; (O): Zn$_3$(PO$_4$)$_2$.

FIGURE 5.4-A shows the FTIR spectra for the samples, where the interaction with phosphate was confirmed by the presence of the band at 1040 cm^{-1} (FIGURE 5.4-A), attributed to the υ_3 (P-O) stretching vibration mode.[111] This was an important indication of the interaction of phosphate with [Zn-Al]-LDH$_{c300}$, despite the fact that the XRD analysis did not reveal any crystalline phosphate phases. Furthermore, the phosphate contents of the samples (TABLE 5.1) increased at higher initial phosphate concentrations. Regardless of the mechanism of interaction of phosphate with calcined [Zn-Al]-LDH, at high phosphate concentrations [Zn-Al]-LDH$_{c600}$ was able to incorporate greater amounts of PO$_4^{3-}$, while better results were obtained for [Zn-Al]-LDH$_{c300}$ at low phosphate concentrations (TABLE 5.1). These results were in agreement with the study of Cheng et al.[60] who found that material calcined at 300 °C presented better phosphate adsorption at an initial PO$_4^{3-}$ concentration of 20 mg L^{-1}, due to the greater specific surface area of the sample.

The thermal stabilities and compositions of [Zn-Al]-LDH calcined at 300°C and 600 °C and loaded with PO$_4^{3-}$ were investigated using TGA (FIGURE 5.5). The main phases for 0.83-[Zn-Al]-LDH$_{c600}$ were zinc oxides (ZnO and ZnAl$_2$O$_4$), as a result of which this sample showed no significant mass loss. Although the XRD patterns for the materials produced with intermediate phosphate concentrations showed the presence of the same zinc oxides, changes were observed in the mass loss profiles. The main mass losses occurred at around 75, 300, 500, and 600 °C, related to the losses of surface water, loosely bound water molecules, and amorphous phosphate compounds leading to the formation of pure ZnO and ZnAl$_2$O$_4$, respectively.[146] At 33.10 mM of phosphate, only two small peaks were present, at

208 and 535 °C, attributed to the loss of adsorbed water and phosphate anions, respectively, culminating in oxide formation.
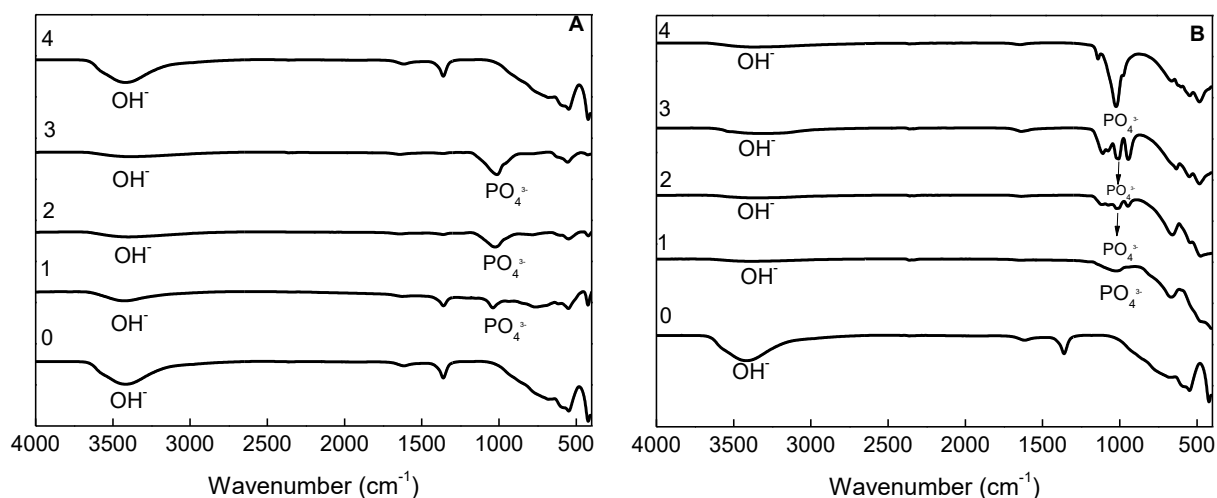
FIGURE 5.4 - FTIR spectra for phosphate adsorption on (A) [Zn-Al]-LDH$_{c300}$ and (B) [Zn-Al]-LDH$_{c600}$. (0): pristine [Zn-Al]-LDH; (1): 0.83 mM PO$_4^{3-}$; (2): 3.31 mM PO$_4^{3-}$; (3): 16.55 mM PO$_4^{3-}$; (4): 33.10 mM PO$_4^{3-}$.

TABLE 5.1 - Phosphate concentrations after interaction with [Zn-Al]-LDH calcined at 300 and 600 °C

Initial PO$_4^{3-}$ (mM)	[Zn-Al]-LDH$_{c300}$ (mg PO$_4^{3-}$ g^{-1})	[Zn-Al]-LDH$_{c600}$ (mg PO$_4^{3-}$g^{-1})
00.83	16.00	06.50
01.65	15.50	04.60
03.31	25.00	14.50
06.62	31.20	28.20
11.58	43.40	67.50
16.55	63.00	53.00
26.48	78.40	85.00
33.10	81.80	92.50

The thermal profiles of [Zn-Al]-LDH$_{c300}$ loaded using phosphate concentrations up to 16.55 mM were typical of LDH, with removal of (i) physically adsorbed water at temperatures below 100 °C, (ii) interlayer water up to 200 °C, (iii) hydroxyl groups from the layers as water around 300 °C, and (iv) anions, with consequent oxide formation, above 400 °C.[19] However, at 33.10 mM of phosphate, the peak related to removal of PO$_4^{3-}$ was no longer observed, indicating thermal stability of the compound formed (Zn$_3$(PO$_4$)$_2$).
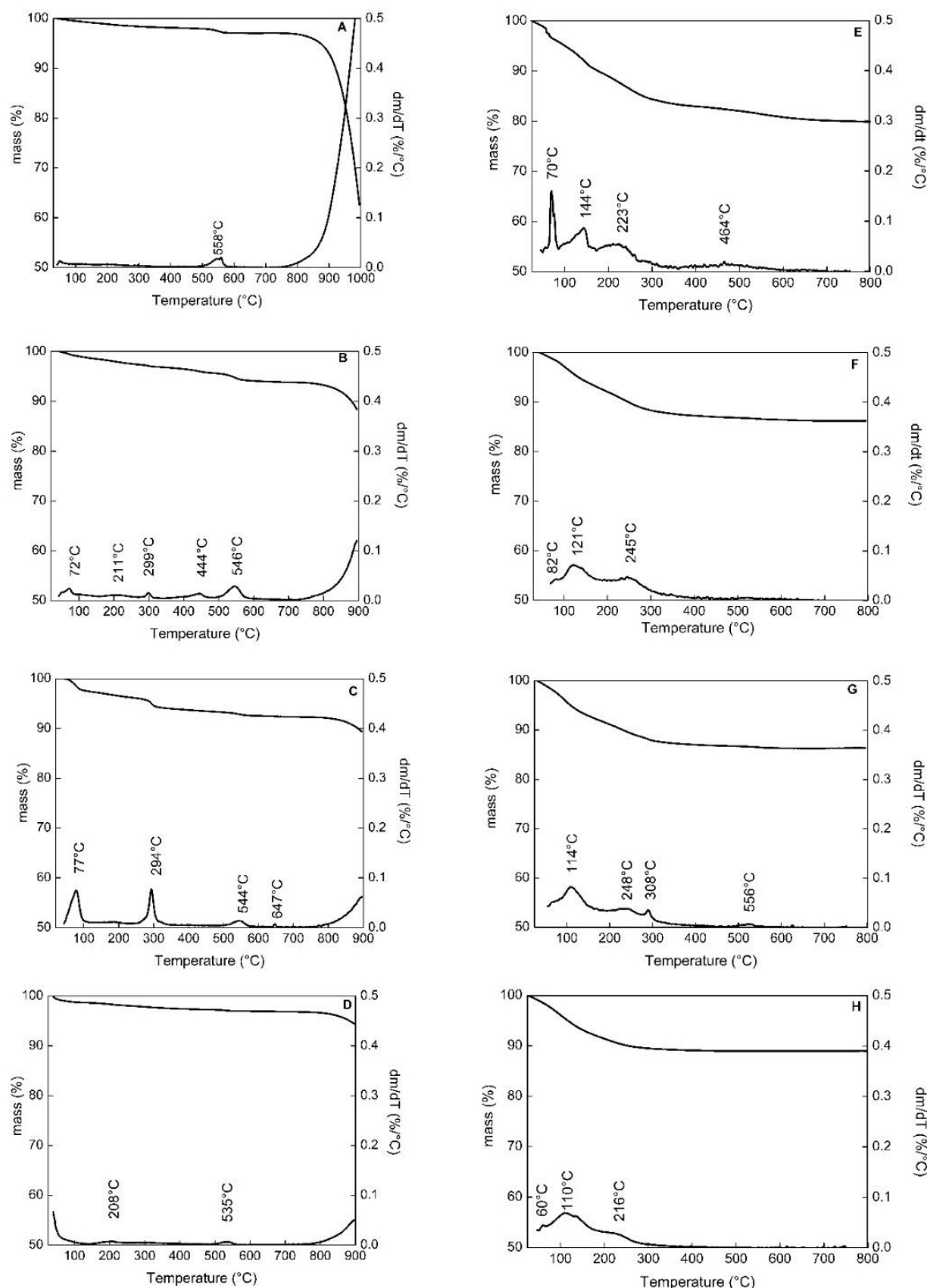
FIGURE 5.5 - Thermogravimetric (TG) and differential thermogravimetric (DTG) curves for samples [Zn-Al]-LDH$_{c300}$ and [Zn-Al]-LDH$_{c600}$ loaded with PO$_4^{3-}$ by structural reconstruction using different initial PO$_4^{3-}$ concentrations: (A) 0.83 mM - [Zn-Al]-LDH$_{c600}$; (B) 3.31 mM - [Zn-Al]-LDH$_{c600}$; (C) 16.55 mM - [Zn-Al]-LDH$_{c600}$; (D) 33.10 mM - [Zn-Al]-LDH$_{c600}$; (E) 0.83 mM - [Zn-Al]-LDH$_{c300}$; (F) 3.31 mM - [Zn-Al]-LDH$_{c300}$; (G) 16.55 mM - [Zn-Al]-LDH$_{c300}$; (H) 33.10 mM - [Zn-Al]-LDH$_{c300}$.

5.3.3 - *An application of P release: reinforcement of dental resin with P-loaded [Zn-Al]-LDH$_c$, and phosphate release*

The mechanical properties of the commercial dental resin added with 33.10-[Zn-Al]$_{c600}$ and 33.10-[Zn-Al]$_{c300}$ at mass ratios of 2.5% and 4% were investigated, due to the high phosphate contents of these samples. TABLE 5.2 summarizes the results of the three-point flexural test applied to these four nanocomposites and the pristine dental resin. The elastic modulus and flexural strength values for the resins containing 4% 33.10-[Zn-Al]$_{c600}$, 2.5% 33.10-[Zn-Al]$_{c600}$, and 4% 33.10-[Zn-Al]$_{c300}$ were lower than the values obtained for the pristine dental resin, while the values for the resin containing 2.5% 33.10-[Zn-Al]$_{c300}$ were similar to those for the pristine resin. This was in agreement with other works, since increased inorganic loadings (with no modifications) in brittle polymers is expected to have negative impacts on their mechanical characteristics. The properties of a dental resin containing inorganic particles such as [Zn-Al]-LDH are determined by the dispersion of the filler particles and the interactions at the polymer-filler interface.[147] A homogenous dispersion of the nanoparticle in the dental resin investigated here might not have been achieved creating failure points, reflecting on the mechanical properties of nanocomposites.

Ideally, a dental resin composite should present high flexural strength, since these materials are subjected to chewing stresses that might induce permanent deformation. [127,148] Considering the application of the dental resin reinforced with [Zn-Al]-LDH, the material calcined at 300 °C and loaded with 33.10 mM of phosphate at a ratio of 2.5% provided slight increase of flexural strength, as required for materials submitted to intense and repeated flexing, bending, and twisting.[147]

TABLE 5.2. Mechanical properties of dental resin reinforced with 33.10-[Zn-Al]-LDH$_c$.

Sample	Flexural strength (MPa)	Elastic modulus (GPa)
Control	459.6	25.04
2.5% 33.10-[Zn-Al]-LDH$_{c300}$	681.2	22.97
4% 33.10-[Zn-Al]-LDH$_{c300}$	104.2	05.60
2.5% 33.10-[Zn-Al]-LDH$_{c600}$	111.4	05.18
4% 33.10-[Zn-Al]-LDH$_{c600}$	255.7	11.16

According to Ferracane, [127] it is very attractive the development of "smart" materials that reacts to its environment to release remineralizing ions. The remineralization may be promoted by the slow release of phosphate ions, followed by the precipitation of

new phases, like calcium-phosphate mineral. Restoratives materials that do release Ca, PO_4, or F ions are relatively weak and cannot be used in large stress-bearing restorations. Therefore, materials that exhibits adequate mechanical properties, while at the same time has sustainable release of ions, like Ca, PO_4 and F, contributes for the inhibition of caries formation.

The kinetics of phosphate release from the dental resins containing PO_4^{3-}-loaded [Zn-Al]-LDH_c was evaluated by exposing the materials to artificial saliva. The results (FIGURE 5.6) showed that all the samples could release phosphate, although a substantially higher concentration of phosphate in the artificial saliva was obtained using the resin containing 2.5% 33.10-[Zn-Al]-LDH_{c300}. Even after 58 days, the materials evidenced an increasing capacity for phosphate release, attesting the great potential of these materials, in special of 2.5% 33.10-[Zn-Al]-LDH_{c300}, to act as controlled phosphate release source.

The phosphate released has the potential to assist in remineralizing carious lesions or minimizing caries development, in conjunction with ions such as calcium and fluoride obtained from other sources such as dentifrices and chewing gums.[136,149] Caries is caused by the bacterial production of organic acids that dissolve the dental minerals, and it has been found that the mineral formed during remineralization is more resistant to acid than the original dental enamel.[150] Therefore, the dental resin containing 2.5% 33.10-[Zn-Al]-LDH_{c300} not only maintained the original flexural strength and increased the elastic modulus, as desired for this type of material, but also acted as a source of phosphorus, which is an element important for mineralization and the avoidance of future dental problems.
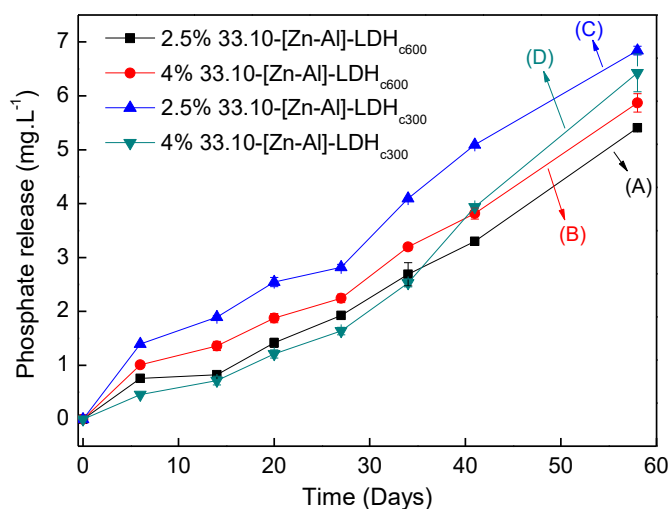
FIGURE 5.6 - Phosphate release profiles for the samples: (A) 2.5% 33.10-[Zn-Al]-LDH$_{c600}$; (B) 4% 33.10-[Zn-Al]-LDH$_{c600}$; (C) 2.5% 33.10-[Zn-Al]-LDH$_{c300}$; (D) 4% 33.10-[Zn-Al]-LDH$_{c300}$.

5.4   - Conclusions

The interaction of phosphate with [Zn-Al]-LDH was evaluated using the reconstruction method with calcination temperatures of 300 and 600 °C. For calcination at 300 °C, the [Zn-Al]-LDH structure was satisfactorily maintained at low phosphate concentration. When the initial phosphate concentration was increased, new crystalline phases with higher phosphate content were formed. Calcination at 600 °C resulted in different interaction of phosphate with [Zn-Al]-LDH, leading to a zinc-phosphate crystalline phase with high phosphate content. Evaluation of the 33.10-[Zn-Al]-LDH$_c$ materials as reinforcement fillers in dental resin showed that the resin containing 2.5% 33.10-[Zn-Al]-LDH$_{c300}$ retained the mechanical properties of the pristine resin, in accordance with the requirements for dental resin, and also released significant amounts of phosphate into an artificial saliva medium. This modified resin could therefore assist in dental remineralization and provide protection against dental problems.

6 - Chapter IV: Is the tendency of phosphate release confirmed by the increase of cation size?

The content of this chapter is an adaptation of the article entitled **"Synthesis and characterization of eco-friendly Ca-Al-LDH loaded with phosphate for agricultural applications"** by Marcela P. Bernardo, Francys K.V. Moreira and Caue Ribeiro, published for Applied Clay Science.

Research paper

Synthesis and characterization of eco-friendly Ca-Al-LDH loaded with phosphate for agricultural applications

Marcela P. Bernardo [a,b,*], Francys K.V. Moreira [c], Caue Ribeiro [a,b]

CrossMark

6.1 - Introduction

Phosphorus (P) is the second major plant growth-limiting nutrient despite the occurrence in different soils in inorganic and organic forms. However, many soils are deficient in phosphorus because the concentration available to plants is generally not higher than 10 µM, even in fertile soils.[151,152] Typical soil P levels are rather low in comparison with levels required for optimal plant growth (external P requirement), which can reach several μM for most demanding crop species, such as beans, cotton, pea, potato, onion, spinach and tomato.[153-155] Phosphorus is an important nutrient involved in several energy conversion and biochemical reactions, including biological nitrogen fixation: for example, soybean production demands considerable amounts of nitrogen and phosphorus.[156] Phosphorus is not only necessary to crop itself but also to microorganisms responsible for high crop production yields.[157] Some of them, such as *Pseudomonas* and *Rhizobium* microorganism genera can promote plant growth and yield due to their efficient capacity of converting insoluble inorganic phosphorus compounds into phosphate forms available to plant roots.[158] Of especially economic importance is the *Bradyrhizobium* genus whose ability in fixing nitrogen from atmosphere is widely recognized. However, microorganisms require proper nutrient supplying to their metabolism prior to promoting large crop yields.[159]

It has been essential the application of materials or structures with anion affinities that can be capable of controlling release of phosphorus according to adequate release profiles. Among materials displaying these features, Layered Double Hydroxides (LDH) are good candidates. LDH are a family of layered materials displaying the general stoichiometry $[M^{2+}_{1-x}M_x^{3+}(OH)_2]^{x+} (A^{n-})_{x/n}.yH_2O$, where M^{2+} are bivalent cations, such as Ni^{2+}, Co^{2+}, Cu^{2+}, Zn^{2+} and Ca^{2+}, and M^{3+} are trivalent cations, as Al^{3+}, Cr^{3+}, Fe^{3+}, Ga^{3+}. A^{n-} is a charge-balancing anion, and x is the molar ratio ($M^{3+}/(M^{3+}+ M^{2+})$) ranging from 0.1 to 0.5.[64,108] The LDH structure is analogous to that of brucite, $Mg(OH)_2$. When a molar fraction of M^{2+} ions at octahedral sites is isomorphically replaced by other of M^{3+} ions, the positive charge excess formed on the metal hydroxide sheet is counter-balanced by inclusion of anions (A^{n-}) in interlayer domains.[11,160] $Ca_2Al(OH)_{6.5}Cl_{0.5}.3(H_2O)$ or hydrocalumite, is a calcium-based layered double hydroxide easily synthesized and normally found in cement pastes and discarded concrete corroded by seawater.[13,161]LDH exhibit high surface area, large anion exchange capacity, and good thermal properties.[13]

Anion adsorption can occur in LDH through two different routes, one of them is the ion exchange (IE) process. IE is possible to happen due to the strongest enthalpy of bond formation within LDH layers, responsible for thermodynamic stability of LDH. The

interlayer domain is typically less stable, therefore readily undergo intercalation/deintercalation reactions.[108] Another route of anion adsorption in LDH is the structural reconstruction (SR) that involves the so-called "memory effect". LDH lose their layered structure when undergoing calcination and form highly active composite metal oxides with high thermal stability, large surface area, basic properties, small crystallite size and high stability against sintering even under extreme conditions.[13]

Calcined LDH can regenerate their original layered stacking by rehydration and sorption of anions. SR occurs only when the calcination is performed at a specific temperature range.[162]

In this investigation, we examined the phosphate (PO_4^{3-}) incorporation in hydrocalumite-like [Ca-Al]-LDH by two mechanisms: ion exchange reaction and structural reconstruction method. To probe the efficiency of [Ca-Al]-LDH in controlling the release of phosphate, an experiment involving growth of *Bradyrhizobium elkanii* in presence of [Ca-Al]-LDH loaded with PO_4^{3-} was carried out, showing evidences of a beneficial PO_4^{3-} controlled release for agricultural applications.

6.2   - Experimental

6.2.1   - Materials

Calcium chloride hexahydrate, aluminum chloride hexahydrate, sodium hydroxide and monobasic potassium phosphate were purchased from Synth, Brazil. All reagents were used as received. Decarbonated ultra-pure H_2O (ρ = 18.2 MΩ cm) obtained by a Milli-Q system (Barnstead Nanopure Diamond, Thermo Fisher Scientific Inc., Dubuque, IA, USA) was used exclusively in all experimental procedures.

6.2.2   - Synthesis of [Ca-Al]-LDH

Hydrocalumite-like [Ca-Al]-LDH with Al^{3+} molar fraction (*x*) of 0.30 was synthesized by the co-precipitation at high supersaturation method.[163] Briefly, the NaOH solution (2.0 mol L^{-1}) was gradually injected at the rate of 16.6 mL h^{-1} into the reactor containing a mixed salt chloride solution 0.5 mol L^{-1}) containing both Ca^{2+} and Al^{3+} cations.[109]

6.2.3   - Adsorption of PO_4^{3-} in LDH by structural reconstruction and ion exchange

For structural reconstruction method, [Ca-Al]-LDH were loaded with PO_4^{3-} anions by using the memory effect.[164] First, [Ca-Al]-LDH samples were calcined at 600ºC for 4 h in a muffle. In the following step, 500 mg of the calcined product was added to 250 mL of KH_2PO_4 solution. For ion exchange route, 500 mg of as-synthesized [Ca-Al]-LDH was added to 250 mL of KH_2PO_4 solution. In both cases the solution were previously

equilibrated at 75°C and the mixture was continuously agitated for 24 h and then centrifuged at 11.200g for 10 min. The incorporation of PO_4^{3-} anions was studied under conditions of molar saturation by varying the PO_4^{3-} concentration from 0.83 mM (1:0.134 Al^{3+}:PO_4^{3-} molar ratio) to 33.10 mM (1:5.4 Al^{3+}:PO_4^{3-} molar ratio). In all cases, the pH of the KH_2PO_4 solutions was adjusted to 7 with 0.1 M NaOH to avoid dissolution of LDH.

6.2.4   - Quantification of phosphorus

The concentration of phosphorus was determined by molybdenum blue method.[69,70]

6.2.5   - Growth of Bradyrhizobium elkanii in presence of [Ca-Al]-LDH loaded with PO_4^{3-}

In order to study the influence of [Ca-Al-PO_4^{3-}]-LDH on growth of *Bradyrhizobium elkanii* SEMIA 5019, it was used a traditional culture medium, composed of: K_2HPO_4 (0.5 g L^{-1}), $Mg.SO_4.7H_2O$ (0.2 g L^{-1}); NaCl (0.1 g L^{-1}); Mannitol (5 g L^{-1}); Yeast extract (0.4 g L^{-1}) and the selected [Ca-Al- PO_4^{3-}]-LDH samples: [Ca-Al]-LDH R-1.65 mM; [Ca-Al]-LDH R-11.58 mM; [Ca-Al]-LDH; [Ca-Al]-LDH R-33.10 mM; [Ca-Al]-LDH IE-1.65 mM; [Ca-Al]-LDH IE-11.58 mM and [Ca-Al]-LDH IE-33.10 mM. The phosphate concentration at each experiment was equivalent to the phosphate level required for *B. elkanii* growth. The culture medium was made without the phosphate source. Also, positive and negative controls were prepared, with and without K_2HPO_4, respectively. All the experiments were conducted in triplicated. Statistical analyses were performed using the software R version 3.3.0. ANOVA and Duncan test of multiples comparisons with 5% of significance level were used in mean comparisons.

6.2.6   - Characterizations

Powder X-ray diffraction (PXRD) measurements were conducted on a Shimadzu XRD 6000 diffractometer using Ni-filtered Cu K_α radiation (λ = 1.5405 Å). PXRD patterns were taken over the 2θ range of 3° − 80° with a scan speed of 2° min^{-1}. Specific surface area measurements were done by isothermal nitrogen adsorption through the BET (Brunauer–Emmett–Teller) method on ASAP 2020 equipment (Micrometrics). Scanning electron microscopy (SEM) was conducted on a JEOL microscope running at 15 kV. Atomic absorption spectrometry was conducted on a PinAAcle 900T (PerkinElmer) atomic absorption spectrometer. Samples were dissolved in acid prior to analysis. ^{27}Al and ^{31}P MAS NMR experiments were carried out on 9.4 T Avance III HD spectrometer (Bruker) operating at a frequency of 104.215 MHz for ^{27}Al and 161.904 MHz for ^{31}P, respectively. The ^{31}P spectra were acquired using a 90º pulse (2.5 μs), proton decoupled, 25 ms of acquisition time, 10 s of recycle delay and 1000 scans. The ^{27}Al spectra were acquired using

a 30° pulse (1.5 μs), without proton decoupling, 16 ms of acquisition time, 1s of recycle delay and 500 scans. The samples for ^{31}P and ^{27}Al analyses were packed in a 5 mm cylindrical zirconium rotor and were spun at the magic angle sample spinning (10 kHz). Thermal degradation was evaluated using a TGA Q500 thermogravimetric analyzer (TA Instruments, New Castle, DE) under the following conditions: nitrogen atmosphere flow 60 mL/min; heating rate 10°C/min; and temperature range of 25°C – 900°C.

6.3   - Results and discussion

6.3.1   - Reconstruction of [Ca-Al]-LDH

[Ca-Al]- LDH was synthetized by co-precipitation. Chemical analysis revealed that the molar ratio (x) of the sample was 0.30, leading to a Ca^{2+}/Al^{3+} molar proportion of 2.2:1.

PXRD patterns of the as-synthesized [Ca-Al]-LDH displays sharp and symmetric reflections typical of hydrocalumite (JCPDS:78-1219) with monoclinic symmetry[165] and basal space of 7.6 Å calculated from the (002) reflection. Also, the pattern shows a little signal relative to gibbsite phase of $Al(OH)_3$ (JCPDS: 1-264) (FIGURE 6.1-A). After calcination at 600°C, the sample presented crystalline phases indexed as Mayenite ($Ca_{12}Al_{14}O_{33}$, JCPDS: 48-1882), resulting from thermal decomposition of [Ca-Al]-LDH (FIGURE 6.1-B). However, when in contact with water, the crystalline phases corresponding to [Ca-Al]-LDH are detected again (FIGURE 6.1-C), demonstrating that the lamellae structure of [Ca-Al]-LDH is regenerated by hydration. SEM micrographs of synthetic, calcined and restructured [Ca-Al]-LDH are presented in Appendix C (FIGURE C1).
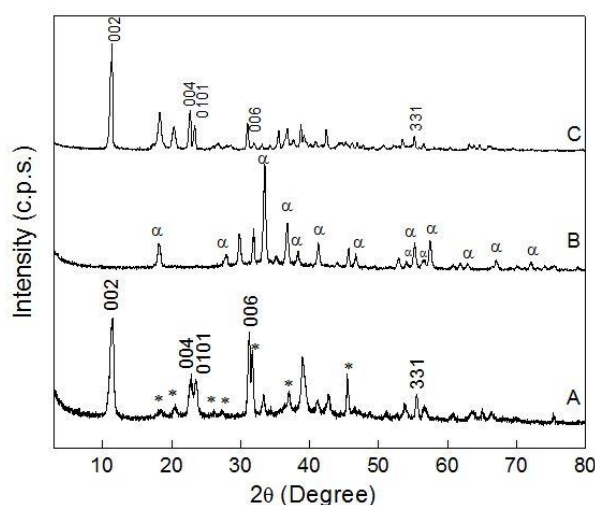
FIGURE 6.1 - PXRD patterns of (A) as-synthesized [Ca-Al]-LDH; (B) calcined sample [Ca-Al]c-LDH; (C) restructured sample in water [Ca-Al]-LDH R-H_2O. α: Mayenite; *: Aluminum hydroxide (gibbsite).

6.3.2 - Adsorption of PO_4^{3-} in [Ca-Al]-LDH

Two possible routes can be used to uptake anions in LDH: ion exchange (IE) and structural reconstruction (SR). The PO_4^{3-} uptake behavior in [Ca-Al]-LDH was evaluated with relation to both routes. Phosphate concentrations were varied between 0.83 mM (1:0.134 Al^{3+}:PO_4^{3-} molar ratio) and 33.10 mM (1:5.4 Al^{3+}:PO_4^{3-} molar ratio). TABLE 6.1 reports the amount of phosphate incorporated in [Ca-Al]-LDH from the different initial phosphate concentrations.

TABLE 6.1 - Amount of phosphate incorporated in [Ca-Al]-LDH through structural reconstruction (SR) and Ion Exchange (IE)

PO_4^{3-} (mM)	Structural Reconstruction (mg PO_4^{3-}/ g LDH)	Ion exchange (mg PO_4^{3-}/ g LDH)
0.83	10.36	15.80
1.65	19.65	35.39
3.31	43.98	62.86
6.62	54.79	54.26
11.58	65.75	94.20
16.55	95.36	91.46
26.48	90.95	92.68
33.10	83.26	127.56

The PO_4^{3-} uptake increased with increasing initial PO_4^{3-} concentration, regardless the adsorption route. For low PO_4^{3-} concentrations (until 11.58mM), the IE process resulted in larger adsorbed PO_4^{3-} amounts, with exception of 6.62 mM, at which both processes led to quite equal uptake rates. Similarly, at high PO_4^{3-} concentrations (16.55 and 26.48 mM) both processes exhibited similar PO_4^{3-} uptake efficiency. This indicates that for this range of PO_4^{3-} concentrations the amount of phosphate adsorbed on the [Ca-Al]-LDH is independent on the adsorption route. However, increasing the initial PO_4^{3-} concentration (33.10 mM), the IE process once again presented higher PO_4^{3-} uptake efficiency than SR. The differences in adsorbed phosphate amounts between SR and IE may be explained by the different kinetic dissolution reactions due to differences in precursor particle size, that is, hydrocalumite for IE and mayenite for SR. Although differences in specific surface area of the precursors, PO_4^{3-} loaded [Ca-Al]-LDH samples obtained from PO_4^{3-} solutions at equivalent initial concentration exhibited quite similar specific surface areas: [Ca-Al]-LDH R- 11.58 mM (SSA = 114.68 m² g^{-1}) and [Ca-Al]-LDH IE- 11.58 mM (SSA = 91.37 m² g^{-1}); [Ca-Al]-LDH R-33.10mM (SSA = 54.31 m² g^{-1}) and [Ca-Al]-LDH IE- 33.10 mM (SSA = 59.88 m² g^{1}).

Structural crystalline changes in [Ca-Al]-LDH because of the PO_4^{3-} uptake were assessed through PXRD (FIGURE 6.2). In general, similar crystalline phases are formed in [Ca-Al-PO_4^{3-}]-LDH with increasing PO_4^{3-} concentration, independent on the adsorption route.
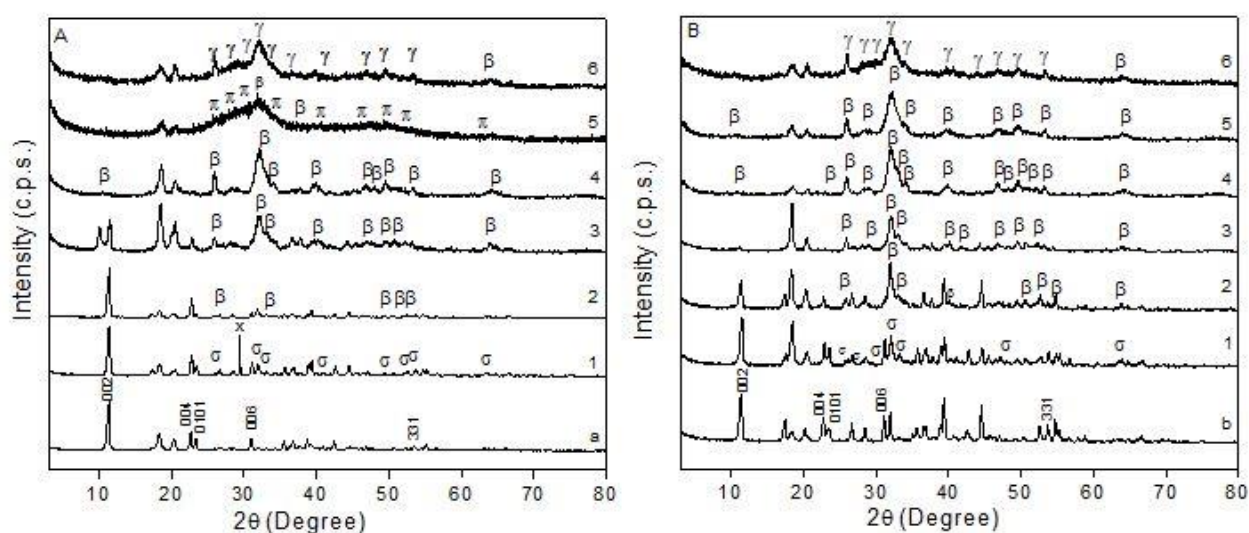
FIGURE 6.2 - PXRD for phosphate adsorption in [Ca-Al]-LDH by (A) structural reconstruction (SR) and (B) ion exchange process (IE) from different initial phosphate concentrations. (a): [Ca-Al]-LDH SR-H_2O; (b) [Ca-Al]-LDH IE-H_2O; (1):0.83 mM; (2):1.65 mM; (3): 3.31 mM; (4):11.58 mM; (5):16.55 mM; (6): 33.10 mM. δ: $Ca_3(PO_4)_2xH_2O$; X: $CaCO_3$; β: $Ca_{10}(OH)_2(PO_4)_6$ π: $Ca_2(P_2O_7)$; Υ: ($Ca_4(PO_4)_2O$).

For concentrations between 0.83 mM and 1.65 mM, the hydrocalumite-like structure is well maintained, and new phases are formed for each concentration, for instance, hydrated calcium phosphate and hydroxyapatite, respectively. At concentration of 3.31 mM, some structural differences are noted with respect to adsorption route. For [Ca-Al-PO_4^{3-}]-LDH obtained by SR, the hydrocalumite phase is clear. Additionally, hydroxyapatite phase is recognized at this concentration. For [Ca-Al-PO_4^{3-}]-LDH obtained by IE, the [Ca-Al]-LDH phase was totally replaced by hydroxyapatite. At phosphate concentrations of 6.62 and 11.58 mM, hydroxyapatite phase is evidently predominant, regardless the adsorption route.

For IE, the hydroxyapatite phase is well maintained up to 16.55 mM PO_4^{3-}. But for SR performed at the same concentration range, the hydroxyapatite phase is replaced by calcium pyrophosphate ($Ca_2(P_2O_7)$) (JCPDS:33-0297). At the very high PO_4^{3-} concentration (26.48 and 33.10 mM), a new phase, tetracalcium phosphate ($Ca_4(PO_4)_2O$) (JCPDS 25-1137) is predominant. All samples became progressively amorphous at the highest PO_4^{3-} concentrations.

The SR mechanism involves rehydration of mixed metal oxides and concurrent intercalation of PO_4^{3-} into the interlayer domains to regenerate the LDH.[13] The

calcined materials have some characteristics including: (i) increased surface area [166,167] (ii) increased porosity due to the calcination process [166,168] and (iii) fewer carbonate anions at the interlayer domains in comparison with the uncalcined LDH.[167,168] It is seen that specific surface area of calcined [Ca-Al]-LDH (28.67 m² g^{-1}) was smaller than that of the uncalcined [Ca-Al]-LDH (63.94 m² g^{-1}). This reduction of specific surface area may be explained by the sintering process, when the mayenite crystals increases in size.[169]

Considering both adsorption routes, at low PO_4^{3-} concentration the structure of hydrocalumite is maintained, in other words, for SR process the memory effect occurs effectively, while for IE process, PO_4^{3-} anions are adsorbed on the unmodified hydrocalumite crystal. According to Yang et al.[32] the phosphate adsorption occurs via electrostatic interaction, ligand exchange and ion exchange. When the interlayer anion is replaced by the PO_4^{3-} anion, the phosphate is said to be intercalated, because it is inserted between the LDH layers. However, the LDH layer surface also displays hydroxyl groups that could be exchanged by the PO_4^{3-} anion following the ligand exchange process. In this case, the PO_4^{3-} anion is externalized of the interlayer space. The electrostatic interaction between negatively charged PO_4^{3-} anions and the positive adsorbent surface is also a possible way of adsorbing PO_4^{3-} anions at the external LDH crystal surface.

Values for the interlayer space when phosphate, arsenate, nitrate and sulfate were adsorbed on different LDH ([Mg-Al], [Ca-Al] and [Zn-Al]) are shown in TABLE 6.2.

TABLE 6.2 - Interlayer spaces for different LDH structures in literature, considering the interlayer anion reported

Article	Interlayer anion	Ion diameter (nm)	Interlayer space (nm)*	Type of LDH
Xu et al. (2010)	Phosphate	0.476	0.320	[Ca-Al]-LDH
Zhou et al. (2012)	Phosphate	0.476	0.280	[Ca-Al]-LDH
Jia et al. (2016)	Phosphate	0.476	0.264	[Ca-Al]-LDH
Qian et al. (2012)	Phosphate	0.476	0.285	[Ca-Al]-LDH
Grover et al. (2010)	Arsenate	0.422	0.294	[Ca-Al]-LDH
Halajnia et al. (2013)	Phosphate	0.476	0.313	[Mg-Al]-LDH
Halajnia et al. (2013)	Nitrate	0.400	0.313	[Mg-Al]-LDH
Halajnia et al. (2013)	Sulfate	0.46	0.322	[Mg-Al]-LDH
Cheng et al. (2009)	Phosphate	0.476	0.305	[Zn-Al]-LDH

In these different cases, none of them showed interlayer space to fit an ion on the regular size, indicating that some other factors – such as the accommodation of structural water in interlayer space – are playing an important role. Therefore, is believed that the interaction between the layers and water molecules leads to the distortions on the interlayer anion verified on the literature and in this work. In fact, the anion distortion was

theoretically predicted for hydrocalumite structure.[170] The values found for the interlayer space in our materials suggests the same pattern from literature, showing that phosphate intercalation between [Ca-Al]-LDH layers is possible (Appendix C- TABLE C1). Then we may consider that the anion (phosphate adsorbed by the [Ca-Al]-LDH in range 0.83mM-3.31 mM) is probably interacting by two main ways: (1) on the external surface of hydrocalumite and (2) on the interlayer space.

Xu et al.[165] and Zhou et al.[171] concluded that [Ca-Al]-LDH are capable of adsorbing high phosphate concentrations by a dissolution-reprecipitation mechanism: LDH with Ca^{2+} ions at the lamellae composition are more soluble that LDH containing Mg^{2+} ions.[108] In this case, PO_4^{3-} anions react with Ca^{2+} cations released from LDH dissolution, forming insoluble hydroxyapatite ($Ca_5(PO_4)_3OH$) because of the much lower hydroxyapatite solubility product ($K_{sp} = 2 \times 10^{-58}$). Furthermore, at different experimental conditions, including temperature, pH and saturation level, other phases may be formed from dissolved Ca^{2+} ions, such as tricalcium phosphate ($Ca_3(PO_4)_2$), octacalcium phosphate ($Ca_8H_2(PO_4)_6 \cdot 5H_2O$), monetite ($CaHPO_4$), brushite ($CaHPO_4 \cdot 2H_2O$), tetracalcium phosphate ($Ca_4(PO_4)_2O$) and amorphous calcium phosphate (amorphous $Ca_9(PO_4)_6 \cdot xH_2O$) (Xu et al., 2010; Zhou et al., 2012). Similarly, [Ca-Al]-LDH calcination leads to formation of mayenite, which is known to react rapidly with water.[172] Once in contact with the high phosphate concentrated solution, new calcium-phosphate phases were formed.

Thermal stability and further compositional data of [Ca-Al]-LDH samples loaded with PO_4^{3-} were assessed by TGA (FIGURE 6.3). Overall, mass loss events occur in three different temperature ranges. TABLE 6.3 summarizes total mass loss percentages of the different PO_4^{3-}-loaded samples obtained by SR and IE along with their qualitative composition at 25°C. The first mass loss stage (40 – 160 °C) may be ascribed to desorption of surface water and dehydration (removal of interlayer water) in case of hydrocalumite-like phase.[122] The second mass loss stage (190 – 270°C) relates to dehydroxylation of hydrocalumite-like phase, or desorption of surface water from hydroxyapatite and tetracalcium phosphate phases, which are highly stable up to 700 °C.[122,123,173] Accordingly, the last mass loss stage occurring above 450°C may be associated with decomposition of PO_4^{3-} anions or transition of non-stoichiometric tetracalcium phosphate to stoichiometric phases.[122,123]
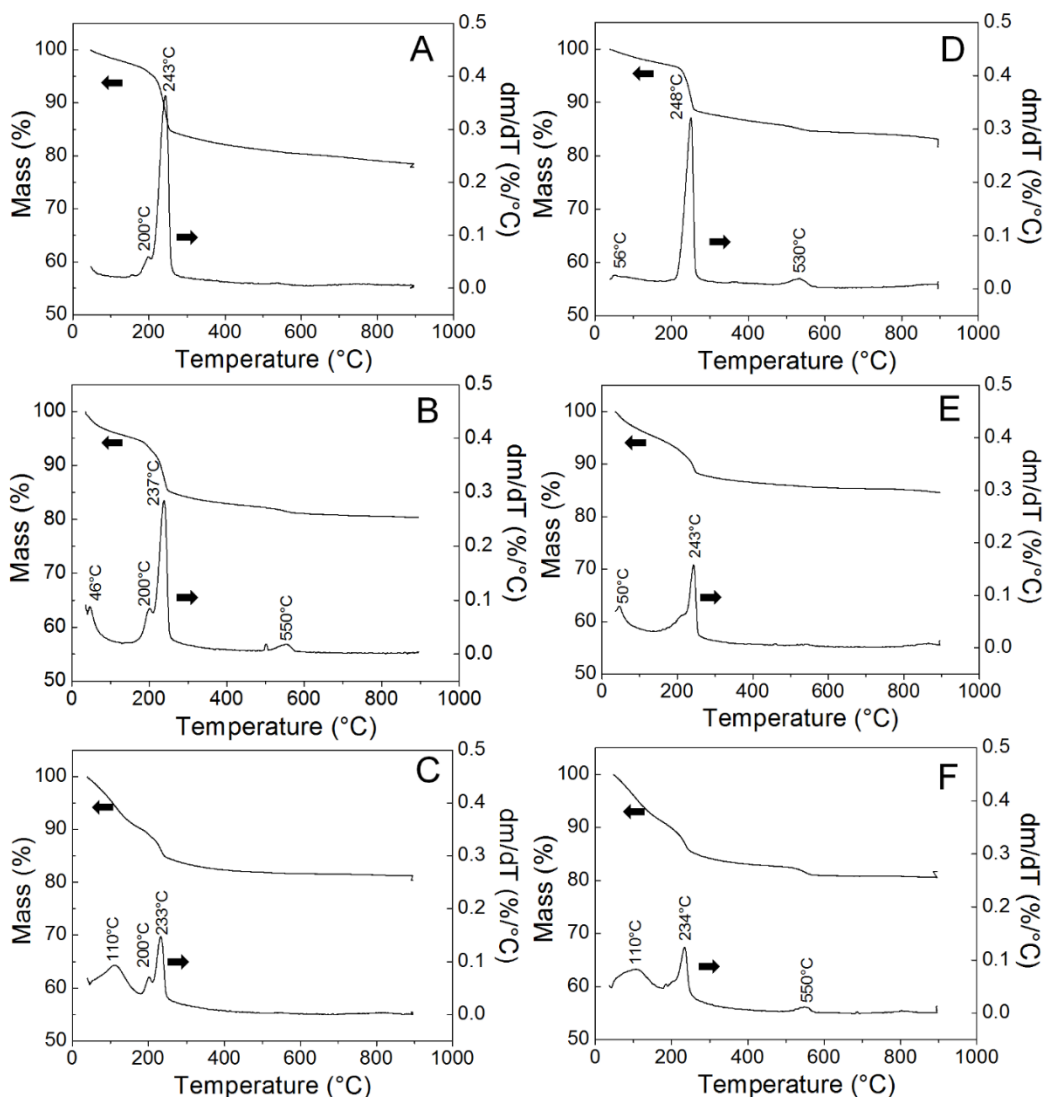
FIGURE 6.3 - Thermogravimetric (TG) and differential thermogravimetric (DTG) curves of samples loaded with PO_4^{3-} by structural reconstruction from initial PO_4^{3-} concentrations of (A) 6.62 mM, (B) 11.58 mM and (C) 33.10 mM, and by ion exchange process from initial PO_4^{3-} concentrations of (D) 6.62 mM, (E) 11.58 mM and (F) 33.10 mM. (TG/DTG curves relating the other initial PO_4^{3-} concentrations are in Appendix C (FIGURE C2a and FIGURE C2b).

TGA results clearly show that mass loss effects in the $[Ca-Al-PO_4^{3-}]$-LDH are reduced with increasing initial PO_4^{3-} concentration. For [Ca-Al]-LDH samples synthesized in pure water, the total mass loss percentage was about 36%. This percentage reduced to approximately 18% in samples obtained either by SR or IE in presence of 33.10 mM PO_4^{3-} (TABLE 6.3).

This behavior confirms transition of hydrocalumite-like phase to hydroxyapatite and tetracalcium phosphate starting at 6.62 mM PO_4^{3-}, as revealed by PXRD. This occurs because hydroxyapatite and tetracalcium phosphate are thermally more stable

than hydrocalumite, and PO_4^{3-} groups entrapped into their crystalline structures are not eliminated at temperatures below 700°C, conversely to the thermal behavior of LDH, whose interlayer anions are usually removed at temperatures exceeding 600 °C.[17]

TABLE 6.3 - TGA data of PO_4^{3-}-loaded samples obtained by SR and IE

PO_4^{3-} (mM)	SR		IE	
	Mass loss (%)	Composition*	Mass loss (%)	Composition*
0	36.24	Hydrocalumite	35.40	Hydrocalumite
0.83	34.48	Hydrocalumite	32.35	Hydrocalumite
1.65	29.43	Hydrocalumite	30.35	Hydrocalumite
3.31	26.97	Hydroxyapatite	20.38	Hydrocalumite
6.62	21.51	Hydroxyapatite	16.88	Hydroxyapatite
11.58	19.64	Hydroxyapatite	15.44	Hydroxyapatite
16.55	19.87	Tetracalcium phosphate	16.17	Hydroxyapatite
26.48	22.19	Tetracalcium phosphate	19.43	Tetracalcium phosphate
33.10	18.81	Tetracalcium phosphate	18.34	Tetracalcium phosphate

From SEM micrographs, the morphological differences in sample structure with increasing PO_4^{3-} concentration are clear. FIGURE 6.4-A shows that hydrocalumite is comprised of plate-like crystals, which is the typical habit of the mineral. For both adsorption routes at concentration of 3.31mM (FIGURE 6.4-B and FIGURE 6.4-E), samples presented evidences of lamellae structure, however, there was no evidence of hexagonal crystals.

At intermediate concentrations (FIGURE 6.4-C and FIGURE 6.4-F) crystals displaying needle-like morphology are seen, which is typical of hydroxyapatite, the main crystalline phase at this concentration.[174] At very high PO_4^{3-} concentrations, it occurs formation of tetracalcium phosphate. For structural reconstruction (FIGURE 6.4-D), the main phase has a granular shape, while for the ion exchange (FIGURE 6.4-G) crystal having irregular morphology are detected.
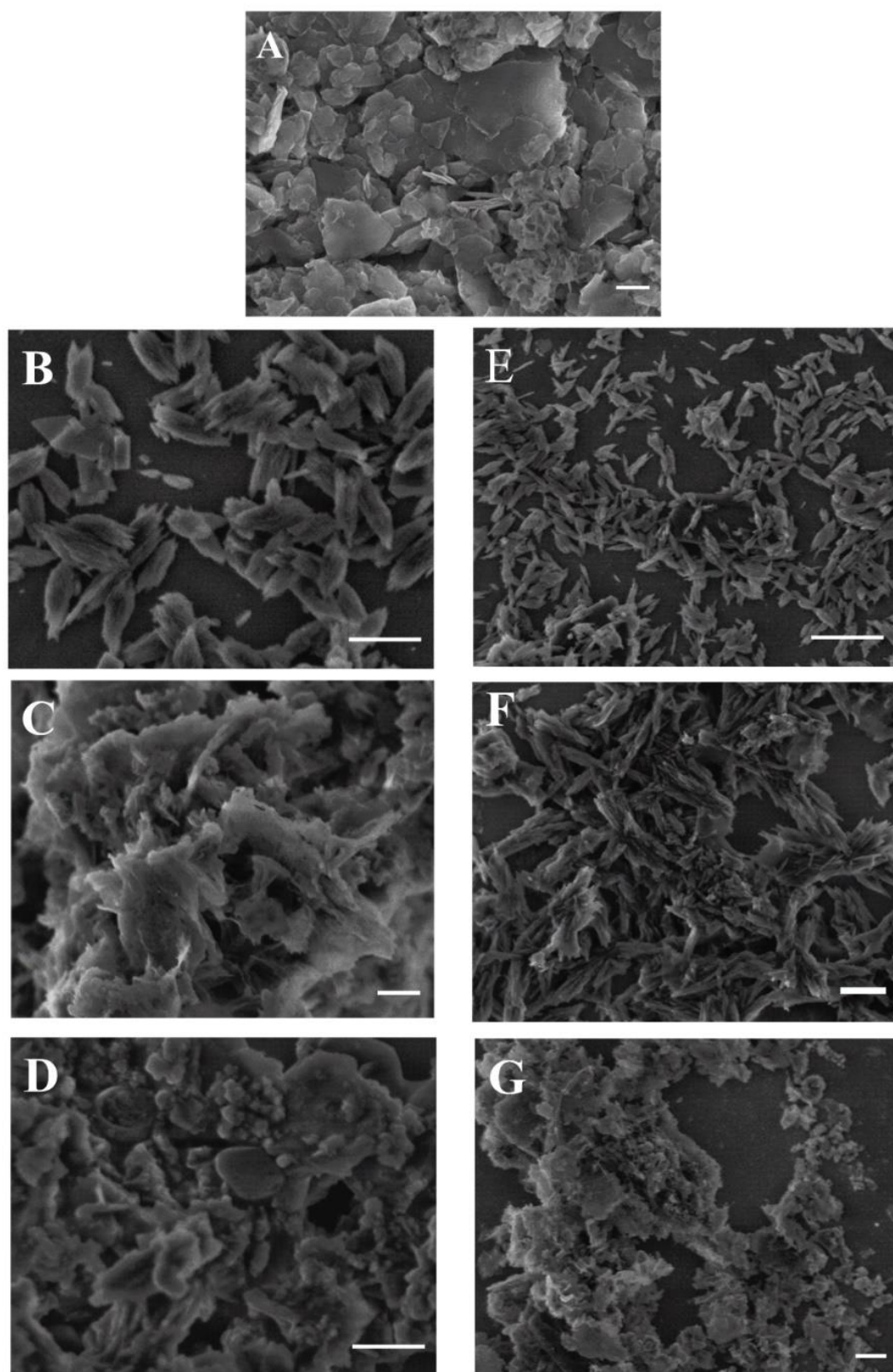
FIGURE 6.4 - SEM micrographics of (A) synthetic [Ca-Al]-LDH; (B) [Ca-Al]-LDH SR-3.31mM; (C): [Ca-Al]-LDH SR- 11.58 mM; (D): [Ca-Al]-LDH SR-33.10mM; (E): [Ca-Al]-LDH IE- 3.31mM; (F): [Ca-Al]-LDH IE- 11.58 mM; (G): [Ca-Al]-LDH IE- 33.10 mM. All scale bars correspond to 300 nm

In order to verify the chemical environment of the ^{31}P and [27]Al atoms in [Ca-Al-PO$_4$[3-]]-LDH, the NMR technique was performed. From ^{31}P NMR, samples obtained from both adsorption routes presented the same shape lines with increasing PO$_4$[3-] concentration. KH$_2$PO$_4$ displays a ^{31}P single resonance at 4.0 ppm indicating that P atoms are in tetrahedral molecular geometry. After PO$_4$[3-] adsorption in the [Ca-Al]-LDH, hydroxyapatite and calcium phosphate are formed and the resonance peak slightly displaced to 2.70 ppm (FIGURE 6.5 and TABLE 6.4). These results are in accordance with previous reports,[78] where Ca-P compounds exhibit faintly cross-polarizes and therefore contains a limited number of protons in the direct vicinity of the P nuclei, identified as apatite. Concerning [27]Al, the chemical shift at about 10 ppm is suggested to represent aluminum at a pentahedrally coordinated environment.[78]
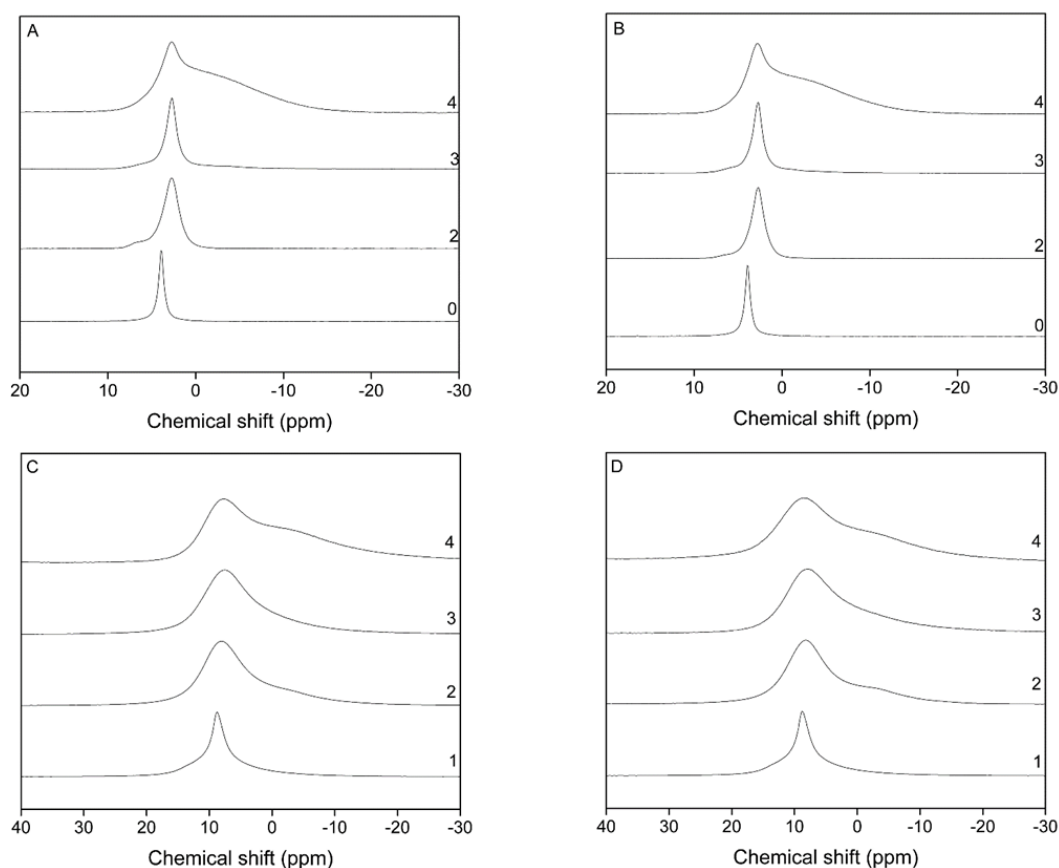
FIGURE 6.5 - (A) ^{31}P NMR spectra for [Ca-Al]-LDH SR (B) ^{31}P NMR spectra for [Ca-Al]-LDH IE; (C) ^{27}Al NMR spectra for [Ca-Al]-LDH SR; (D) ^{27}Al NMR spectra for [Ca-Al]-LDH IE. (0): KH$_2$PO$_4$; (1) Pristine [Ca-Al]-LDH; (2) 3.31 mM; (3) 11.58 mM; (4) 33.10 mM.

Despite no changes in aluminum coordination have been noted, peaks are broad and it is generally characteristic of multiple different chemical environments, probably due to formation of new crystalline phases.[80]

TABLE 6.4 - Chemical shifts of ^{31}P NMR and ^{27}Al NMR resonances for [Ca-Al]-LDH SR and [Ca-Al]-LDH IE in different PO_4^{3-} solutions.

PO_4^{3-} (mM)	[Ca-Al]-LDH SR		[Ca-Al]-LDH IE	
	^{31}P	^{27}Al	^{31}P	^{27}Al
0		8.74		8.74
0.83	2.63	9.56	2.69	8.75
1.65	2.63	9.47	2.69	8.53
3.31	2.72	8.01	2.69	8.23
6.62	2.74	7.87	2.78	7.93
11.58	2.72	7.59	2.69	7.80
16.55	2.67	7.71	2.69	7.78
26.48	2.67	7.87	2.74	7.72
33.10	2.68	7.65	2.78	8.38

6.3.3 - *Influence of [Ca-Al]-LDH loaded with PO₄³⁻ on Bradyrhizobium elkanii growth*

In order to examine the influence of the different main PO_4^{3-}-rich phases on *Bradyrhizobium elkanii* growth, selected [Ca-Al]-LDH samples loaded with PO_4^{3-} (1.65 mM, 11.58 mM and 33.10 mM) by IE and SR were examined. *Bradyrhizobium* is a genus well-known for their interaction with legume crops.[158,175] It is responsible for nitrogen (N_2) fixation, other important element for plant growth. Also, due to its ability to expel acids, *Bradyrhizobium elkanii* can convert insoluble inorganic phosphorus compounds into available phosphate forms for plant roots.[158] The results are presented as colonies forming units (CFU) in FIGURE 6.6.
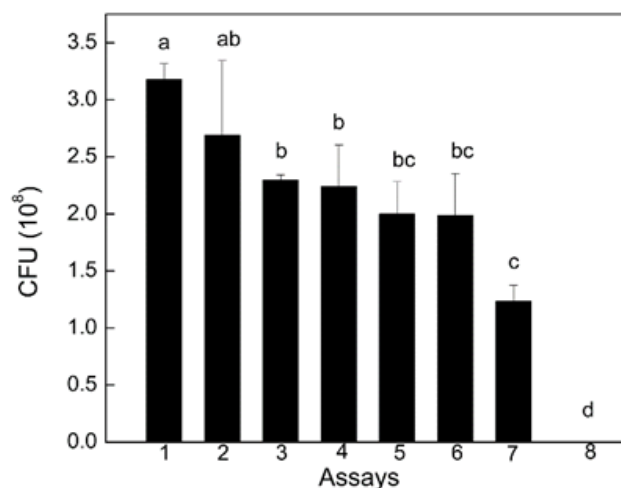
FIGURE 6.6 - Microorganisms assays for growth on the different materials: (1): [Ca-Al]-LDH IE-33.10 mM; (2): [Ca-Al]-LDH SR-11.58 mM; (3): [Ca-Al]-LDH SR-33.10 mM; (4): Negative control (without phosphate addition on regular medium); (5): [Ca-Al]-LDH IE-11.58 mM; (6): Positive control (regular medium); (7): [Ca-Al]-LDH IE-1.65 mM; (8): [Ca-Al]-LDH SR-1.65 mM. Averages with the same letter are not significantly different according to Duncan test.

Significant increase in bacterial growth was found for [Ca-Al]-LDH IE-33.10 mM, whose major crystalline phase is tetracalcium phosphate. However, no differences in growth were recognized when the samples [Ca-Al]-LDH R-33.10 mM, [Ca-Al]-LDH R-11.58 mM, [Ca-Al]-LDH IE-11.58 mM were used. This behavior may occur due to differences in solubility of the materials.

In addition, the negative control also showed some bacterial growth, which may be explained by the presence of other nutrients within the medium that can supply the *B. elkanii* requirements. On the other hand, the [Ca-Al]-LDH 1.65 mM sample, in which hydrocalumite is the principal crystalline phase, inhibited or reduced bacterial growth. In this case, pH may be determining on the bacteria growth. The ideal pH for *B. elkanii* growth is between 6.0 - 7.0.[159,176] When hydrocalumite is added to the culture medium the pH is increased to 10.0 - 11.0. This may explain the reduction or inhibition of *B. elkanii* growth.

The sample [Ca-Al]-LDH IE-33.10 mM may have acted as a controlled PO_4^{3-} release source. The PO_4^{3-} anions are gradually released to the medium as it is necessary to the bacterium. As the microbial mass increases, more PO_4^{3-} anions will be available to growth of the bacteria as well as they will be bioavailable to legume crops (FIGURE 6.7). Additionally, with increasing microbial mass, more N_2 could be fixed into the soil. Thus, the [Ca-Al-PO_4^{3-}]-LDH demonstrates enormous potential to be applied as a phosphate source

for legume crops and to promote development of microbial mass, contributing indirectly to the nitrogen requirements of cultivation.
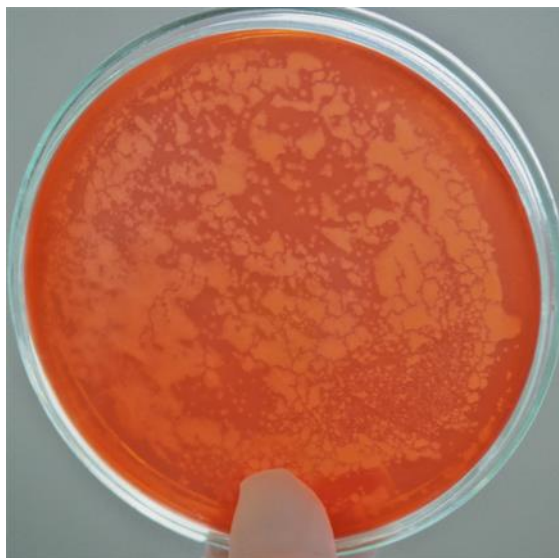
FIGURE 6.7 - Colonies of *Bradyrhizobium elkanii* at solid medium with congo red dye.

6.4   - Conclusions

In conclusion, the adsorption of PO_4^{3-} in [Ca-Al]-LDH was examined with respect to ion exchange process and the so-called "memory effect". In both routes, similar crystalline phases were formed (at lower concentrations, hydrocalumite with adsorbed phosphate; at intermediate concentrations, hydroxyapatite; and higher concentrations calcium phosphate), however the amount of phosphate adsorbed on [Ca-Al]-LDH was superior for ion exchange process to that found from the "memory effect", due to the differences in surface area of the materials. *Bradyrhizobium elkanii* is an important microorganism for nitrogen fixation in soil and consequent improvement of legume crops yields. The [Ca-Al]-LDH IE-33.10mM sample significantly increased the growth of this bacterium. As [Ca-Al-PO_4^{3-}]-LDH are eco-friendly compounds, they have enormous potential to be used in leguminous crops and raise agriculture production.

7 - Chapter V: The profile of [Mg-Al]-LDH of release is confirmed on dynamic systems?

The content of this chapter is an adaptation of the article entitled **"Controlled Release of Phosphate from Layered Double Hydroxide Structures: Dynamics in Soil and Application as Smart Fertilizer"** by Marcela P. Bernardo, Gelton G. F. Guimarães, Vinicius F. Majaron and Caue Ribeiro, published for ACS Sustainable Chemistry and Engineering.

Controlled Release of Phosphate from Layered Double Hydroxide Structures: Dynamics in Soil and Application as Smart Fertilizer

Marcela P. Bernardo,*[†,‡] Gelton G. F. Guimarães,[‡] Vinicius F. Majaron,[†,‡] and Caue Ribeiro[†,‡]

7.1 - Introduction

Phosphorus is an essential nutrient for plant growth and its deficiency causes major abiotic stress that limits crops productivity.[177,178] Highly weathered acidic Oxisols and Ultisols account for over 70% of phosphorus-deficient soils in the tropics, of which nearly 50% are found in tropical America. [179,180] Consequently, poor phosphorus uptake from soil is an important limiting factor for achieving optimal yields in agriculture. [181,182]

According to the International Plant Nutrition Institute (IPNI) the consumption of phosphate fertilizers in Brazil (one of the world leaders in the production and export of agricultural products) was 5.000 tons in 2016, three times more than rate register for the world. Appropriate fertilizer management is crucial from economic perspective, to maximize productivity and profitability, optimize the use of the soil, and reduce the need for new cultivated areas.[12] In addition, has to consider possible "side effects" of mismanagement of phosphate fertilizer, specifically nutrient pollution of streams or other surface water near crop fields. Water can be polluted with phosphorus primarily by erosion and runoff of phosphate from the soil. These losses may have serious effects on the quality of water. The main problem with phosphorus pollution is eutrophication resulting in excessive growth of plants and algae in the water. [183]

Conventional agricultural techniques are often associated with poor fertilizer management and inefficient use of nutrients by plants, leading to low yields and potential damage to the environment. Excessive phosphate applications are unhelpful, because phosphate becomes unavailable to plants due to immobilization by precipitation with cations, especially Fe^{3+} and Al^{3+}.[184,185]

The use of controlled release fertilizers can avoid excessive application of phosphate, preventing its immobilization in the soil and providing a more constant phosphate availability after soil fertilization.[186] Therefore, the actual effect of these materials regarding the phosphate stock for soil fertility, being available for use in future harvests. The benefits provided by controlled release in immediate plant production increase are still under debate.[187-191]

Various techniques can be employed for the controlled release of phosphate,[185,187] including the use of layered double hydroxides (LDH),[20] known as "anionic clays" due to structural resemblance with the cationic clays, exhibit high anion exchange capacity and good affinity for phosphate.[56] LDH have the general formula $[M^{2+}_{1-x}M^{3+}_{x}(OH)_2]^{x+}[A^{n-}]_{x/n} \cdot yH_2O$, where M^{2+} and M^{3+} are di- and trivalent metallic cations, respectively, A^{n-} is a charge-balancing anion, and x is the molar ratio $M^{3+}/(M^{3+} + M^{2+})$,

ranging from 0.1 to 0.5.[57] The LDH crystalline structure consists of positively charged brucite-like ($Mg(OH)_2$) lamellae in which trivalent cations replace isomorphic divalent cations at the octahedral sites.[193] The net positive charge of the LDH lamellae is then counterbalanced by A^{n-} species in the interlamellar domains.[109] Due to its characteristic structure, LDH provides physical protection to intercalated phosphate ions, decreasing the direct contact of these ions with the soil. [12] The potential of LDH as matrices for the controlled release of phosphate into solution has been explored,[34,76] and promising results have been obtained for release of the nutrient in soil.[12,125] However, the mechanism of phosphate release in the soil environment has not been described, and information is lacking concerning possible phosphate immobilization and the performance of this fertilizer class compared to other available sources of phosphate.

The present work proposes a simple methodology for the preparation of phosphate-loaded LDH, the structural reconstruction, with analysis of the behavior of this fertilizer in the soil environment, as the phosphate dynamics at soil, and its effect on the growth of wheat. The interaction of phosphate with the soil was evaluated by sequential extraction and NMR techniques, and investigation was made of the phosphate contents of grown crops and the amounts of phosphate remaining in the soil.

7.2   - Experimental Section

7.2.1   - Materials

Monobasic potassium phosphate was purchased from Synth (Brazil). Commercial hydrotalcite ($Mg_6Al_2(CO_3)(OH)_{16}.4H_2O$) was purchased from Sigma-Aldrich. Monoammonium phosphate (MAP) was provided by Adubos Vera Cruz (Ibaté, São Paulo, Brazil). All reagents were used as received. Decarbonated deionized water ($\rho = 18.2$ MΩ cm) obtained from a Milli-Q system (Barnstead Nanopure Diamond, Thermo Fisher Scientific Inc., USA) was used in all the experimental procedures.

7.2.2   - Phosphate adsorption by the reconstruction method

The adsorption of phosphate was performed using the so-called "memory effect" or reconstruction method.

The commercial [Mg-Al]-LDH was thermally treated at 600 °C for 4 h in a muffle furnace, using a programmed heating rate of 30 °C.min^{-1}. The experimental conditions required to form crystalline LDH products were previously set by testing the structural reconstruction of calcined LDH samples in pure water at temperatures of 25 °C and 75 °C (Appendix D- FIGURE D1).

Then, 500 mg of the calcined material were added to 250 mL of 16.6 mM

KH_2PO_4 solution previously equilibrated at 75 °C, with pH adjusted to 7 using 0.1 M NaOH, to prevent hydroxyl from occupying the interlayer space. The mixture was continuously agitated for 24 h, followed by centrifugation at 11,200 g for 10 min. The final pH of the suspension was found to be approximately 12. Considering the pKa^{III} of the phosphoric acid ($pKa^{III} = 12.67$) the predominant anion in suspension is phosphate after achieving the pKa^{III} value, but it may also be possible that other dissociated forms of phosphoric acid ($H_2PO_4^-$ and HPO_4^{2-}) occurred in the medium at some extent. The solid was resuspended in water for storage in a freezer, and was lyophilized under vacuum of 1.33×10^{-4} bar (SuperModulyo freeze dryer, Thermo Fisher Scientific Inc., USA), yielding a white powder used for solid characterization.

7.2.3 - *Characterization*

Powder X-ray diffraction (PXRD) measurements were performed using a Shimadzu XRD 6000 diffractometer with Ni-filtered Cu K_{α} radiation ($\lambda = 1.5405$ Å), in the 2θ range 5–70°, with a scan speed of 2° min^{-1}. Interlamellar spaces were calculated using Bragg's law. Scanning electron microscopy (SEM) employed a JEOL microscope operated at 15 kV. ^{27}Al and ^{31}P MAS-NMR analyses were carried out using a Bruker 9.4 T Avance III HD spectrometer operated at frequencies of 104.215 and 161.904 MHz for ^{27}Al and ^{31}P, respectively. The ^{31}P spectra were acquired with proton decoupling, using a 90° pulse (2.5 µs), 25 ms acquisition time, 10 s recycle delay, and 1000 scans. The ^{27}Al spectra were acquired without proton decoupling, using a 30° pulse (1.5 µs), 16 ms acquisition time, 1 s recycle delay, and 500 scans. For both ^{31}P and ^{27}Al analyses, the samples were packed in a 5 mm cylindrical zirconium rotor and subjected to magic angle spinning at 10 kHz. Fourier transform infrared analyses (FTIR) were performed using a Bruker spectrometer, with spectral resolution of 2 cm^{-1}. Thermal degradation was evaluated using a TGA Q500 thermogravimetric analyzer (TA Instruments, USA) operated with an atmosphere of nitrogen (60 $mL.min^{-1}$) and heating from 25 to 500 °C at a rate of 10 $°C.min^{-1}$.

7.2.4 - *Kinetics of phosphate release in water*

The kinetics of phosphate release from $[Mg-Al-PO_4]$-LDH ($[Mg_{0.75}Al_{0.25}(OH)_2]$ ($0.1PO_4$).$0.92H_2O$) was compared with the release from a soluble phosphate source (KH_2PO_4) and a soluble phosphate fertilizer (MAP). Amounts of the powdered materials corresponding to 2.5 mg of phosphate were added to 125 mL of water (pH 6.5), with initial $(HCO_3)^-$ content of $3.33. 10^{-3}$ $mol.L^{-1}$. After 2, 4, 6, 8, 10, 15, 20, 30, 60, and 120 minutes, samples were removed and centrifuged at 11,200 g for 10 min. The pH after phosphate release was 7.5. The solid was then resuspended in water for freezing and

lyophilization prior to the characterization analyses. Quantification of magnesium was performed by ICP-AES (VISTA PRO-CCD, Varian, Mulgrave, Australia). The operating conditions are represented at Appendix D (TABLE D1). Quantification of phosphate was performed by the phosphoantimonylmolybdenum blue complex method.[70] For this, 5 mL of supernatant was mixed with 2 mL of ascorbic acid solution (0.4 M), 0.2 mL of citric acid solution (0.03 M), and 2 mL of a reagent consisting of sulfuric acid solution (4.7 M), 5.5 mL of ammonium molybdate (0.08 M), and 0.6 mL of antimony and potassium tartrate (0.05 M). This mixture was then allowed to react for 15 min in a water bath at 50 °C to form the phosphoantimonylmolybdenum blue complex, which was measured using a PerkinElmer Lambda 25 UV-Vis spectrophotometer operated at a wavelength of 880 nm. All the experiments were performed in triplicate.

For each phosphate material, fitting was performed using a nonlinear logistic model (Equation 1), adopting a significance level of 5%. These procedures employed R software (v. 3.3.3).

$$Y = a/(1+b*\exp(-c*\text{time})) \quad\quad\quad (7)$$

where a is the asymptote, $a/(1+b)$ is the initial value, and c is the velocity parameter.

7.2.5 - Release and availability of phosphate in soil

The release into soil of phosphate from the [Mg-Al-PO$_4$]-LDH, KH$_2$PO$_4$, and MAP materials was evaluated using a typical tropical soil (Oxisol) collected from the surface layer (0-20 cm) of an agricultural plot in the region of São Carlos (São Paulo State, Brazil). The soil was air-dried and sieved through a 2 mm screen, prior to physicochemical characterization. Textural analysis by the pipette method[196] showed that the soil consisted of 631 g.kg^{-1} sand, 37 g.kg^{-1} silt, and 332 g.kg^{-1} clay. The water-holding capacity was 150 g.kg^{-1}.[197] The pH (H$_2$O) was 4.63, measured with a glass electrode, and the organic carbon content was 9.65 g.kg^{-1}, measured by the Walkley-Black method.[198] A standard technical procedure[197] was used to determine the following parameters: potential extractable acidity (H+Al) (3.5 cmol$_c$.kg^{-1}); exchangeable Al^{3+} (0.4 cmol$_c$.kg^{-1}); exchangeable Ca^{2+} (0.54 cmol$_c$.kg^{-1}); available Fe (50 mg.kg^{-1}); cation exchange capacity (CEC) (4.27 cmol$_c$.kg^{-1}); and available phosphorus (P) (0.5 mg.kg^{-1}). The method described by Alvarez et al.[199] was used to determine the remaining phosphorus (P-rem) (14.5 mg.L^{-1}).

To compare the release and dynamics of phosphate from [Mg-Al-PO$_4$]-LDH, KH$_2$PO$_4$, and MAP in soil, 20 g portions of soil (in triplicate) were placed in 100 mL polyethylene bottles, followed by application and homogenization in the soil of each

fertilizer source to supply a dose 5 mg of phosphorus, in other words a concentration of 250 mg $P.kg^{-1}$. The moisture content was adjusted to 80% of water holding capacity (WHC) by adding 2.4 mL of deionized water to 20 g of soil. Individual samples for each period were incubated for 0, 3, 7, 14 and 30 days kept at 25 °C under aerobic conditions and constant moisture, with periodic addition of deionized water whenever necessary. After different incubation periods, the total soil sample was air-dried and then crushed to pass through a 2 mm screen.

The available phosphate was extracted with anionic resin using anion exchange membranes (AMI-7001S, Membranes International Inc., USA), as described elsewhere.[200] The membranes were cut into strips of 2.0 x 5.0 cm and were treated as described by Gatiboni,[201] employing washes with HCl (0.5 mol L^{-1}), water, and $NaHCO_3$ (0.5 mol L^{-1}).

Samples (2.5 g) of the incubated soil were transferred to 50 mL polyethylene centrifuge tubes containing 40 mL of distilled water, followed by insertion of a strip of AMI (10 cm^2), treated as described above, and the suspensions were gently agitated for 16 h in an orbital shaker. The phosphate absorbed by the membrane was extracted into 40 mL of HCl (0.5 mol L^{-1}), with agitation for 2 h in a shaker. The phosphate contents in the soil extracts were then measured by the phosphoantimonylmolybdenum blue method. Sequential chemical fractionation of phosphate was performed as described previously.[202] Samples (2.5 g) of the incubated soil were sequentially extracted (in triplicate) by addition of 40 mL volumes of different extractant solutions, in the following order: 1 M NH_4Cl, 0.5 M NH_4F (pH 8.2), 0.5 M $NaHCO_3$ (pH 8.5), 0.1 M NaOH + 1 M NaCl, and 1 M HCl. For the first two extractions, the soil and solution were shaken for 1 h, while all the other extractions employed shaking for 18 h. After each extraction, the solution was centrifuged at 11,200 g for 10 min, the supernatant was collected for subsequent phosphate determination, and the remaining soil was resuspended in the next extraction. These extractions solubilized phosphate present in forms ranging from the most labile to the most stable, operationally defined as follows: easily desorbable (1 M NH_4Cl); Al-associated (0.5 M NH_4F at pH 8.2); easily mineralizable organic P ($NaHCO_3$ at pH 8.5); Fe-bound P (0.1 M NaOH + 1 M NaCl); and Ca-bound P (1 M HCl). The phosphate contents of the soil extracts were determined as described previously, and the amounts of available phosphate and the phosphate associated with each chemical fraction of the soil were expressed as percentages of the total phosphate incorporated into the soil.

7.2.6   - Phosphate uptake by wheat

Experiments were performed using 300 mL plastic pots containing 0.25 kg of the same soil described above. At the start of the trial, a soil correction was performed with the addition of limestone 880 mg.kg^{-1} soil (size lower of 100 µm) to provide soil base saturation of 60% (pH after correction: 5.4).[203] The soil samples were mixed and incubated for 30 days, maintaining the soil at 80% of WHC (30 mL of water per pot). After this period, equivalent amounts of phosphorus (P) (150 mg.kg^{-1}) from each phosphate source (MAP, KH_2PO_4, and [Mg-Al-PO$_4$]-LDH) were applied to the individual pots, with mixing. A control treatment without phosphorus addition was also included. Seven wheat seeds (*Triticum aestivum*: BRS 254) were placed in each pot, followed by moisture adjustment and application of a nutrient solution containing NH_4NO_3, $MgCl_2$, K_2SO_4, H_3BO_3, $CuSO_4$, $ZnSO_4$, and $(NH_4)_6Mo_7O_{24}$.[204] A nutrient solution containing KCl was also applied only to the pots treated with MAP and LDH, in order to provide the same K dose as the KH_2PO_4 treatment. A smaller dose of the NH_4NO_3 solution was applied to the soil fertilized with MAP to maintain the same N dose of the other treatments and the Mg content on [Mg-Al-PO$_4$]-LDH exercises no influence on the availability of this nutrient to crops because this nutrient is not present in limited quantities and the LDH structure is well maintained, as following discussed. The pots were exposed to natural light, at 17-29 °C, under humidity of 40-50% (measured on a daily basis). After germination, five plants were retained in each pot. Soil moisture content was maintained constant by applying distilled water with a pipette. After 30 days of growth, the wheat plants were collected, dried at 70 °C for 72 h, and the aerial parts were ground in a Wiley mill to obtain samples with granulometry smaller than 1 mm. The samples were digested with nitro-perchloric acid,[205] and phosphate analyses were performed using the phosphoantimonylmolybdenum blue method.[70]

For all the samples, the soil pH was determined after 30 days of plant growth. For this, 10 g of soil was mixed with 25 mL of water for 30 min, under agitation, followed by decanting and measurement of the pH of the supernatant using a glass electrode.

The labile phosphate remaining in the soil after the incubation was determined by mixing 10 g of soil with 100 mL of Mehlich 1 extractant (0.05 M HCl + 0.0125 M H_2SO_4) overnight, according to a standard procedure,[197] with analysis by the phosphoantimonylmolybdenum blue method.

The results of dry matter production and phosphate uptake by the wheat plants were presented as mean values and standard deviations. Differences among the

treatments were evaluated by statistical analysis using ANOVA and Tukey's test, performed with Statistica® software.

7.3 - *Results and Discussion*

7.3.1 - *Memory effect and phosphate interaction*

The reconstruction method was first examined by PXRD after reconstruction in pure water. FIGURE 7.1A shows PXRD patterns for commercial LDH, the calcined product, and the material obtained in water. The [Mg-Al]-LDH diffractogram corresponded to a hexagonal lattice with rhombohedral 3R symmetry, typical of the LDH structure. In addition, the basal spacing of the (003) reflection was calculated to be 7.56 Å, which is in accordance with values typically reported for hydrotalcite.[17,206]

After calcination at 600 °C, the LDH structure was completely lost and reflections indexed to MgO (Fm-3m, JCPDS 45-0946) appeared, meaning that the LDH structure was efficiently collapsed by thermal dehydration.[109] However, when the calcined materials were hydrated, typical LDH PXRD patterns were again identified, but the basal spacing increased to 7.64 Å. This slight increase is related to arrangement of carbonate anion on the interlayer space, which presence was essential to re-organize the layered structure in the absence of other counterions. However, at $2\theta = 44°$ is possible to observe one peak related to spinel phase (MgO), remaining from the calcination process. The success in the instauration of structural reconstruction in water provided a possible route for phosphate adsorption.

Once in contact with 16.6 mM KH_2PO_4 solution, the calcined product showed the typical LDH PXRD patterns, with a shift of the (003) peak to low angles, indicating a 0.2 Å increase of the *d* space, according to Bragg's law (FIGURE 7.1B) (basal space = 7.80 Å). This increase on the interlayer space suggested that accommodation of the phosphate anions in the interlayer spaces was associated with distortions of the layers and interactions with water molecules.[67,110] In addition, new peaks index as monoclinic bobierrite phase of $Mg_3(PO_4)_2 \cdot 8H_2O$ (C2/c, JCPDS 33–0877) are found. This suggests that intercalation of phosphate and the precipitation of bobierrite on [Mg-Al]-LDH occurred in parallel.

Preservation of the crystalline structure during equilibrium between LDH and phosphate is essential in order to obtain LDH able to act as a phosphate fertilizer. Phosphate content analysis revealed a phosphorus (P) concentration of 42.4 mg.g LDH^{-1}. The vibrational spectra for the materials are represented at Appendix D- FIGURE D2.
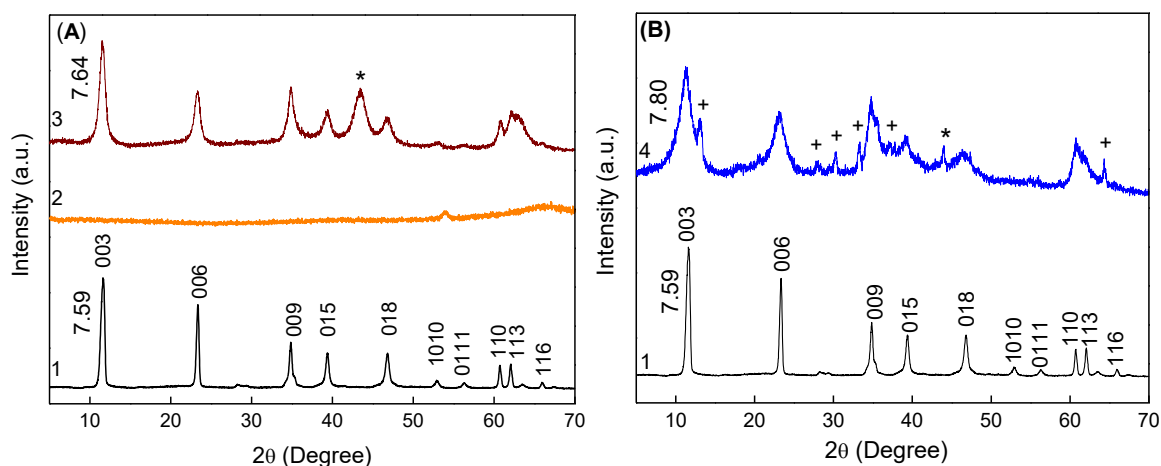
FIGURE 7.1 - PXRD patterns for structural reconstruction in water (A) and in phosphate solution (B): (1) pristine [Mg-Al]-LDH; (2) calcined [Mg-Al]-LDH; (3) [Mg-Al]-LDH reconstructed in water; (4) [Mg-Al]-LDH reconstructed in 16.6 mM of phosphate. The basal space value is in angstrom. *: spinel phase; +: bobierrite phase.

The SEM micrographs revealed changes in the LDH structure after phosphate adsorption and indicate the incorporation of phosphate in the LDH (FIGURE 7.2). The morphology of the commercial [Mg-Al]-LDH was characterized by the presence of hexagonal plate-like crystals, as expected for crystalline LDH structure (FIGURE 7.2-A). After phosphate adsorption, it is possible to observe a resembling hollow architecture particle agglomerated and a small secondary phase appeared, probably due to the large amount of adsorbed phosphate. These structural modifications have been described in previous work.[109]

The thermal stability of [Mg-Al]-LDH and the product obtained after phosphate adsorption were assessed by TGA. Figure 3A clearly shows four events for weight loss of [Mg-Al]-LDH. The first mass loss stage (at 220 °C) was related to the desorption of water from the surface equivalent to 11% of mass loss. [122] The second significant mass loss, at 298 °C, could be attributed to dehydroxylation of the LDH structure (~8%). The third event (298-411°C) are related to the loss of water interleaved between the LDH layers(~17%). The final mass loss, at 411-500 °C, was due to the loss of CO_3^{2-} as CO_2 (~7%).[121,207] The thermal stability of the material reconstructed in water present similar mass losses, however the mass loss temperature was slight lower (FIGURE D3- Appendix D). After phosphate adsorption, only three mass loss events were observed (FIGURE 7.3B), and there is no mass loss related to adsorbed phosphate in accordance with the work of Benicio et al.[12] and Bernardo et al.[110] Frost et al.[208] working with intercalation of

different anions also noticed no mass loss related to the adsorbed anion. The first one at 30-155 °C of 14% mass loss corresponding to dehydration due to the loss of H_2O molecules.
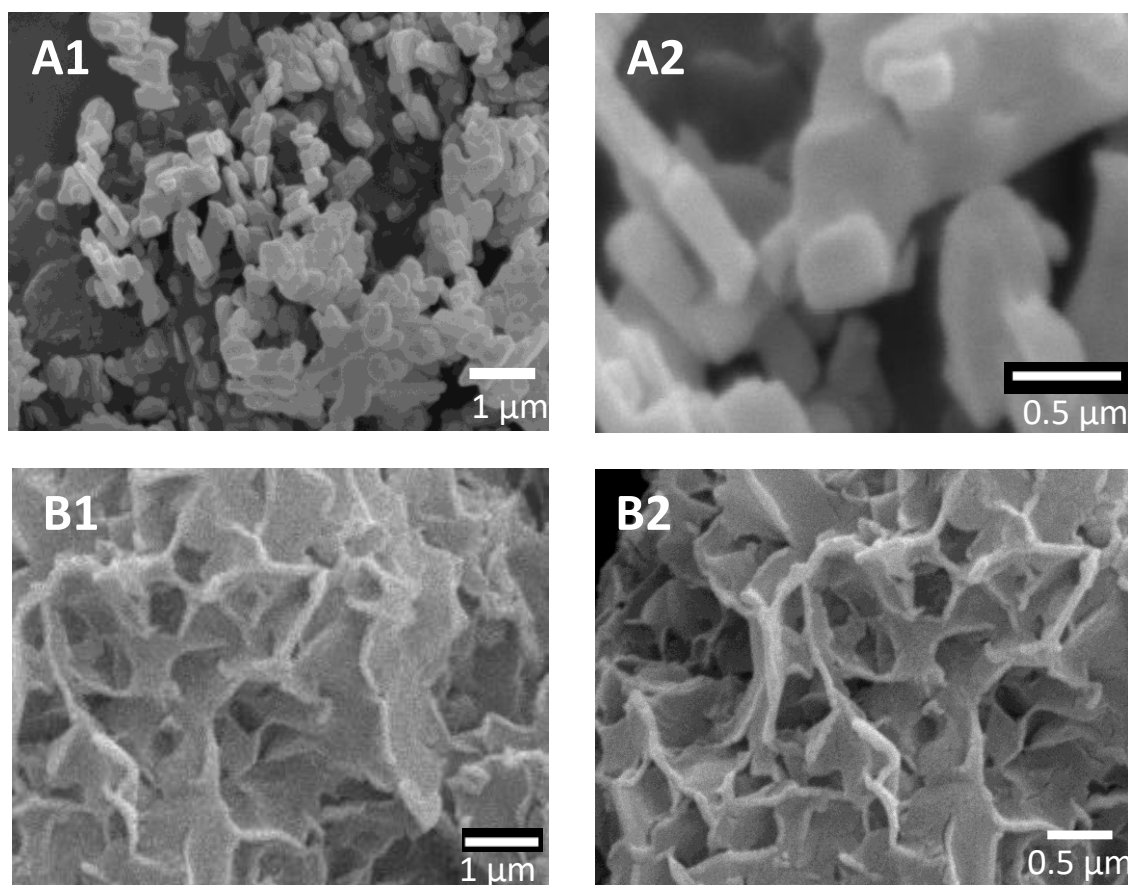
FIGURE 7.2 - Scanning electron micrographs of (A1 and A2) commercial [Mg-Al]-LDH and (B1 and B2) [Mg-Al-PO$_4$]-LDH.

The second one (155-300°C) attributed to the release of intercalated water molecules linked to phosphate ions by strong hydrogen bonds, of 11%. Finally, the third event at 300-500°C the mass loss of 7% are related to loss of water molecules from layers dihydroxylation.[121]
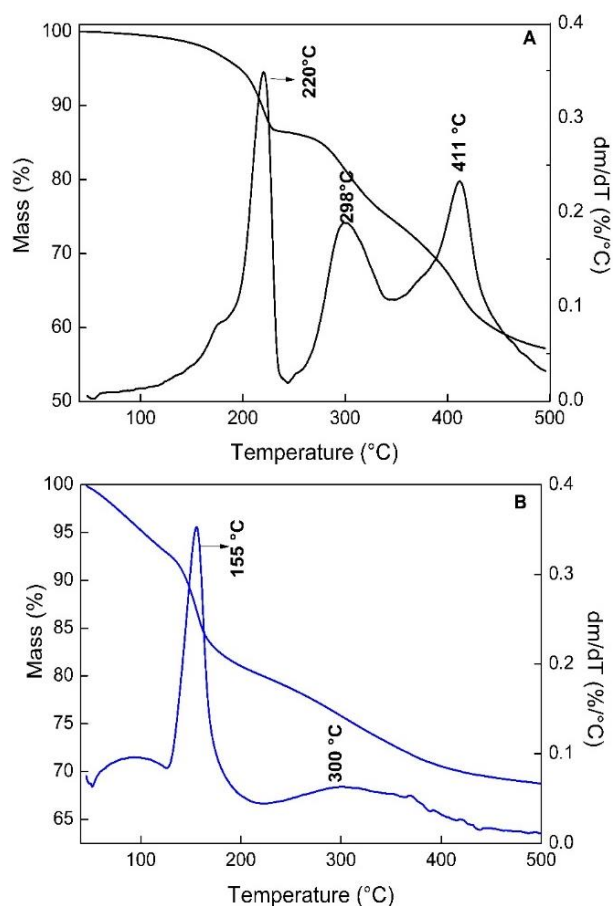
FIGURE 7.3 - Thermogravimetric (TG) and differential thermogravimetric (DTG) curves of (A) the commercial [Mg-Al]-LDH and (B) the [Mg-Al]-LDH sample loaded with phosphate by structural reconstruction.

7.3.2 - *Kinetics of phosphate release in water*

The kinetics of phosphate release was investigated to understand the release behaviors of the different phosphate sources in water (TABLE 7.1, FIGURE 7.4A). KH_2PO_4 and MAP showed 90% phosphate release within 5 min, as expected for soluble phosphate sources and indicating that the nonlinear logistic model (Equation 7) was not applicable. The different initial P availabilities of the soluble sources could be related to the surface reactivity, which is determined by the crystal habit and morphology (Figure D4- Appendix D). These differences were not significant for longer times and only influenced the initial solubility. The behavior exhibited by [Mg-Al-PO4]-LDH for immediate release of the phosphate associated with the external surfaces of [Mg-Al-PO4]-LDH is given mainly by ion exchange with hydroxyl groups, while the intercalated anions were delivered slowly by ion exchange with carbonate and hydroxyl ions present in the water, considering the LDH scale of affinity (multivalent inorganic anions> OH^- > F^-> Cl^- > Br^- > NO_3^- > I^-).[12] The LDH material protected the phosphate against rapid release, with 90% release after ~53 min. Considering that KH_2PO_4 was the phosphate source for [Mg-Al]-LDH, the release time was extended 10-fold exclusively due to the presence of LDH. Concerning about the bobierrite

phase formed during the phosphate adsorption phase, it was dissolved after water release, without increase the Mg concentration in solution, and the LDH structure is well maintained (Appendix D- FIGURE D5). [Mg-Al-PO$_4$]-LDH is a proper material to be used for phosphate release, once presents superior release rates in water in comparison with release in alkaline mediums,[34,66,73,76] showing that phosphate interacts with [Mg-Al]-LDH is reversible which allows the use of [Mg-Al-PO$_4$]-LDH as phosphate source.

TABLE 7.1 - Statistical parameters for the release into water of phosphate from each source.

Fertilizer	R²	Fitted parameters			Initial release	Time for 90% release
		a	b	c	%	min
KH$_2$PO$_4$	0.87	100.02***	15.2**	1.08***	6.16	5:36
MAP[#]	-	-	-	-	$\hat{y} = \bar{y} = 92.72$	0:02
[Mg-Al-PO$_4$]-LDH[@]	0.92	92.39***	12.32**	0.12***	6.93	52:42

Nonlinear model: y=a/(1+b*exp(-c*time)). Significance (t-test): *** 0.001; ** 0.01. #: Fitting was not possible for MAP because the P was released immediately, with an average value of $\hat{y} = \bar{y} = 92.72$. @ Mg concentration in solution after phosphate release was ~1.86mg.L^{-1}, equivalent to ~2.3% of total content of Mg, according to ICP-AES measurements.

After 120 min, 6.7% of the phosphate was retained in the LDH structure. The NMR technique is an important tool to comprehend the phosphate interaction in this case. The ^{31}P NMR analysis of [Mg-Al-PO$_4$]-LDH before phosphate release (Figure 7.4B) showed one intense and sharp peak at 4.82 ppm, attributed to phosphorus tetrahedral coordination,[78,80] as expected for phosphate intercalated in LDH at this concentration.[109] Side bands related to the rotor rotation were also present. After the release process, two peaks were found, at 1.96 and 4.82 ppm. Broad peaks (such as the peak at 1.96 ppm) are characteristic of elements with less mobility in the matrix, while sharp and well defined peaks (such as the peak at 4.82 ppm) are related to elements with greater flexibility. [209] Therefore, that phosphate released until 120 min are expressed in ^{31}P NMR by the peak at 4.82 ppm, which has more mobility and was easily released. However, the fraction that was not release after 120 min (~10%) are strongly interacting with LDH structure and are represented at ^{31}P NMR by the peak 1.86 ppm, typical of elements with less mobility.

Prior the phosphate release, the peak at 1.96 ppm was probably overlapped by the 4.82 ppm peak, due to the high concentration of phosphate easily released.
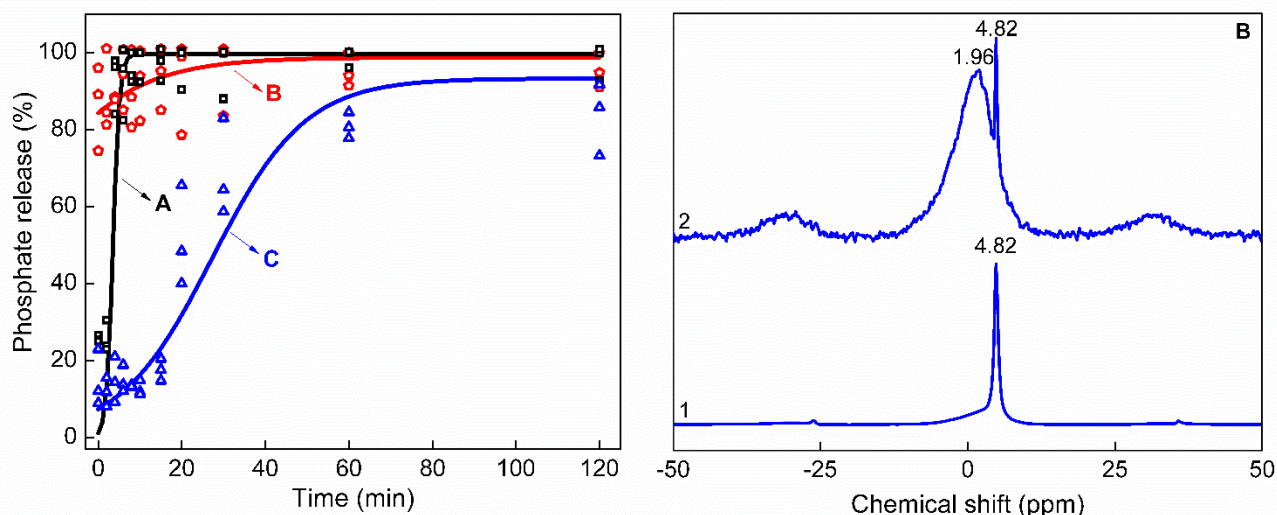
FIGURE 7.4 - (A) Kinetics of phosphate release into water (measurements in triplicate) and fitted curves obtained using the logistic model: (A) KH_2PO_4, (B) MAP, and (C) [Mg-Al-PO_4]-LDH; (B) ^{31}P NMR analysis of [Mg-Al-PO_4]-LDH before (1) and after (2) phosphate release.

Once the ability of [Mg-Al-PO_4]-LDH to release phosphate in water has been established, it was important to understand the release behavior in soil, as well as the dynamics of this macronutrient and its interactions with other elements present in tropical soils that have high capacities for phosphate adsorption.

7.3.3 - *Release and availability of phosphate in soil*

In the soil incubation experiments, the MAP-treated soil samples presented initial phosphate recovery (as available phosphate, extracted with anionic resin) of around 85% (FIGURE 7.5), while the samples treated with KH_2PO_4 and [Mg-Al-PO_4]-LDH showed values of 40 and 50%, respectively. The different recoveries of phosphate from the soluble sources could be attributed to the rapid availability of P from MAP (FIGURE 7.4 and D4(Appendix D)), as well as the different counterions of the phosphate sources, which resulted in different diffusivity coefficients. The high MAP solubility also has some influence on the results. [210,211] In [Mg-Al-PO_4]-LDH, the phosphate is protected by the interlayer space of LDH, which explains the low rate of recovery of phosphate by the anionic resin. [212]

After three days of incubation, all the phosphate recovery rates were quite similar, regardless the source, and similar trends were observed during the course of the trial. In addition to the available phosphate, other phosphate interactions could be identified, for instance, immobilization by soil microbiota followed by subsequent release during mineralization processes, as well as complexation by Fe^{3+}, which makes phosphate unavailable for further use by plants. [4] In the next step, sequential extraction was performed

in order to investigate the influence of the phosphate source on the dynamics of the element in the soil.
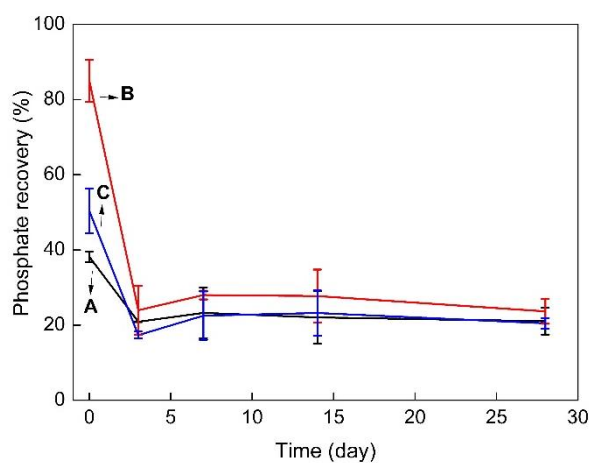
FIGURE 7.5 - Analysis of available phosphate extracted with anionic resin using anion exchange membranes after incubation of soil with (A) KH_2PO_4, (B) MAP, and (C) [Mg-Al-PO_4]-LDH**.**

The results of the sequential chemical fractionations of soil incubated with MAP, KH_2PO_4, and [Mg-Al-PO_4]-LDH are shown in FIGURES 7.6A, 7.6B, and 7.6C, respectively. No interaction between the phosphate and calcium was observed, due to the low calcium concentration (0.54 $cmol_c.kg^{-1}$) in this Oxisol, as reported elsewhere.[213] The interaction of phosphate with Ca is more significant in soils with basic pH.[214] The sequential chemical extraction enabled distinction between the interactions of phosphate with Al^{3+} and Fe^{2+}/Fe^{3+}. Despite the high exchangeable Al^{3+} concentration (0.4 $cmol_c.kg^{-1}$), little interaction of Al with phosphate was observed during the incubation period (FIGURES 7.6A, 7.6B, and 7.6C). The results of the ^{27}Al NMR analyses of the soils at the start and end of the incubations revealed that there were no changes in Al^{3+} coordination (FIGURE 7.7), which remained octahedral in a stable compound (probably as $Al(OH)_3$).[50] These results were in agreement with the findings of Reeve and Sumner,[215] which showed no apparent relationship between phosphate fixation and exchangeable Al^{3+}, suggesting that phosphate fixation was the result of an adsorption reaction rather than a precipitation reaction. An important point is that even the aluminum present in the LDH structure did not restrict the availability of phosphate in soil (consequently to the plants), probably due to preservation of the LDH structure during the phosphate release process.

Around 30-34% of the extracted phosphate showed interaction with Fe^{3+}. The tropical soil (Oxisol) used in this experiment did not undergo pH correction and therefore maintained its acidic characteristics (pH 4.63 and potential extractable acidity (H + Al) of

3.5 $cmol_c.kg^{-1}$). At low pH, Fe^{3+} ions presents high solubility, which favors the interaction with phosphate.[216] The commercial fertilizer (MAP) showed a slightly higher interaction of phosphate with Fe^{3+} ions (34%), compared to $[Mg-Al-PO_4]$-LDH (30%). The amounts of easily desorbed phosphate (the phosphate immediately available to plants) decreased during the course of the incubation period, probably due to interaction with Fe^{3+} ions.

The easily mineralizable organic phosphate is an important phosphate fraction that is readily available to crops. For all the phosphate sources used in the soil release experiment, the concentration of phosphate associated with easily mineralizable organic matter decreased slightly between 15 and 30 days, at the same time that the Fe-phosphate interaction increased. The microorganisms present in the soil can act as mineralization agents that convert phosphate into forms able to react with the other elements present in the environment. Nevertheless, significant amounts of phosphate were found for the easily mineralizable organic fraction, which remained available to crops. Similar rates of phosphate recovery from the organic fraction, of around 25%, were obtained for the $[Mg-Al-PO_4]$-LDH and KH_2PO_4 treatments. A slightly higher recovery of approximately 35% was obtained for the MAP treatment, although the amount of phosphate that interacted with Fe^{3+} ions was correspondingly higher, so a significant part of the phosphate present in the commercial fertilizer was immobilized and consequently was unavailable to crops. The values for the sequential extraction for the pure soil are represent in Appendix D (FIGURE D6).

Considering the total amount of phosphate recovered at the end of 30 days- that means, the sum of the identified phosphate fractions- (FIGURE 7.6D), 50% of the fractions of phosphate released from KH_2PO_4 and $[Mg-Al-PO_4]$-LDH could be identified, while 65% of the phosphate from MAP had identifiable interactions with the soil. The remaining P fraction that was not quantified in the sequential extraction was likely to have been present in organic or residual recalcitrant forms (which represent a substantial fraction of soil phosphate).[202] These forms were not extracted in the procedure employed in the present work.
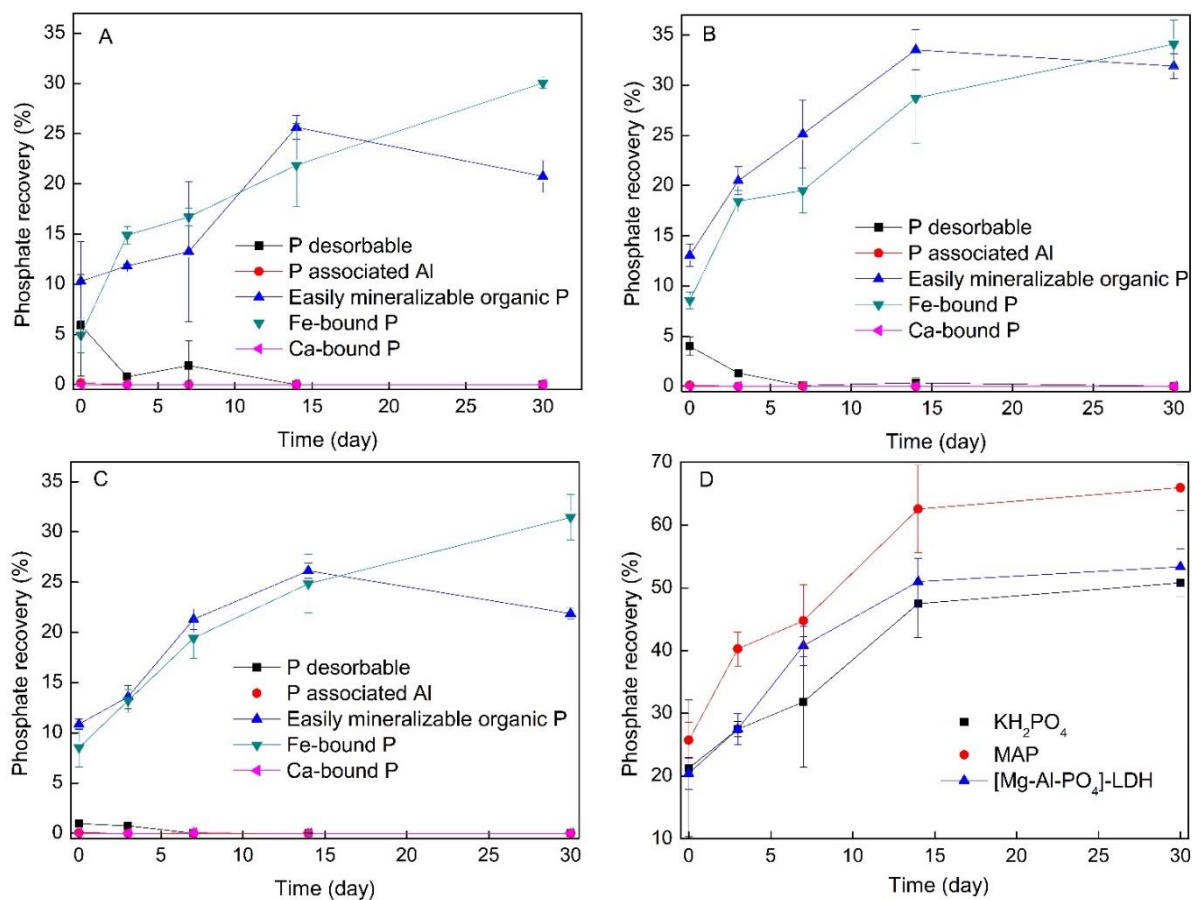
FIGURE 7.6 - Phosphate determination by sequential extraction of soil incubated with (A) KH₂PO₄, (B) MAP, and (C) [Mg-Al-PO₄]-LDH. (D) Total P recovered in the sequential extractions for the materials studied.
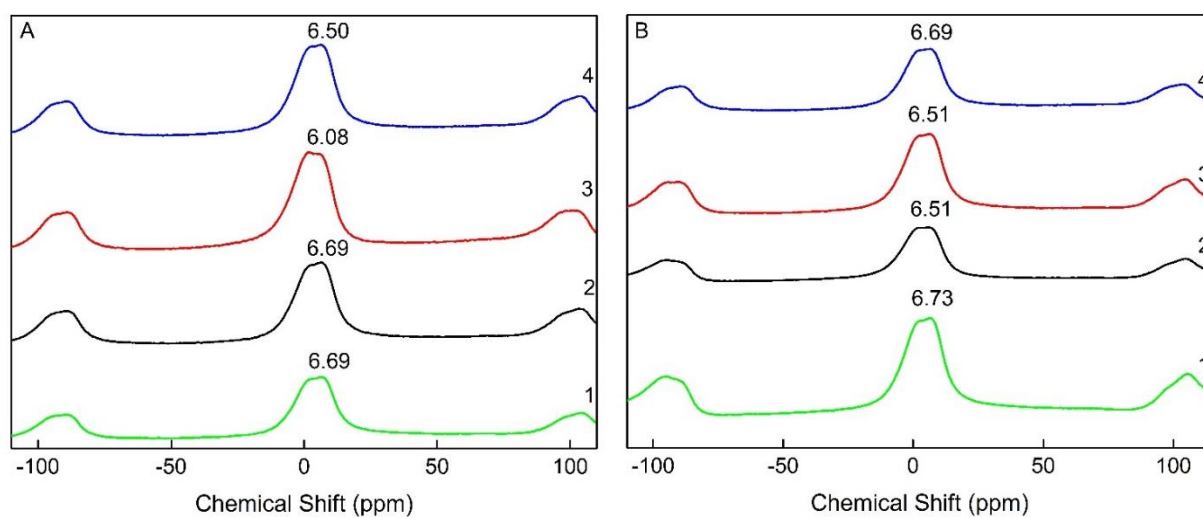

FIGURE 7.7 - ^{27}Al NMR spectra of soil (A) before and (B) after the incubation for 30 days: (1) soil (control); (2) soil incubated with KH₂PO₄; (3) soil incubated with MAP; (4) soil incubated with [Mg-Al-PO₄]-LDH.

7.3.4 - Phosphate uptake by wheat crops

The potential of [Mg-Al-PO$_4$]-LDH for use as a controlled release fertilizer for crops was evaluated in the cultivation of wheat plants, using the same soil type employed in the previous assays.

Equivalent doses of phosphorus (150 mg.kg^{-1}) from each phosphate source studied were applied individually to wheat plants. Analysis of the phosphate contents showed that [Mg-Al-PO$_4$]-LDH provided performance equivalent to the commercial phosphate fertilizer (MAP) and the soluble phosphate salt (KH$_2$PO$_4$) (TABLE 7.2). Thirty days after planting (FIGURE 7.8), the dry masses of the aerial parts were in the range 0.8-0.89 g.pot^{-1}, while the phosphate contents were 2.13 and 2.57 mg.pot^{-1} for [Mg-Al-PO$_4$]-LDH and KH$_2$PO$_4$, respectively. These results demonstrated that [Mg-Al-PO$_4$]-LDH was able to provide phosphate in a short time and in a similar way as the commercial fertilizer. However, the extraction with Mehlich 1 solution showed that the amount of phosphate available for release to plants from LDH was significantly higher than the amounts available from the other sources (TABLE 7.2). In other words, only a fraction of the phosphate content of [Mg-Al-PO$_4$]-LDH was released after 30 days.

TABLE 7.2 - Statistical analysis of wheat dry matter production, P content, pH, and available P.

Treatment	Dry matter (g.pot^{-1})	Phosphate content (mg.pot^{-1})	pH	Available phosphate (mg.pot^{-1})
Soil	0.36 (0.06) b	0.15 (0.03) b	5.25 (0.05) b	0.330 (0.01) c
KH$_2$PO$_4$	0.88 (0.03) a	2.57 (0.40) a	5.15 (0.06) b	4.694 (0.25) b
MAP	0.89 (0.04) a	2.34 (0.21) a	5.15 (0.19) b	4.564 (0.80) b
[Mg-Al-PO$_4$]-LDH	0.80 (0.08) a	2.13 (0.11) a	7.18 (0.05) a	7.448 (0.75) a

Values within a column followed by the same letter do not differ significantly (Tukey's test; $P < 0.05$). The values in parentheses are the standard deviations.
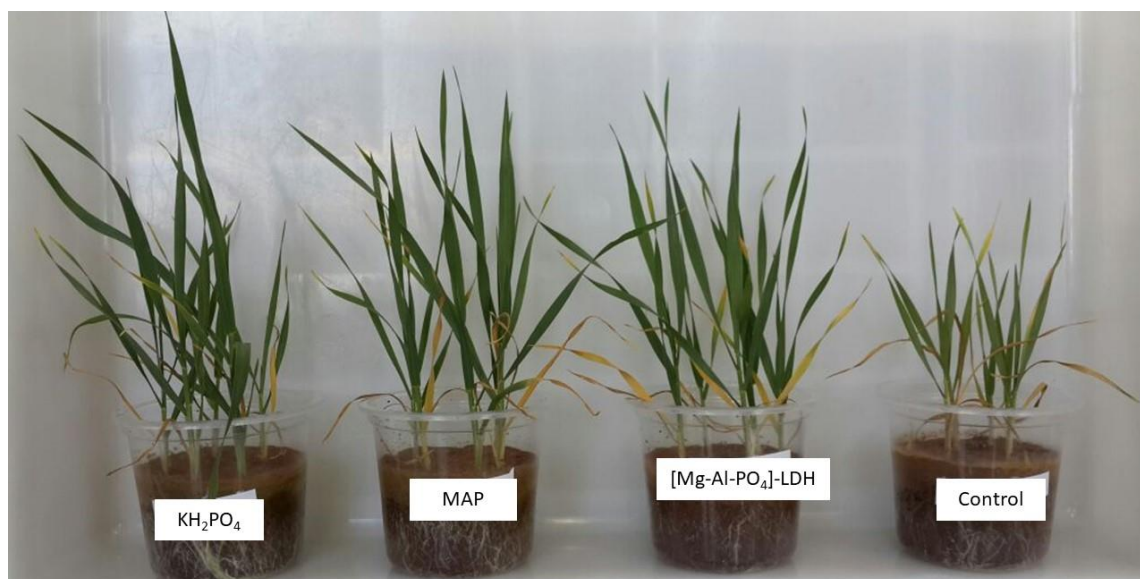
FIGURE 7.8. Wheat crops 30 days after sowing for the different treatments: control (without any phosphate source), KH_2PO_4, MAP, and $[Mg-Al-PO_4]$-LDH.

The release profile shown by $[Mg-Al-PO_4]$-LDH is desirable for a smart fertilizer, since a significant fraction of the phosphate remains protected from interaction with the soil (fixation or losses) and is available to be released over an extended period (around 1.5 times longer than for the other sources tested- see TABLE 7.2: available phosphate). $[Mg-Al-PO_4]$-LDH was able to stock phosphate for soil fertility, leaving available for use in future harvests. An important difference between $[Mg-Al-PO_4]$-LDH and the other phosphate treatments was the pH of the soil after the cultivation period. A higher pH was obtained when $[Mg-Al-PO_4]$-LDH was used as the phosphate fertilizer for the wheat seedlings, compared to the other phosphate sources. This capacity of $[Mg-Al-PO_4]$-LDH to increase pH is especially significant in the case of tropical soils, since the phosphate is maintained in solution and its availability to crops is enhanced due to reduced anion adsorption.[217,218] Substantial improvements in fertilization efficiency can be obtained using phosphate fertilizers capable of generating environmental pH conditions that favor the formation of anionic forms that can be absorbed by plants. [210] This increase on soil pH of $[Mg-Al-PO_4]$-LDH involves the exchanging of phosphate by CO_3^{2-} anion, which is the anion with higher affinity for LDH structure. Phosphate is a weaker Lewis base compared to CO_3^{2-} then, during this release process, pH should increase since phosphate will be consumed by plants.

Overall, the productivity obtained with $[Mg-Al-PO_4]$-LDH was statistically similar to the results obtained with KH_2PO_4 and MAP, while both the pH and the

availability of phosphate to the plants were higher for the [Mg-Al-PO$_4$]-LDH treatment. As demonstrated in other studies, the aluminum present in the LDH structure had no effect on the immobilization of phosphate.[12,125] No alteration of the Al^{3+} chemical environment was observed after the soil incubation.

7.4   - Conclusions

A layered double hydroxide ([Mg-Al]-LDH) was investigated for the controlled release of phosphate in soil, which is a desirable feature for phosphate fertilizers. Our main interest was to understand how the anionic change, which takes place in LDH structures, could favor the long-term phosphate management in soil, which was benefic in terms of low immobilization. Physicochemical characterization revealed that the LDH was able to maintain the layered structure and to incorporate phosphorus at a concentration of 42.4 mg.g^{-1}, using a structural reconstruction strategy. The results indicated that structural reconstruction provided a fertilizer with higher phosphate loading (compared to similar controlled release fertilizers), which was able to maintain a significant amount of phosphate available in the soil after the development of wheat plants. The release was not influenced by the Al^{3+} content of the LDH (which could have been a major drawback for its use). Fe^{3+} was shown to be the most important phosphate immobilizing agent in soil, and ^{27}Al and ^{31}P NMR analyses elucidated the interactions of phosphate with Al^{3+}. The findings highlighted the potential of this new class of fertilizers, as keeper of long term soil fertility, supporting their use in agricultural applications. Therefore, we believe that this paper is not enough for designing a full product (which was not the aim of this paper) but supports further research to apply LDH as fertilizer adjuvants, illustrating which are the clear advantages and limitations of these materials for fertilizer design.

8 - Chapter VI: General Conclusions

In this thesis we have demonstrated that the cation M^{2+} size has remarkable influence on the release mechanism of the interlayer anion and it is an important characteristic to be considered for the applications of these materials. Also, other remarks may be highlighted:

❖ LDH composed of Mg^{2+} and Al^{3+}, with open structures, has higher adsorption and desorption capacity than other possible LDH structures, thus application as phosphate reservoirs are a potential field for use of this material;

❖ Phosphate desorption phases is essentially an ion-exchange reaction that occurs at both interlamellar domains and outer surface of LDH structure.

❖ LDH with tiny structure, as [Ca-Al]-LDH and [Zn-Al]-LDH, strongly interacts with phosphate – leading to phase changes – and keep phosphate more stable. However, at proper mediums (such as artificial saliva and culture medium) they are able to release phosphate;

❖ [Mg-Al]-LDH may be used as fertilizer, being capable of providing adequate nutrition in a short time; and is able to stock phosphate for further release, avoiding phosphate interaction to plants with soil elements;

❖ The important role that LDH may have in different application fields is highlighted, confirm LDH as an important multifunctional material.

9 - Chapter VII: Future Research Propositions

In this work we search to use LDH as matrix for phosphate interaction. Great results were achieved, but the LDH has more potential to be explored:

❖ Other cations on the LDH structure can be studied for phosphate interaction; The interactions with nitrate, for instance, can be explored as well, for agricultural applications;

❖ Experiments with crops may be conduct at green house with different cultivars and prolongated times;

❖ The combination of LDH and polymers can be explored for slow up the release. Also, the nanocomposite formation would allow better manipulation of the material.

10 - References

1 . ISHERWOOD, K. F. O uso de fertilizantes minerais e o meio ambiente. ANDA, São Paulo, 2000. p. 63.

2. GOMES, A. S.; FERREIRA, L. H. G. & BENDER, R. R.; Uso do fosfato natural no cultivo de arroz, soja e milho em rotação, no sistema plantio direto. Pelotas, Embrapa Clima Temperado, 2005. p. 37.

3 . LOUREIRO, F. E. V. L. & MELAMED, R. O fósforo na agricultura brasileira: uma abordagem minero-metalúrgica. Rio de Janeiro, CETEM (Centro de Tecnologia Mineral), 2006. p.76.

4 . FERREIRA, L. H. G.; GOMES, A. S. & POSSER, C. A. Fosfatos naturais na adubação de sistema de culturas de verão com ênfase no arroz irrigado. Pelotas, Embrapa Clima Temperado, 2008. p.8.

5 . CONAB; Insumos fertilizantes entregues ao consumidor. [2013]. Disponível em: < http://www.conab.gov.br/OlalaCMS/uploads/arquivos/8547f3d5c1d69ca4c2c9d7920954516 a..pdf >. Acesso em: Dezembro 2017.

6 . FERNANDES, E.; GUIMARÃES, B. A. & MATHEUS, R. R. Principais empresas e grupos brasileiros do setor de fertilizantes. Rio de Janeiro, BNDES setorial, 2009. p. 228.

7 . NELSON, D. L. & COX, M. Princípios de Bioquímica de Lehninger. 6ª Ed. Porto Alegre, Artmed, 2014. p.1328.

8 . SHAW, L.; MURRAY, J.J.; BURCHELL, C.K. & BEST, J.S. "Calcium and phosphorus content of plaque and saliva in relation to dental caries." Caries Res., 17(6): 543, 1983.

9 . ELENA, M.; BENNETT, S. R.; CARPENTER N. & CARACO F. "Human impact on erodable phosphorus and eutrophication: a global perspective: increasing accumulation of phosphorus in soil threatens rivers, lakes, and coastal oceans with eutrophication." BioScience, 51 (3): 227, 2001.

10 . MANASSE, E. "Idrotalcite e piroaurite." Atti Soc. Toscana Sci. Nat., **24**: 92, 1915.

11 . KHAN, A. I. & O'HARE, D. "Intercalation chemistry of layered double hydroxides: recent developments and applications". J. Mater. Chem., 12(11): 3191, 2002.

12 . BENÍCIO, L. P. F.; CONSTANTINO, V.R.L.; PINTO, F.G.; VERGUTZ, L. TRONTO, J. & DA COSTA, L.M. "Layered double hydroxides: new technology in phosphate fertilizers based on nanostructured materials" ACS Sustainable Chem. Eng., 5(1): 399, 2017.

13 GOH, K.H.; LIM, T-T. & DONG, Z. "Application of layered double hydroxides for removal of oxyanions: A review." Water research. **42**:1343, 2008.

14 . EVANS, D.G. & SLADE, R.C.T. "Structural Aspects of Layered Double Hydroxides." In: Duan, X. & Evans, D. G. "Layered Double Hydroxides, Structure and Bonding Series." Springer Berlin Heidelberg, New York, 1-88, 2006.

15 . CREPALDI, E. L. & E VALIM, J.B. "Hidróxidos duplos lamelares: síntese, estrutura, propriedades e aplicações". Química Nova, 21(3): 300, 1998.

16 . WANG, Q. & O'HARE, D. "Recent advances in the synthesis and application of layered double hydroxide (LDH) nanosheets" Chem. Rev. **112**: 4124, 2012.

17 . CAVANI, F.; TRIFIRO, F. & VACCARI, A. "Hydrotalcite-type anionic clays: preparation, properties and applications." Catal. Today., **11**: 173, 1991.

18 . REICHLE, W.T. "Synthesis of anionic clay minerals (mixed metal hydroxides, hydrotalcite)." Solid State Ion., **22**:135, 1986.

19 . RIVES, V. "Characterisation of layered double hydroxides and their decomposition products" Mater. Chem. Phys., **75**:19, 2002.

20 . CARLINO, S. & HUDSON, M.J. "Thermal intercalation of layered double hydroxides: capric acid into an Mg–Al LDH." J. Mater. Chem. **5**: 1433, 1995.

21 . HOFMEISTER, W. & VON PLATEN, H. "Crystal Chemistry and Atomic Order in Brucite-related Double-layer Structures." Cryst Rev., **3**:3, 1991.

22 . MIYATA, S. "Physico-chemical properties of synthetic hydrotalcites in relation to composition." Clay Clay Miner. **28**:50, 1980.

23 . NEWMAN, S.P. & JONES, W. "Synthesis, characterization and applications of layered double hydroxides containing organic guests." New J Chem., **22**:105, 1998.

24 . RIVES, V.; ARCO, M. & MARTÍN, C. "Intercalation of drugs in layered double hydroxides and their controlled release: A review." Appl. Clay. Scien. **88**:239, 2014.

25 . ASHEKUZZAMAN, S.M. & JIANG, J.Q. "Study on the sorption–desorption–regeneration performance of Ca-, Mg and CaMg-based layered double hydroxides for removing phosphate from water." Chem. Eng. J., **246**: 97, 2014.

26 . SIPICZKI, M. Functional materials-syntheses, characterisation and catalytic applications, Szeged, Doctoral School of Chemistry, University of Szeged, 2013, PhD Dissertation, 79p.

27 . LI, F. & DUAN, X. "Applications of layered double hydroxides. Structure and Bonding." **119**: 193, 2005.

28 . SZILAGYI, I.; PAVLOVIC, M. & ROUSTER. P. "Immobilization of superoxide dismutase enzyme on layered double hydroxide nanoparticles" Int. J. Chem. Mol. Eng., 12(2):1,2018.

29 . DJEBBI, M.A.; BRAIEK, M.; HIDOURI, S.; NAMOUR, P.; RENAULT, N.J. & AMARA, A.B.H. "Novel biohybrids of layered double hydroxide and lactate dehydrogenase enzyme: Synthesis, characterization and catalytic activity studies." J. Mol. Struct., **1105**: 381, 2016.

30 . RAHMAN, M.B.A.; BASRI, M.; HUSSEIN, M.Z.; RAHMAN, R.N.Z.A.; ZAINOL, D.H. & SALLEH, A.B." Immobilization of lipase from Candida rugosa on layered double hydroxides for esterification reaction." Appl Biochem Biotech., **118**:313, 2004.

31 . CORMA, A.; FORNES, V.; MARTIN-ARANDA, R.M. & REY, F. "Determination of base properties of hydrotalcites: condensation of benzaldehyde with ethyl acetoacetate." J. Catal, **134**:58, 1992.

32 . YANG, K.; YAN, L.; YANG, Y.; YU, S.; SHAN, R.; YU, H.; ZHU, B. & DU, B. "Adsorptive removal of phosphate by Mg–Al and Zn–Al layered double hydroxides: kinetics, isotherms and mechanisms." Sep. Purif. Technol., **124**:36,2014.

33 . BISH, D.L. "Anion-exchange in takovite: applications to other hydroxide minerals." Bull Mineral, **103**:170, 1980.

34 . DAS, J.; PATRA, B.S.; BALIARSINGH, N. & PARIDA, K.M. "Adsorption of phosphate by layered double hydroxides in aqueous solutions." Appl. Clay Scien. **32**:252, 2006.

35 . MIYATA, S. "The Syntheses of Hydrotalcite-Like Compounds and Their Structures and Physico-Chemical Properties I: The Systems Mg2+-Al3+-NO3, Mg2+-Al3+-Cl-,

Mg2+-Al3+-ClO4-, Ni2+-Al3+-Cl- and Zn2+-Al3+-Cl-." Clays and Clay Miner., 23(5):369, 1975

36. SUN, J.; YUAN, L.; DAI Z.; LIU, X.; HUANG, T.; WU, J.; XU, Z. P. & XINGHUAI, SUN. "Sustained release of brimonidine from a new composite drug delivery system for treatment of glaucoma". ACS Appl. Mater. Interfaces, 9 (9): 7990, 2017.

37. LIANG, R.; WEI, M.; EVANS, D.G. & DUAN, X. "Inorganic nanomaterials for bioimaging, targeted drug delivery and therapeutics." Chem. Commun., **50**: 14071, 2014.

38. KHAN, A. I.; NORQUIST, A. J. & O'HARE, D. "Intercalation and controlled release of pharmaceutically active compounds from a layered double hydroxide" Chem. Commun., **0**: 2342, 2001.

39. WILLIAMS, G.R. & O'HARE, D. "Towards understanding, control and application of layered double hydroxide chemistry." J. Mater. Chem., **16**: 3065, 2006,

40. VERMA, A.; SHARMA, S.; GUPTA, P.K.; SINGH, A.; TEJA, B. V.; DWIVEDI, P.; GUPTA, G.K.; TRIVEDI, R. & MISHRA, P.R**.** "Vitamin B12 functionalized layer by layer calcium phosphate nanoparticles: A muco adhesive and pH responsive carrier for improved oral delivery of insulin" Acta Biomaterialia, **31**: 288, 2016.

41. CHOY, JH., KWAK, Y. S.; PARK, JS.; JEONG, YJ. & PORTIER, J. "Intercalative nanohybrids of nucleoside monophosphates and DNA in layered metal hydroxide." J. Am. Chem. Soc., 121 (6): 1399, 1999.

42. SHICHI, T.; TAKAGI, K.; SAWAKI, Y. " Stereoselectivity control of [2+2] photocycloaddition by changing site distances of hydrotalcite interlayers." Chem. Commun., **0**: 2027, 1996

43. ZU, Y.; LAIPAN, M.; ZHU, R.; XU, T.; LIU, J.; ZHU, J.; XI, Y.; ZHU G. & HE, H. "Enhanced photocatalytic activity of Zn/Ti-LDH via hybridizing with C60." Molec. Cat. **427**: 54, 2017.

44. DINARI, M.; MOMENI, M.M. & GHAYEB, Y. "Photodegradation of organic dye by ZnCrLa-layered double hydroxide as visible-light photocatalysts." J. Mater. Sci.: Mater. Electron. 27 (9): 9861, 2016.

45. LEI, C.; PI, M.; KUANG, P.; GUO, Y. & ZHANG, F. " Organic dye removal from aqueous solutions by hierarchical calcined Ni-Fe layered double hydroxide: Isotherm, kinetic and mechanism studies." J. Colloid Interface Sci., **496**:158, 2017.

46. LUO, L.; HE, B.; KONG, W. & WANG, Z.; "NiCo$_2$S$_4$/Ni–Co layered double hydroxide nanocomposite prepared by a vapor-phase hydrothermal method for electrochemical capacitor application." J. Alloys Compd.**705**:349, 2017.

47. CHEN, Y.Z.; HWANG, C.M. & LIAW, C.W. "One-Step synthesis of methyl isobutyl ketone from acetone with calcined Mg/Al hydrotalcite-supported palladium or nickel catalysts." Appl Catal A., **169**:207, 1998.

48. LIU, J.; CHENA, G. & YAN, J. "Preparation and characterization of poly(vinyl chloride)/layered double hydroxide nanocomposites with enhanced thermal stability." Polymer, 49(18):3923, 2008.

49. MANZI-NSHUTI, C.; HOSSENLOOP, J.M. & WILKIE, C.A. "Comparative study on the flammability of polyethylene modified with commercial fire retardants and a zinc aluminum oleate layered double hydroxide." Polym. Degrad. Stab., 94(5):782, 2009.

50 . BEYKE, M.H.; MOHAMMADIRAD, M.; SHEMIRANI, F.; SABOURY, A.A. "Magnetic cellulose ionomer/layered double hydroxide: An efficient anion exchange platform with enhanced diclofenac adsorption property" Carbohydr. Polym., **157**:438, 2017.

51 RAJAN, S.S.S.; O'CONNOR, M.B. & SINCLAIR, A.G. "Partially acidulated phosphate rocks: Controlled release phosphorus fertilizers for more sustainable agriculture." Fert Res., **37**:69, 1994.

52 . BERBER, M.R.; HAFEZ, I.H.; MINAGAWA, K. & MORI, T. "A sustained controlled release formulation of soil nitrogen based on nitrate-layered double hydroxide nanoparticle material." J Soil Sedim., **14**: 60, 2014.

53 . GILBERT, N. "The disappearing nutrient.", Nat., **461**:716, 2009.

54 . NAKAMURA, E. & SATO, K. "Managing the scarcity of chemical elements." Nat. Mater., **10**:158, 2011.

55 . SHAVIV, A. "Advances in controlled-release fertilizers." Adv Agron., **71**:1, 2001.

56 . HOSNI, K. & . SRASRA, E. "Evaluation of Phosphate Removal from Water by Calcined LDH Synthesized from the Dolomite." Colloid J., **72**:423, 2010.

57 . GHORBEL, S.B.; MEDINA, F.; GHORBEL, A. & SEGARRA, A.M. "Phosphoric acid intercalated Mg–Al hydrotalcite-like compounds forcatalytic carboxylation reaction of methanol in a continuous system." Appl Catal., A. **493**:142, 2015.

58 . COSTA, F.R.; SAPHIANNIKOVA, M. & WAGENKNECHT, G.H. "Layered Double hydroxide based polymer nanocomposites." Adv. Res. Polym. Sci., **210**:101, 2008.

59 . PFEIFFER, H.; LIMA, E.; LARA, V. & VALENTE, J.S. "Thermokinetic study of the rehydration process of a calcined mgal-layered double hydroxide." Langmuir, 26(6):4074, 2010.

60 . CHENG, X.; HUANG, X.; WANG, X.; ZHAO, B.; CHEN, A. & SUN, D. "Phosphate adsorption from sewage sludge filtrate using zinc–aluminum layered double hydroxides." J. Hazard. Mater. **169**:958, 2009.

61 . GUÉRARD-HÉLAINE, C.; LÉGERET, B.; FERNANDES, C.; PRÉVOT, V.; FORANO, C. & LEMAIRE, M. "Efficient immobilization of fructose-6-phosphate aldolase in layered double hydroxide: improved stereoselective synthesis of sugar analogues." New J. Chem., **35**:776, 2011.

62 . DAS, D.P.; DAS, J. & PARIDA, K.M. "Physicochemical characterization and adsorption behaviour of calcined Zn/Al hydrotalcite-like compound ([Mg-Al]clc) towards removal of fluoride from aqueous solution." J. Colloid Interface Sci., **261**:213, 2003.

63 . DAS, J.; DAS, D.; DASH, G.P. & PARIDA, K.M. "Studies on Mg/Fe hydrotalcite-like compound ([Mg-Al]clc) I. Removal of inorganic selenite (SeO_3^{2-}) from aqueous medium." J. Colloid Interface Sci., **251**:26, 2002.

64 . WANG, S. L.; LIU, C.H.; WANG, M.K.; CHUANG, Y.H. & CHIANG, P.N. "Arsenate adsorption by Mg/Al–NO_3 layered double hydroxides with varying the Mg/Al ratio." Appl Clay Sci., **43**:79, 2009.

65 . YANG, Y.; GAO, N.; CHU, W.; ZHANG, Y. & MA, Y. "Adsorption of perchlorate from aqueous solution by the calcination product of Mg/(Al–Fe) hydrotalcite-like compounds." J. Hazard. Mater., **209**:318, 2012.

66 . CHITRAKAR, R.; TEZUKA, S.; SONODA, A.; SAKANE, K.; OOI, K. & HIROTSU, T. "Adsorption of phosphate from seawater on calcined MgMn-layered double hydroxides." J. Colloid Interface Sci., **290**:45, 2005.

67 . HALAJNIA, A.; OUSTAN, S.; NAJAFI, N.; KHATAEE, A.R. & LAKZIAN, A. "Adsorption–desorption characteristics of nitrate, phosphate and sulfate on Mg–Al layered double hydroxide." App Clay Sci., **80**:305, 2013.

68 . DEL ROY, A.; FORANO, C. & BESSE, J.P. "Layered Double Hydroxides; Synthesis and Post-synthesis modifications." In: 'Layered Double Hydroxides: Present and Future." Ed: Vicent Rives. Nova Science Publishers, 1, 2006.

69 . PAI, S.C., YANG, C.C. & RILEY, J.P. "Effects of acidity and molybdate concentration on the kinetics of the formation of the phosphoantimonylmolybdenum blue complex." Anal. Chim Acta., **229**:115, 2009.

70 . DRUMMOND,L. & MAHER, W. "Determination of phosphorus in aqueous solution via formation of the phosphoantimonylmolybdenum blue complex Re-examination of optimum conditions for the analysis of phosphate." Anal. Chim Acta., 302:69, 1995.

71 . LIMOUSIN, G.; GAUDET, J.P.; CHARLET, L.; SZENKNECT, S.; BARTHE, V. & KRIMISSA, M. "Sorption isotherms: A review on physical bases, modeling and measurement." Appl Geochem., **22**:249, 2007.

72 . CAI, P.; ZHENG, H.; WANG, C.; MA, H.; HU, J.; PU,Y. & LIANG, P. "Competitive adsorption characteristics of fluoride and phosphate on calcined Mg–Al–CO_3 layered double hydroxides." J. Hazard. Mater., **213**:100, 2012.

73 . NOVILLO, C.; GUAYA, D.; ALLEN-PERKINS, A.; ARMIJOS, A.C.; CORTINA, J.L. & COTA, I. "Evaluation of phosphate removal capacity of Mg/Al layered double hydroxides from aqueous solutions." Fuel., **138**:72, 2014.

74 . HIEMSTRA, T. & VAN RIEMSDIJK, W.H. "A Surface Structural Approach to Ion Adsorption: The Charge Distribution (CD) Model." J. Colloid Interface Sci., **179**:488, 1996.

75 . HIEMSTRA, T. Surface Complexation at Mineral Interfaces: Multisite and Charge Distribution Approach." Guéldria, Soil Chemistry and Chemical Soil Quality- Wageningen University, 2015, PhD dissertation, 384p.

76 . KUZAWA, K.; JUNG, Y.J.; KISO, Y.; YAMADA, T.; NAGAI, M. & LEE, T.G. "Phosphate removal and recovery with a synthetic hydrotalcite as an adsorbent." Chemosphere., **62**:45, 2006.

77 . XING, K.; WANG, H.; GUO, L.; SONG, W. & ZHAO, Z. "Adsorption of tripolyphosphate from aqueous solution by Mg–Al–CO_3-layered double hydroxides." Colloids Surf. A., **328**:15, 2008.

78 . LOOKMAN, R.; GROBET, P.; MERCKX, R. & VAN RIEMSDIJK, W.H. "Application of ^{31}P and ^{27}Al MAS NMR for phosphate speciation studies in soil and aluminium hydroxides: promises and constraints." Geoderma., **80**: 369, 1997.

79 . WARMADEWANTHI, J.C.L. "Selective Precipitation of Phosphate from Semiconductor Wastewater." J. Environ. Eng., **135**:1063, 2009.

80 . JOHNSON, B.B.; IVANOV, A.V.; ANTZUTKIN, O.N. & FORSLING, W. "^{31}P Nuclear Magnetic Resonance Study of the Adsorption and of Phosphate and Phenyl Phosphates on ç-Al_2O_3." Langmuir., **18**:1104, 2002.

81 . PRABAKAR, S.; RAO, K. J. & RAO, C.N.R. "A Study of $AlPO_4$ By ^{27}Al And ^{31}P MAS NMR Spectroscopy." Mater. Res. Bull., **26**:805, 1991.

82 . VYALIK, A.; MASSIOT, D. & SCHELER, U. "Structural characterization of aluminium layered double hydroxides by ^{27}Al solid-state NMR." Solid State Nucl. Magn. Reson., **36**:19, 2009.

83 . CONSTANTINO, V.R.L.; ARAKI, K.; SILVA, D.O.; OLIVEIRA, W. "Preparation of aluminum compounds from bauxite: aspects of a didactic experiment." Quim. Nova., **25**:490, 2002.

84 . MOREIRA, A. & FAGERIA, N. K. "Soil Chemical Attributes of Amazonas State, Brazil." Commun. Soil Sci. Plant Anal., **40**:2912, 2009.

85 . ABREU JR, C.H.; MURAOKA T. A. & LAVORANTE, F. "Relationship between acidity and chemical properties of brazilian soils." Sci. Agric., **60**:337, 2003.

86 . CAIRES, E. F.; BANZATTO, D. A. & FONSECA, A. F. "Limestone surface in planting direct system." R. Bras. Ci. Solo., **24**:161, 2000.

87.. SHIMAMURA, A.; JONES, M.I.; KANEZAKI, E. & METSON, J.B. "Complete desorption of interlayer hydrogen phosphate in Mg/Al-layered double hydroxides by means of anion exchange with 1-octanesulfonate." J Mater Sci., **47**:1142, 2012.

88 . VARELAS, C.G.; DIXON, D.G. & STEINER, C. "Zero-order release from biphasic polymer hydrogels." J. Control. Release., **34**:185, 1995.

89 . MANADAS, R.; PINA, M.E. & VEIGA, F. "In vitro dissolution as prediction of oral absorption of drugs in pharmaceutics ways of modificate release." Braz. J. of Pharm. Sci., **38**:11, 2002.

90 . LOPES, C.M.; LOBO, J.M.S. & COSTA, P. "Formas farmacêuticas de liberação modificada: polímeros hidrifílicos." Braz. J. of Pharm. Sci., **41**:143, 2005.

91 . GHODKE, S.A.; SONAWANE, S.H.; BHANVASE, B.A.; MISHRA, S. & JOSHI, K.S. "Studies on Fragrance Delivery from Inorganic Nanocontainers: Encapsulation, Release and Modeling Studies." J. Inst. Eng. India Ser. E., **96**:45, 2015.

92 . DASH, S.; NARASIMHA, P.; MURTHY, N.; NATH, L. & CHOWDHURY, P. "Kinetic Modeling On Drug Release From Controlled Drug Delivery Systems." Acta Pol. Pharm-Drug Resear., **67**:217, 2010.

93 . LI, L. & STANFORTH, R. "Distinguishing Adsorption and Surface Precipitation of Phosphate on Goethite (alpha-FeOOH)." J Colloid Interface Sci., **230**: 12, 2000.

94 . ZACH-MAOR, A.; SEMIAT, R. & SHEMER, H. "Adsorption–desorption mechanism of phosphate by immobilized nano-sized magnetite layer: Interface and bulk interactions." J. Colloid Interface Sci., **363**:608, 2011.

95 . BURNS, R.T.; MOODY, L.B. & CELEN, I. "Optimization of phosphorus precipitation from swine manure slurries to enhance recovery." Water Sci. Technol., **48**:139, 2003.

96 . CHIMENOS, J.M.; FERNÁNDEZ, A.I. & VILLALBA, G."Removal of ammonium and phosphates from wastewater resulting from the process of cochineal extraction using MgO-containing by-product." Water Research., 37:1601, 2003.

97 . FARIA, O.L.V.; KOETZ, P.R. & DOS SANTOS M.S. "Rice parboilization wastewater phosphorus removal by enhanced biological assimilation in sequencing batch reactor (SBR)." Ciência e Tecnologia de Alimentos., **26**:309, 2006.

98 . PALHARES, J.C.P. & CALIJURI, M.D.C. "Characterization of affluents and effluents in swine feeding system and environmental impact qualification." Ciência Rural., **37**:502,2007.

99 . CARBALLA, M.; MOERMAN, W. & DE WINDT, W. "Strategies to optimize phosphate removal from industrial anaerobic effluents by magnesium ammonium phosphate (MAP) production." Journal of Chemical Technology and Biotechnology., **84**:63, 2009.

100 . LATIFIAN, M.; HOLST, O. & LIU, J. "Nitrogen and Phosphorus Removal from Urine by Sequential Struvite Formation and Recycling Process." Clean - Soil, Air, Water., **42**:1157, 2014.

101 . CORRELL, D.L. "The role of phosphorus in the eutrophication of receiving waters: a review." Journal of Environmental Quality., **27**: 261, 1998.

102 . TCHAMANGO, S.; NANSEU-NJIKI, C.P. & NGAMENI, E. "Treatment of dairy effluents by electrocoagulation using aluminium electrodes." Science of the Total Environment., **408**:947,2010.

103 . YILDIZ, E. "Phosphate removal from water by fly ash using crossflow microfiltration." Separation and Purification Technology., **35**: 241, 2004.

104 . ZHOU, J.; YANG, S. & YU, J. "Novel hollow microspheres of hierarchical zinc–aluminum layered double hydroxides and their enhanced adsorption capacity for phosphate in water." Journal of Hazardous Materials., **192**: 1114, 2011.

105 . OOKUBO, A.; OOI, K. & HAYASHI, H. "Preparation and phosphate ion-exchange properties of a hydrotalcite-like compound." Langmuir., **9**: 1418, 1993.

106 . WANG, S.L.; LIU, C.H. & WANG, M.K. "Arsenate adsorption by $Mg/Al–NO_3$ layered double hydroxides with varying the Mg/Al ratio." Applied Clay Science., **43**:79, 2009.

107 . DAS, J.; DAS, D. & DASH, G.P. "Studies on Mg/Fe hydrotalcitelike compound (HTlc): Removal of chromium (VI) from aqueous solution." International Journal of Environmental Studies., **61**: 605,2004.

108 . RADHA, A.V.; KAMATH, P.V. & SHIVAKUMARA, C. "Mechanism of the anion exchange reactions of the layered double hydroxides (LDH) of Ca and Mg with Al." Solid State Science., **7**: 1180, 2005.

109 . BERNARDO, M.P.; MOREIRA, F.K.V.; COLNAGO, L.A. & RIBEIRO, C. "Physico-chemical assessment of $[Mg-Al-PO_4]$-LDH obtained by structural reconstruction in high concentration of phosphate." Colloids and Surfaces, A: Physicochemical and Engineering Aspects., **497**, 53:2016.

110 . BERNARDO, M.P.; MOREIRA, F.K.V. & RIBEIRO, C. "Synthesis and characterization of eco-friendly Ca-Al-LDH loaded with phosphate for agricultural applications." Applied Clay Science., **137**: 143, 2017.

111 . BADREDDINE, M.; LEGROURI, A. & BARROUG, A. "Influence of pH on phosphate intercalation in zinc–aluminum layered double hydroxide." Materials Letters., **38**: 391,1999.

112 . XIONG, J.; HE, Z. & MAHMOODA, Q. "Phosphate removal from solution using steel slag through magnetic separation." Journal of Hazardous Materials., **152**:211, 2008.

113 . HUANG, W.; ZHANG, Y. & LI, D. "Adsorptive removal of phosphate from water using mesoporous materials: A review." Journal of Environmental Management. **193**:470, 2017.

114 . JIA, Y.; WANGA, H. & ZHAO, X. "Kinetics, isotherms and multiple mechanisms of the removal for phosphate by Cl-hydrocalumite." Appl. Clay Scien., **129**: 116, 2016.

115 . CHANG, Z.; EVANS, D.G. & DUAN, X. "Synthesis of $Zn-Al-CO_3$ layered double hydroxides by a coprecipitation method under steady-state conditions." Journal of Solid State Chemistry., **178**: 2766, 2005.

116 . LABAJOS, F.M.; RIVERS, V. & ULIBARRI, M.A. "Effect of hydrothermal and thermal treatments on the physicochemical properties of Mg-Al hydrotalcite-like materials." Journal of Materials Science., **27**: 1546, 1992.

117 . DESTAINVILLE, A.; CHAMPION, E. & BERNACHE-ASSOLLANTE, D. "Synthesis, characterization and thermal behavior of apatite tricalcium phosphate." Materials Chemistry and Physics., **80**: 269, 2003.

118 . RAYNAUD, S.; CHAMPION, E. & BERNACHE-ASSOLLANT, D. "Calcium phosphate apatites with variable Ca/P atomic ratio I. Synthesis, characterisation and thermal stability of powders." Biomaterials., **23**: 1065, 2002.

119 . KANARI, N.; MISHRA, D. & GABALLAH, I. "Thermal decomposition of zinc carbonate hydroxide." Thermochim Acta., **410**: 93, 2004.

120 . PALMER, S.J.; FROST, R.L. & NGUYEN, T. "Thermal decomposition of hydrotalcite with molybdate and vanadate anions in the interlayer." Journal of Thermal Analysis., **92**: 879, 2008.

121 . PALMER, S.J.; SPRATT, H.J. & FROST, R.L. "Thermal decomposition of hydrotalcites with variable cationic ratios." Journal of Thermal Analysis., **95**:123, 2009.

122 . GRISHCHENKO, R.O.; EMELINA, A.L. & MAKAROV, P.Y. "Thermodynamic properties and thermal behavior of Friedel's salt." Thermochim Acta., 74:570, 2013.

123 . SIPAUT, C.S.; JAFARZADEH, M. & SUNDANG, M. "Size control in porosity of hydroxyapatite using a mold of polyurethane foam." Journal of Inorganic and Organometallic Polymers. **26**: 1066, 2016.

124 . BENÍCIO, L.P.F.; CONSTANTINO, V.R.L. & PINTO, F.G. "Layered Double Hydroxides: New Technology in Phosphate Fertilizers Based on Nanostructured Materials." ACS Sustainable Chemistry Engineering., **5**:399, 2017.

125 . EVERAERT, M.; WARRINNIER, R. & BAKEN, S. "Phosphate-Exchanged Mg-Al Layered Double Hydroxides: A New Slow Release Phosphate Fertilizer." ACS Sustainable Chemistry Engineering., **4**:4280, 2016.

126 . SADOWSKY, S.J. "An overview of treatment considerations for esthetic restorations: A review of the literature." J. Prosthet. Dent., **96**: 433, 2006.

127 . FERRACANE, J.L. "Resin composite - State of the art." Dent. Mater., **27**:29, 2011.

128 . CRAMER, N.B.; STANSBURY, J.W. & BOWMAN, C.N. "Recent advances and developments in composite dental restorative materials." J. Dent. Res., **90**: 402, 2011.

129 . DRAUGHN, R.A. "Compressive fatigue limits of composite restorative materials." J. Dent. Res., **58**:1093, 1979.

130 . DRUMMOND, J.L. "Cyclic fatigue of composite restorative materials." J. Oral Rehabil., **16**: 509, 1989.

131 . DRUMMOND, J.L. "Degradation, fatigue, and failure of resin dental composite materials." J. Dent. Res., **87**:710, 2008.

132 . KLAPDOHR, S. & MOSZNER, N. "New inorganic components for dental filling composites." Monatshefte für Chemie, **136**: 21,2005.

133 . CHEN, M.H. "Update on dental nanocomposites." J. Dent. Res. **89**: 549, 2010.

134 . GHORBEL, S. B.; MEDINA, F. A.; GHORBEL, A.M. & SEGARRA. "Phosphoric acid intercalated Mg-Al hydrotalcite-like compounds for catalytic carboxylation reaction of methanol in a continuous system." Appl. Catal. A Gen., **493**:142, 2015.

135 . LIVI, S.; SAR, G.; BUGATTI, V.; ESPUCHE, E. & DUCHET-RUMEAU, J.

"Synthesis and physical properties of new layered silicates based on ionic liquids: improvement of thermal stability, mechanical behaviour and water permeability of PBAT nanocomposites.", RSC Adv., **4**:26452, 2014.

136 . ALIBAKHSHI, E.; GHASEMI, E.; MAHDAVIAN, M.; RAMEZANZADEH, B. & FARASHI, S. "Fabrication and characterization of PO_4^{3-} intercalated Zn-Al-Layered Double Hydroxide nanocontainer." J. Electrochem. Soc., **163**:495, 2016.

137 . YANG, Z.; FISCHER, H. & POLDER, R. "Modified hydrotalcites as a new emerging class of smart additive of reinforced concrete for anticorrosion applications: A literature review." Mater. Corros., **64**:1066, 2013.

138 . TAMMARO, L.; VITTORIA, V.; CALARCO, A.; PETILLO, O.; RICCITIELLO, F. & PELUSO, G. "Effect of layered double hydroxide intercalated with fluoride ions on the physical, biological and release properties of a dental composite resin." J. Dent., **42**:60, 2014.

139 . REYNOLDS, E.C. "Calcium phosphate-based remineralization systems: Scientific evidence?" Aust. Dent. J., **53**:268, 2008.

140 . GERLACH, A.; VINCENT, B.; LISSAC, M.; ESNOUF, X. & THOLLET, G. "Distribution of zinc ions from orthophosphate cements at the cement-tooth interface in fixed dental prosthesis." Biomaterials, **14**:770, 1993.

141 . SU-CHENG, P.; CHUNG-CHENG, Y. & RILEY, J.P. "Effects of acidity and molybdate concentration on the kinetics of the formation of the phosphoantimonylmolybdenum blue complex." Anal. Chim. Acta, **229**:115, 1990.

142 . APPEL, G.; & REUS, M. Formulations Applied to Dentistry. 2nd ed., RCN, São Paulo, 2005. p. 143.

143 . TIARA, A.M.; CHAKRABORTY, S.; SARKAR, I.; PAL, S.K. & CHAKRABORTY, S. "Synthesis and characterization of Zn-Al layered double hydroxide nanofluid and its application as a coolant in metal quenching." Appl. Clay Sci., **143**:241, 2017.

144 . HE, H.; KANG, H.; MA, S.; BAI, Y. & YANG, X. "High adsorption selectivity of ZnAl layered double hydroxides and the calcined materials toward phosphate." J. Colloid Interface Sci., **343**:225, 2010.

145 . LV, J.; ZHANG, S.; LUO, L.; HAN, W.; ZHANG, J.; YANG, K. & CHRISTIE, P. "Dissolution and microstructural transformation of ZnO nanoparticles under the influence of phosphate." Environ. Sci. Technol., **46**:7215, 2012.

146 . MOUSA, M.A.; DIEFALLAH, E.M.; ABDEL FATTAH, A.A. & OMRAN, Z.A. "Physicochemical studies on ZnO-Al_2O_3 system." J. Mater. Sci., **25**: 3067, 1990.

147 . PRADHAN, S.; COSTA, F.R.; WAGENKNECHT, U.; JEHNICHEN, D.; BHOWMICK, A.K. & HEINRICH, G. "Elastomer/LDH nanocomposites: Synthesis and studies on nanoparticle dispersion, mechanical properties and interfacial adhesion." Eur. Polym. J., **44**:3122, 2008.

148 . WANG, L.; D'ALPINO, P.H.P.; LOPES, L.G. & PEREIRA, J.C. "Mechanical properties of dental restorative materials: relative contribution of laboratory tests." J. Appl. Oral Sci., **11**:162, 2003.

149 . ABUDIAK, H.; ROBINSON, C.; DUGGAL, M.S.; STRAFFORD, S. & TOUMBA, K.J. "Effect of fluoride sustained slow-releasing device on fluoride, phosphate and calcium levels in plaque biofilms over time measured using ion chromatography." J. Dent., **40**:632,

2012.

150 . FEATHERSTONE, J.D.B. "Remineralization, the natural caries repair process: The need for new approaches." Adv. Dent. Res., **21**:4, 2009.

151 . GYNESHWAR, P.; KUMAR, G.N.; PARESH, L.J. & POLE, P.S. "Role of soil microorganisms in improving P nutritions of plants." Plant Soil., **245**:83, 2002.

152 . SON, T. T. N.; DIEP, C. N. & GIANG,T. T. M. "Effect of bradyrhizobia and phosphate solubilizing bacteria application on soybean in rotational system in the mekong delta." Omonrice., **14**:48, 2006.

153 . ASHER, C. J. & LONERAGAN J. F. "Response of plants to phosphate concentration in solution culture: I. Growth and phosphorus content." Soil Sci., **103**:225,1967.

154 . FÖHSE, D.; CLAASSEN, N. & JUNGK, A."Phosphorus efficiency of plants. I. External and internal requirement and P uptake efficiency of different plant species." Plant Soil., **110**: 101,1988.

155 . HINSINGER, P. "Bioavailability of soil inorganic P in the rhizosphere as affected by root-induced chemical changes: a review." Plant Soil., **237**:173, 2001.

156 . SERVANI, M.; MOBASSER, H. R.; SOBHKHIZI, A.; ADIBIAN, M. & NOORI M. "Effect of phosphorus fertilizer on plant height, seed weight and number of nodes in soybean." Int. J. Plan and Env. Sci., **4**: 696, 2014.

157 . BODDEY, L.H. & HUNGRIA, M. "Phenotypic grouping of Brazilian Bradyrhizobium strains which nodulate soybean." Biol Fertil Soils., **25**: 407, 1997.

158 . ROSAS, S. B.; ANDRE, J.A.; ROVERA, M. & CORREA, N.S. "Phosphate-solubilizing *Pseudomonas putida* can influence the rhizobia-legume symbiosis." Soil Biol. Biochem., **38:** 3502, 2006.

159 . HUNGRIA, M. & VARGAS, M. A.T. "Environmental factors affecting N_2 fixation in grain legumes in the tropics, with an emphasis on Brazil." Field Crops Res., **65**:151, 2000.

160 . QIAN, G.; FENG, L.; ZHOU, J. Z.; XU, Y.; LIU, J.; ZHANG, J. & XU, Z. P. "Solubility product (Ksp)-controlled removal of chromate and phosphate by hydrocalumite." Chem. Eng. J., **181**:25, 2012.

161 . LIU, Q.; LI, Y.; ZHANG, J.; CHI, Y.; RUAN, X.; LIU, J. & QIAN, G. "Effective removal of zinc from aqueous solution by hydrocalumite." Chem. Eng. J., **175**:33, 2011.

162 . YAN, L.; YANG, K.; SHAN, R.; YU, H. & DU, B. "Calcined ZnAl- and Fe_3O_4/ZnAl–layered double hydroxides for efficient removal of Cr(VI) from aqueous solution." RSC Adv. **5**: 96495, 2015.

163 . DUAN, X. & EVANS, D.G. "Layered double hydroxides, structure and bonding series." IN: Structural Aspects of Layered Double Hydroxides. DUAN, X. & EVANS, D.G. (Eds.). Springer Berlin Heidelberg New York, 2006.p.1-87

164 . RIVES, V. Layered Double Hydroxides: Present and Future. 1a ed. New York, Nova Science Publishers, 2006, p. 439.

165 . XU, Y.; DAI, Y.; ZHOU, J.; XU, Z. P.; QIAN, G. & MAX LU, G. Q. J. "Removal efficiency of arsenate and phosphate from aqueous solution using layered double hydroxide materials: intercalation vs. precipitation." Mater. Chem., **20**: 4684, 2010.

166 . CARJA, G.; NAKAMURA, R. & NIIYAMA, H. "Tailoring the porous properties of iron containing mixed oxides for As(V) removal from aqueous solutions." Micropor. Mesopor. Mater., **83**: 94, 2005.

167 . YANG, L.; SHAHRIVARI, Z.; LIU, P.K.T.; SAHIMI, M. & TSOTSIS, T.T. "Removal of trace levels of arsenic and selenium from aqueous solutions by calcined and uncalcined layered double hydroxides (LDH)." Ind. Eng. Chem. Res., **44**: 6804, 2005.

168 . LAZARIDIS, N.K.; MATIS, K.A. & WEBB, M. "Sorption removal of anions and cations in single batch systems by uncalcined and calcined Mg-Al-CO$_3$ hydrotalcite." Chemosphere, **42**:373, 2001.

169 . PFEIFFER, H.; ÁVALOS-RENDÓN, T.; LIMA, E. & VALENTE, J. S. "Thermochemical and cyclability analyses of the CO$_2$ absorption process on a Ca/Al layered double hydroxide." J. Environ. Eng., **137**: 1058, 2011.

170 . WANG, J.; KALINICHEV, A. G.; KIRKPATRICK, R.J. & HOU, X. "Molecular Modeling of the Structure and Energetics of Hydrotalcite Hydration." Chem. Mater., **13**:145, 2001.

171 . ZHOU, J. Z.; FENG, L.; ZHAO, J.; LIU, J.; LIU, Q.; ZHANG, J. & QIAN, G. "Efficient and controllable phosphate removal on hydrocalumite by multi-step treatment based on pH-dependent precipitation." Chem. Eng. J. **185**: 219, 2012.

172 . ENGSTRÖM, F.; ADOLFSSON, D.; SAMUELSSON, C.; SANDSTRÖM, Å. & BJÖRKMAN, B. "A study of the solubility of pure slag minerals." Miner. Eng., **41**: 46, 2013.

173 . KARAMIAN, E.; ABDELLAHI, M.; KHANDAN, A. & ABDELLAH, S. J. "Introducing the fluorine doped natural hydroxyapatite-titania nanobiocomposite ceramic." Alloys Compd., **679**:375, 2016.

174 . ROOHANI-ESFAHANI, S.; NOURI-KHORASANI, S.; LU, Z.; APPLEYARD, R. & ZREIQAT, H. "The influence hydroxyapatite nanoparticle shape and size on the properties of biphasic calcium phosphate scaffolds coated with hydroxyapatite-PCL composites." Biomaterials., **31**: 5498, 2010.

175 . ZHANG, F.; DASHTI, N.; HYNES, R. K. & SMITH. "Plant growth promotion rhizobacteria and soybean [*Glicine max* (L.) Merr.] nodulation and nitrogen fixation at suboptimal root zone temperatures." D. L. Ann. Bot., **77**: 453, 1996.

176 . KRIEG, N.R. & HOLT, J.G. Bergey's Manual of Systematic Bacteriology. 1a ed. William and Wilkins, Baltimore/London, 1984, p 1105.

177 . SANCHES, P. A. & SALINAS, J. G. "Low input technology for managing oxisol and utisols in tropical America." Adv. Agron., **34**:229, 1981.

178 . WISSUWA, M. "How do plants achieve tolerance to phosphorus deficiency? Small causes with big effects." Plant Physiol., 133(4): 1947, 2003.

179 . FAIRHURST, T.; LEFROY, R.; MUTERT, E. & BATJES, N. "The importance, distribution and causes of phosphorus deficiency as a constraint to crop production in the tropics." Agrofor. Forum, 9(4):2, 1999.

180 . OBERSON, A.; FRIESEN, D. K.; RAO, I. M.; BUHLER, S. & FROSSARD, E. "Phosphorus Transformations in an Oxisol under contrasting land- use systems: The role of the soil microbial biomass." Plant Soil, 237(2):197, 2001.

181 . SMIT, A.L; BINDRABAN; P.S, SHROEDER, J.J; CONIJIN, J. & V. D. M. H. G. "Phosphorus in agriculture: global resources, trends and developments." Rep. to Steer., **5**:1, 2009.

182 . VAN DE WIEL, C. C. M.; VAN DER LINDEN, C. G. & SCHOLTEN, O. E. "Improving phosphorus use efficiency in agriculture: opportunities for breeding." Euphytica,

207(1):1, 2016.

183 . BEEGLE, D. & DURST, P. T. "Managing phosphorus for crop production." Agron. Facts, **13**:35, 2014.

184 . GYANESHWAR, P.; NARESH KUMAR, G.; PAREKH, L. J. & POOLE, P. S. "Role of soil microorganisms in improving P nutrition of plants." Plant Soil, **245**:83, 2002.

185 . OLIVEIRA, C. A.; ALVES, V. M. C.; MARRIEL, I. E.; GOMES, E. A.; SCOTTI, M. R.; CARNEIRO, N. P.; GUIMARÃES, C. T.; SCHAFFERT, R. E. & SÁ, N. M. H. "Phosphate solubilizing microorganisms isolated from rhizosphere of maize cultivated in an oxisol of the Brazilian Cerrado Biome." Soil Biol. Biochem., **41**:1782, 2009.

186 . DA CRUZ, D. F.; BORTOLETTO-SANTOS, R.; GUIMARÃES, G. G. F.; POLITO, W. L. & RIBEIRO, C. "Role of Polymeric Coating on the Phosphate Availability as a Fertilizer: Insight from Phosphate Release by Castor Polyurethane Coatings." J. Agric. Food Chem., **65**:5890, 2017.

187 . PAULY, D. G.; MALHI, S. S. & NYBORG, M. "Controlled-release P fertilizer concept evaluation using growth and P uptake of barley from three soils in greenhouse." Can. J. Soil Sci., **82**:201, 2002.

188 . ANSTOETZ, M.; ROSE, T. J.; CLARK, M. W.; YEE, L. H.; RAYMOND, C. A. & VANCOV, T. "Novel applications for oxalate-phosphate-amine metal-organic-frameworks (OPA-MOFs): Can an iron-based OPA-MOF be used as slow-release fertilizer?" PLoS One, 10:1, 2015

189 . COLE, J. C.; SMITH, M. W.; PENN, C. J.; CHEARY, B. S. & CONAGHAN, K. J. "Nitrogen, phosphorus, calcium, and magnesium applied individually or as a slow release or controlled release fertilizer increase growth and yield and affect macronutrient and micronutrient concentration and content of field-grown tomato plants." Sci. Hortic., **211**:420, 2016.

190 . DEGRYSE, F.; BAIRD, R.; DA SILVA, R. C. & MCLAUGHLIN, M. J. "Dissolution rate and agronomic effectiveness of struvite fertilizers – effect of soil pH, granulation and base excess." Plant Soil, **410**:139, 2017.

191 . EVERAERT, M.; DEGRYSE, F.; MCLAUGHLIN, M. J.; DE VOS, D. & SMOLDERS, E. "Agronomic Effectiveness of Granulated and Powdered P-Exchanged Mg-Al LDH Relative to Struvite and MAP." J. Agric. Food Chem., **65**:6736, 2017.

192 . MALHI, S.; HADERLEIN, L.; PAULY, D. & JOHNSTON, A. "Improving fertilizer phosphorus use efficiency." Development, **86**: 8, 2002.

193 . SENGUPTA, S. & PANDIT, A. "Selective removal of phosphorus from wastewater combined with its recovery as a solid-phase fertilizer." Water Res., **45**: 3318, 2011.

194 . ZHAN, F.; LIU, M.; GUO, M. & WU, L. "Preparation of superabsorbent polymer with slow-release phosphate fertilizer." J. Appl. Polym. Sci., **92**:3417, 2004.

195 . CUNHA, V. R. R.; MARIA, A. & FERREIRA, C. "Hidróxidos Duplos Lamelares: Nanopartículas inorgânicas para armazenamento e liberação de espécies de interesse biológico e terapêutico." Quim. Nova, **33**:159, 2010.

196 . KILMER, V. J. & ALEXANDER, L. "Methods of making mechanical analysis of soils." Soil Sci, **68**:15, 1949.

197 . EMBRAPA SOLOS, M. "Manual de métodos de análise de solo". Empresa Brasileira de Pesquisa Agropecuária , Rio de Janeiro. 247, 1979.

198 . NELSON, D. & SOMMERS, L. "Total carbon, organic carbon, and organic matter."

IN: Methods of Soil Analysis. AL, S. D. (Eds.). SSSA Book Series No. 5, SSSA and ASA, Madison, 1996, 1010.

199 . ALVAREZ, V. V. H.; NOVAIS, R. F.; DIAS, L. E. & OLIVEIRA, J. A. "Determinação e uso do fósforo remanescente." Bol. Inf. Soc. Bras. Ci. Solo, **25**: 27, 2000.

200 . MIOLA, G. R. Extração de P, K, Ca e Mg do solo por diferentes métodos e avaliação da disponibilidade de P para as plantas. Porto Alegre, Programa de Pós-Graduação em Agronomia- Universidade Federal do Rio Grande do Sul, 1995. Tese de doutorado, 140p.

201 . GATIBONI, L. C. Disponibilidade de formas de fósforo do solo as plantas. Santa Maria, Programa de Pós-Graduação em Agronomia- Universidade Federal de Santa Maria, 2003. Tese de doutorado, 247p.

202 . ABDALA, D. B.; DA SILVA, I. R.; VERGÜTZ, L. & SPARKS, D. L. "Long-term manure application effects on phosphorus speciation, kinetics and distribution in highly weathered agricultural soils." Chemosphere, **119**: 504, 2015.

203 . RAIJ, B. VAN; CANTARELLA, H.; QUAGGIO, J. A. & FURLANI, A. M. C. "Recomendações de adubação e calagem para o Estado de São Paulo." rev. atual., **100**: 48, 1997.

204 . MALAVOLTA, E. Elementos de nutrição mineral de plantas. 1ªed.; São Paulo, 1980, p. 251.

205 . MALAVOLTA, E.; VITTI, G. C. & OLIVEIRA, S. A. Avaliação do estado nutricional das plantas: princípios e aplicações. 2ª ed. Associação Brasileira para Pesquisa da Potassa e do Fosfato, Piracicaba, 1997, p. 201.

206 . WAN, D.; LIU, Y.; XIAO, S.; CHEN, J. & ZHANG, J. "Uptake fluoride from water by caclined Mg-Al-CO3 hydrotalcite: Mg/Al ratio effect on its structure, electrical affinity and adsorptive property." Colloids Surfaces A Physicochem. Eng. Asp., **469**:307, 2015.

207 . HU, P.; ZHANG, Y.; LV, F.; TONG, W.; XIN, H.; MENG, Z.; WANG, X. & CHU, P. K. "Preparation of layered double hydroxides using boron mud and red mud industrial wastes and adsorption mechanism to phosphate." Water Environ. J., **31**:45, 2017.

208 . FROST, R. L.; MUSUMECI, A. W.; BOSTROM, T.; ADEBAJO, M. O.; WEIER, M. L. & MARTENS, W. "Thermal decomposition of hydrotalcite with chromate, molybdate or sulphate in the interlayer." Thermochim. Acta, **429**: 179, 2005.

209 . COLNAGO, L. .; VALENTINE, K. & OPELLA, S. "Dynamics of fd Coat Protein in the Bacteriophage." Biochemistry, **26**:847, 1987

210 . HANSEL, F. D.; AMADO, T. J. C.; BORTOLOTTO, R. P.; TRINDADE, B. S. & HANSEL, D. S. S. "Influence of different phosphorus sources on fertilization efficiency." Brazilian J. Appl. Technol. Agric. Sci., **6325**: 103, 2014.

211 . LEWIS, D. & QUIRK, J. "Phosphate diffusion in soil and uptake by plants: iv. computed uptake by model roots as a result of diffusive flow." Plant Soil, **26**:454, 1967.

212 . OH, J.; BISWICK, T. & CHOY, J. "Layered nanomaterials for green materials." J. Mater. Chem., **19**:2553, 2009.

213 . MOTTA, P. E. F.; CURI, N.; SIQUEIRA, J. O.; VAN RAIJ, B.; FURTINI NETO, A. E. & LIMA, J. M. "Adsorção e formas de fósforo em Latossolos: influência da mineralogia e histórico de uso." Rev. Bras. Ciência do Solo, **26**:349, 2002.

214 . SHARPLEY, A. N. "Dependence of runoff phosphorus on extractable soil phosphorus." J. Environ. Qual., **24**:920, 1995.

215 . REEVE, N. G. & SUMNER, M. E. Z. "Effects of aluminum toxicity and phosphorus

fixation on crop growth on oxisols in natal 1." Soil Sci. Soc. Amer. Proc., **34**:263, 1965.

216 . SMECK, N. E. "Phosphorus dynamics in soils and landscapes." Geoderma, **36**:185, 1985.

217 . AKINREMI, O. O. & CHO, C. M. "Phosphate Transport in Calcium-Saturated Systems: II. Experimental Results in a Model System." Soil Sci. Soc. Am. J., **55**:1282, 1990.

218 . DEVAU, N.; CADRE, E. LE; HINSINGER, P.; JAILLARD, B. & GÉRARD, F. "Soil pH controls the environmental availability of phosphorus : Experimental and mechanistic modelling." Appl. Geochemistry, **24**:2163, 2009

Appendix A

Supporting Information of Chapter I
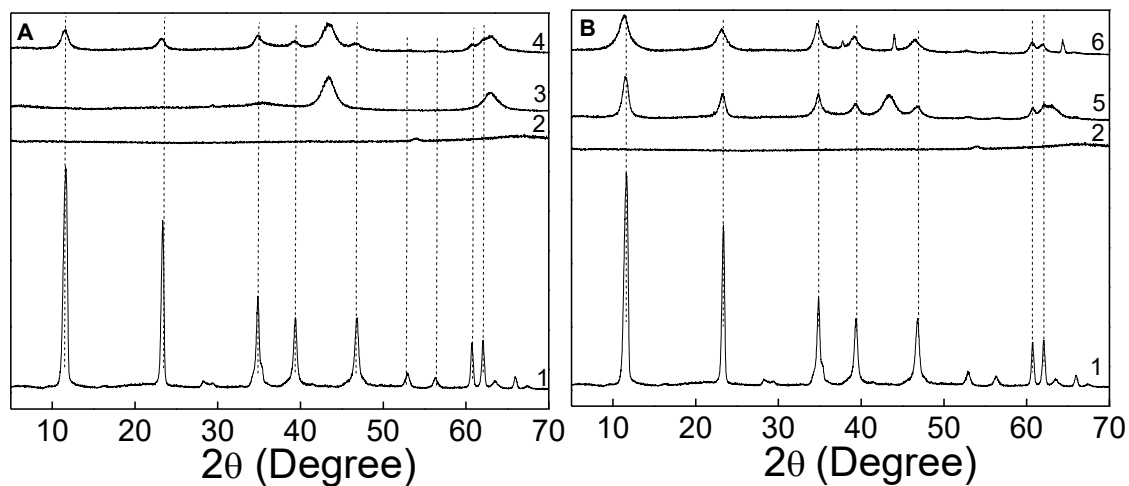
FIGURE A1. (A): PXRD patterns of [Mg-Al]c reconstructed in water at 25 ºC for 4 and 24 hours. 1= [Mg-Al]c; 2= C-[Mg-Al]c; 3= R-[Mg-Al]c for 4 hours; 4= R-[Mg-Al]c for 24 hours. (B): PXRD patterns of [Mg-Al]c reconstructed at 75 ºC for 4 and 24 hours. 1= [Mg-Al]c; 2= C-[Mg-Al]c; 5= R-[Mg-Al]c for 4 hours; 6= R-[Mg-Al]c for 24h.
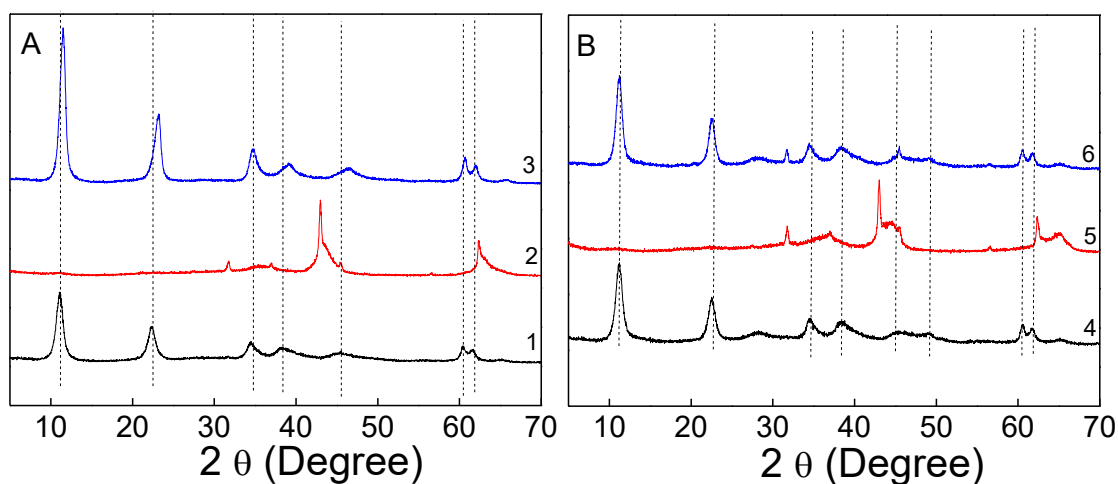
FIGURE A2. (A) PXRD patterns of [Mg-Al$_{0.30}$] reconstructed in water at 75 ºC for 24 hours. 1= [Mg-Al$_{0.30}$]; 2= C- [Mg-Al$_{0.30}$]; 3= R- [Mg-Al$_{0.30}$]. (B) PXRD patterns of [Mg-Al$_{0.40}$] reconstructed in water at 75 ºC for 24 hours. 4= [Mg-Al$_{0.40}$]; 5= C-[Mg-Al$_{0.40}$]; 6= R- [Mg-Al$_{0.40}$].
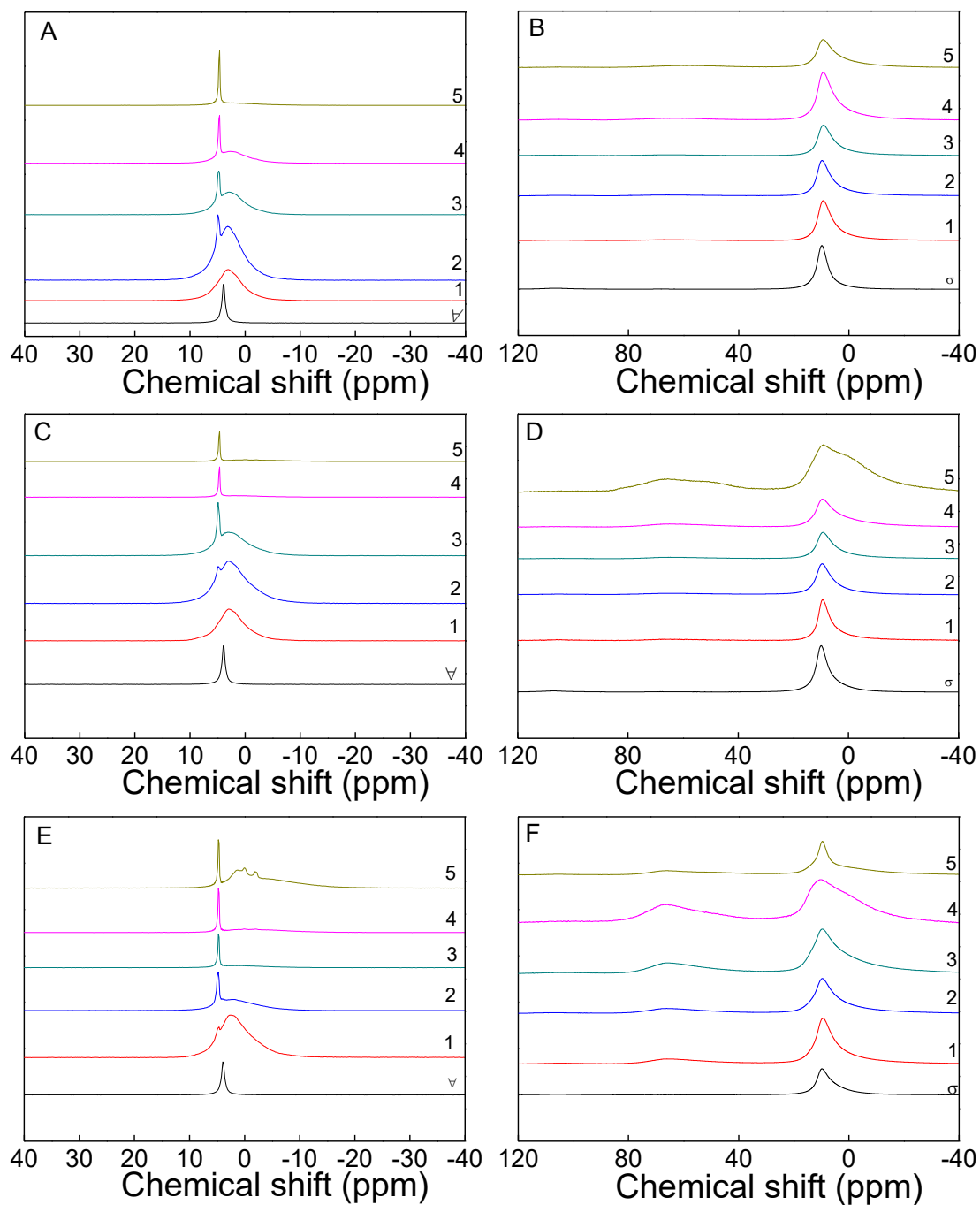
FIGURE A3. ^{31}P NMR spectra (A,C,E)   B: ^{27}Al NMR (B,D,F) ∀ spectra.= KH$_2$PO$_{4;}$ σ = Synthesis; 1 =6.6 mM; 2 = 1:1,75 (11.6 mM); 3 = 1:2.5   (16.6 mM); 4 = 1:4 (26.5 mM); 5 = 1:5 (33.1 mM). A and B = [Mg-Al$_{0.25}$]; C and D = [Mg-Al$_{0.30}$]; E and F = [Mg-Al$_{0.40}$].

Appendix B

Supporting Information of Chapter II

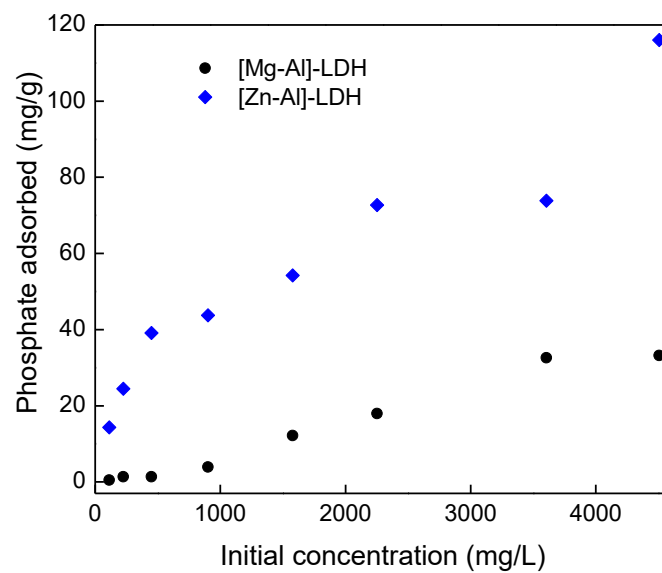FIGURE B1. Adsorption isotherms for [Mg-Al]-LDH and [Zn-Al]-LDH
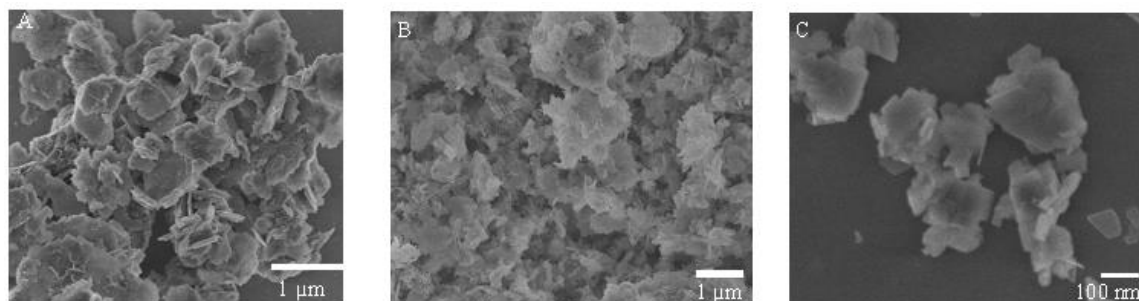
Appendix C

Supporting Information of Chapter IV

FIGURE C1. Scanning electron microscopy (SEM) micrographs of (A) as-synthesized [Ca-Al]-LDH; (B) calcined [Ca-Al]c-LDH and (C) [Ca-Al]-LDH R-H_2O reconstructed in water.

TABLE C1. d-002 Interlayer space values of [Ca-Al]-LDH loaded with PO_4^{3-} as calculated by Bragg equation.

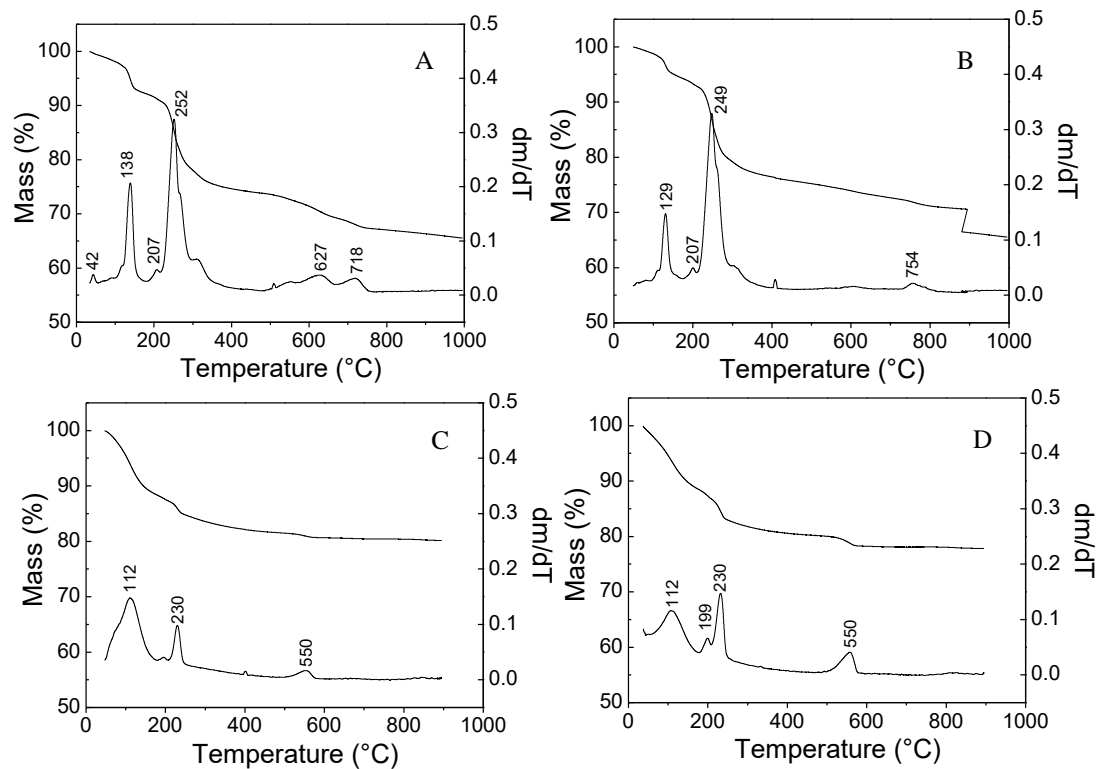| PO_4^{3-} (mM)	Interlayer space (Å)	
	Structural Reconstruction (SR)	Ion Exchange (IE)
Pristine [Ca-Al]-LDH	2.96	2.96
H_2O	2.96	2.96
0.83	2.98	2.90
1.65	2.94	2.99
3.31	($2\theta=10.06$) 3.99 ($2\theta =11.49$)2.90	3.14
6.62	3.30	3.38
11.58	3.46	3.40
PO_4^{3-} (mM)	Interlayer space (Å)	
	Structural Reconstruction (SR)	Ion Exchange (IE)
Pristine [Ca-Al]-LDH	2.96	2.96
H_2O	2.96	2.96
0.83	2.98	2.90
1.65	2.94	2.99
3.31	($2\theta=10.06$) 3.99 ($2\theta =11.49$)2.90	3.14
6.62	3.30	3.38
11.58	3.46	3.40

FIGURE C2a. Thermogravimetric (TG) and differential thermogravimetric (DTG) curves of [Ca-Al]-LDH loaded with PO_4^{3-} by structural reconstruction (SR) from initial PO_4^{3-} concentrations of (A) 0.125 mM, (B) 1.65 mM and (C) 16.55 mM and (D) 26.48 mM.
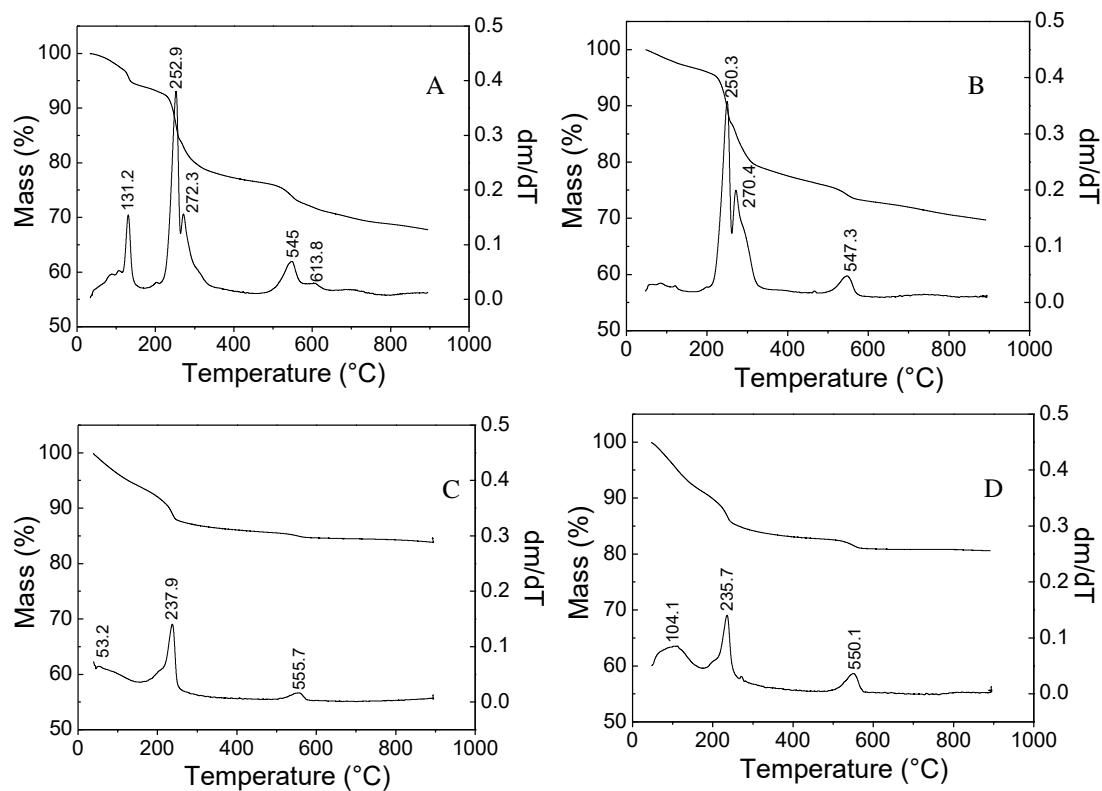
FIGURE C2b. Thermogravimetric (TG) and differential thermogravimetric (DTG) curves of [Ca-Al]-LDH loaded with PO_4^{3-} by ion exchange (IE) reaction from initial PO_4^{3-} concentrations of (A) 0.125 mM, (B) 1.65 mM and (C) 16.55 mM and (D) 26.48 mM.

Appendix D

Supporting Information of Chapter V

TABLE D1: Description and operational condition of ICP-AES

Frequency generator (MHz)	40
Observation mode	radial
Height of observation (mm)	8
Diffraction system	Littrow polychromator with grille echelle
Detector	Coupled charging device
Potential of radiofrequency (kW)	1.3
Nebulizer	Concentric
Nebulizer camera	Cyclonic
Flow rate of plasma gas generation (L.min^{-1})	15
Flow rate of auxiliary gas (L.min^{-1})	1.5
Flow rate of fogging gas (L.min^{-1})	0.6
Replicates	3
Integrations time (s)	10
Element and wavenumber (nm)	
Mg (I)- Atomic line	279.553
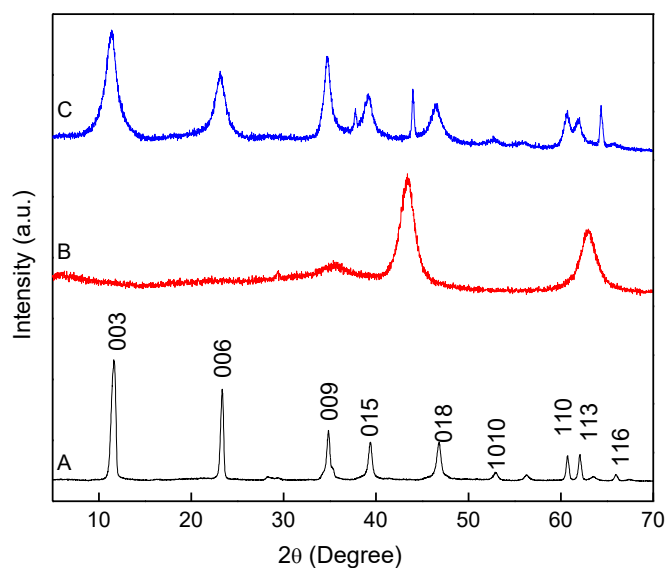
FIGURE D1: PXRD for (A) Commercial [Mg-Al]-LDH and [Mg-Al]-LDH reconstructed in water at (B) 25°C and (C) 75°C, proving that full structural reconstruction only occurs at 75°C.
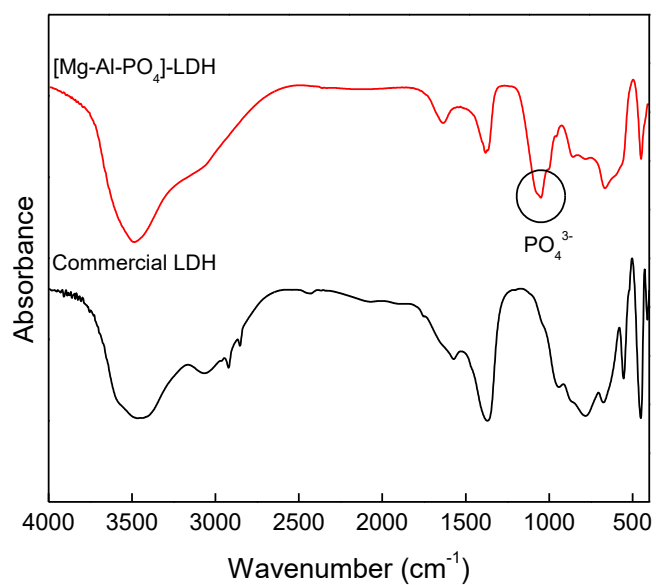
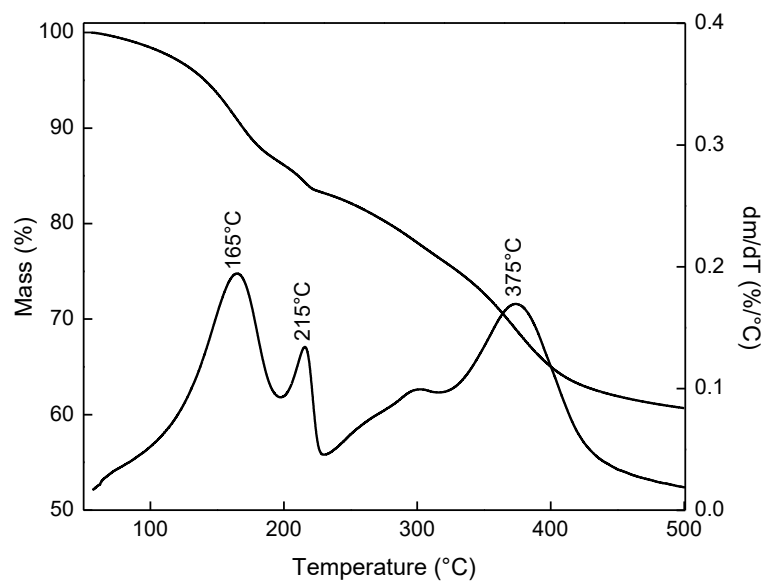FIGURE D2: FTIR spectra for [Mg-Al]-LDH and [Mg-Al-PO₄]-LDH.

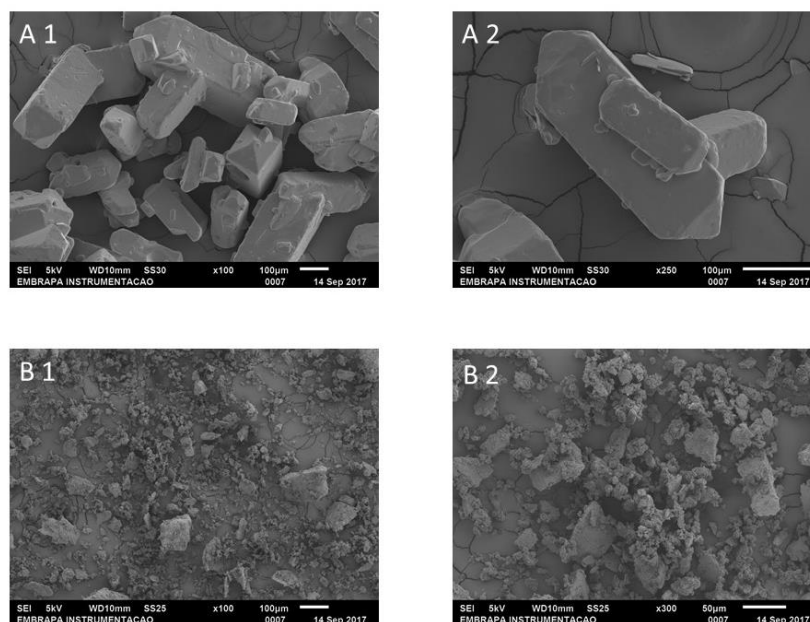FIGURE D3: TG/DTG data for [Mg-Al]-LDH reconstructed in water.

FIGURE D4: Scanning Electron Microscopy for KH$_2$PO$_4$ (A1 e A2) and MAP (B1 e B2)
Figure D4 evidence the differences at crystal habit and morphology for KH$_2$PO$_4$ and MAP, where MAP is formed by crystals with small size than KH$_2$PO$_4$, justifying the quick phosphate release.
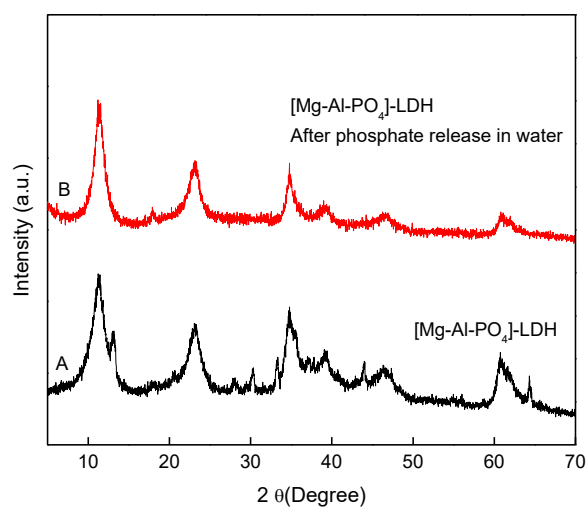

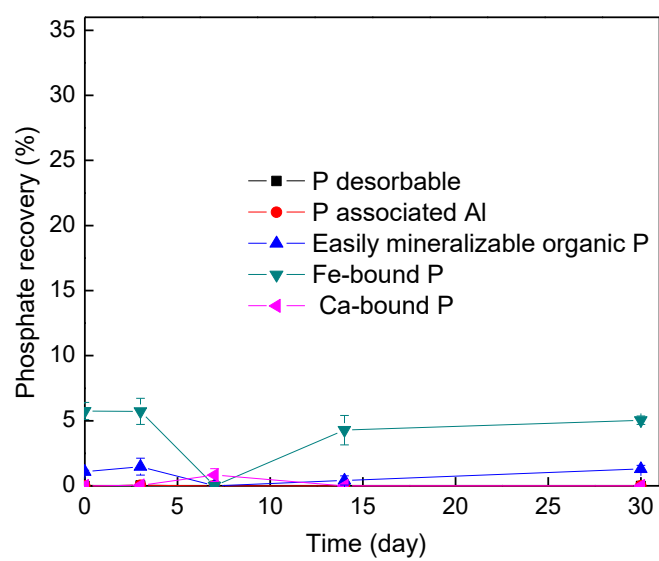FIGURE D5: [Mg-Al-PO4]-LDH (A) before and (b) after phosphate release in water.

FIGURE D6: Sequential extraction for pure soil.